5-6-2010

Providing flow parameters for approximate die design models and the improvement and verification of those models using cfd analysis

Mark Livelli

Providing Flow Parameters for Approximate Die Design Models and the Improvement and Verification of Those Models Using CFD Analysis

Mark Andrew Livelli

A Thesis Submitted in Partial Fulfillment of the Requirement

for Master of Science in Mechanical Engineering

Approved by:

Dr. Steve Weinstein — *Thesis Advisor* _____

Department Head of Chemical and Biomedical Engineering

Dr. Kenneth Ruschak — *Thesis Advisor* _____

Department of Chemical Engineering

Dr. Kathleen Lamkin-Kennard _____

Department of Mechanical Engineering

Dr. Alan Nye _____

Associate Department Head of Mechanical Engineering

Department of Mechanical Engineering

Rochester Institute of Technology

Rochester, New York 14623

May 6, 2010

Permission for Duplication

Providing Flow Parameters for Approximate Die Design Models and the Improvement and Verification of Those Models Using CFD Analysis

I, Mark Andrew Livelli, hereby grant permission to the Wallace Memorial Library of Rochester Institute of Technology to reproduce my thesis in the whole or part. Any reproduction will not be for commercial use or profit.

Signature: _____

Date: _____

Abstract

The role of a coating die is to distribute a uniform, two dimensional liquid film over a solid surface, often formed as an intermediate step in the manufacturing process of polymeric sheet products. The goal of coating die design is to deliver, with a single die, the largest range of fluid rheologies and flow conditions to within specified uniformity limits. Demanding applications require the film thickness nonuniformity to be as little as one percent across the entire coating surface for acceptable quality of the final product, necessitating optimized design as well as precision manufacturing.

There are two principal techniques used for the prediction of optimal die geometry and the analysis of flow uniformity at the slot exit, which includes full numerical computation and theoretical approximate models. Three dimensional computational solutions are numerically intensive, often requiring long computational times to accurately simulate a single die flow condition, and for this reason it is difficult to optimize coating die design solely through the use of full numerical computation. In the alternative approximate modeling approach, the complete set of three dimensional equations governing flow are averaged across the cavity cross section. As a result, the details of the flow and pressure fields at each node point specified within the cavity geometry is exchanged for average flow properties. The advantage of these simplified approximate models is that they are much easier to solve, allowing for many flow conditions and geometric parameters to be tested quickly; however, quantifiable error is incurred due to the approximations of the complete three dimensional set of governing momentum equations.

Much of the initial work on theoretical single cavity die design and the approximate modeling approach focused on the viscous dominated analysis of both the cavity and slot regions for a generalized Newtonian fluid obeying a power law dependence of viscosity on shear rate. Since this initial work, the viscous dominated model has been generalized to include the inertial and gravitational effects within the cavity as well as expanded to incorporate more complex geometries for which the cavity cross sectional area, slot lengths, and slot heights may vary widthwise along the die. For the solution of the single cavity approximate die design model, additional parameters, known as the kinetic and viscous shape factors, are

necessary inputs; these parameters incorporate the specific cross sectional shape of the cavity domain into the pressure drop flow relationship.

In more complex but often superior designs, a secondary cavity and slot are added to improve flow distribution, where the function of the inner cavity and slot are identical to those respective of the single cavity coating die design, however significant flow occurs in the cross section of the outer cavity between the exit of the inner slot and entrance to the outer slot. Despite the complication of this flow in the outer cavity cross section, much of the initial work on theoretical dual cavity die design directly applied the established governing equations of flow in the inner cavity, represented in the approximate models, to both the inner and outer cavities. Ruschak and Weinstein (1997a) obtain a different outer cavity equation for the analysis of dual cavity coating dies, utilizing a perturbation technique to derive a flow equation which accounts for the three dimensional nature of the outer cavity flow and considers the nonlinearities occurring due to inertia or generalized Newtonian rheology. Here, a similar, yet generalized, shape factor for the outer cavity arises which is defined to be consistent with the usual definition for the inner cavity for purely viscous, Newtonian flow.

The focus of this research is to utilize Computational Fluid Dynamics as idealized experimental data, which is to be used for the improvement and verification of the theoretical outer cavity approximate die design model. Additionally, this research provides the first numerical computations of the outer cavity shape factor, incorporating shear thinning fluids as well as fluid inertia. Here, a two dimensional validation of the fundamental assumptions utilized in the derivation of the outer cavity approximate model is performed, while an attempted three dimensional validation of the predicted flow per unit cavity width exiting the outer slot provides confidence in the validity of the approximate modeling approach. A final, practical demonstration of the solution of the outer cavity approximate model provides valuable information for the investigation into the the optimum design of the outer cavity cross section. Ultimately, this research provides a firmer foundation for the design of the outer cavity in a dual cavity coating die, while further demonstrating the utility and importance of the theoretical approximate die design modeling approach.

Dedicated to David and Susan Livelli, Jackie Livelli,
and Rebecca Jaiven

Table of Contents

List of Figures

List of Tables

Nomenclature

Roman

$\dot{\bar{V}}_z$ Lowest order superposition of the first order dimensionless z-component of velocity . . . 20

$\ddot{\bar{V}}_z$ First order superposition of the first order dimensionless z-component of velocity 20

$\breve{\bar{V}}_z$ Constructed form of the first order superposition of the first order dimensionless z-component of velocity . . . 21

W_{is} Width of the inner slot . . . 86

W_{oc} Width of the outer cavity . . . 15

W_{os} Width of the outer slot . . . 86

x Spatial coordinate . . . 15

$\bar{x}$ Dimensionless spatial coordinate . . . 15

y Spatial coordinate . . . 15

$\bar{y}$ Dimensionless spatial coordinate . . . 15

Y_j Mass fraction . . . 33

z Spatial coordinate . . . 15

$\bar{z}$ Dimensionless spatial coordinate . . . 15

Greek

α_ι Condensed Fourier coefficient . . . 28

β_ι Condensed Fourier coefficient . . . 28

$\dot{\gamma}$ Fluid rate of strain . . . 14

δ Ratio of the outer cavity length to width . . . 15

ϵ Measure of flow perturbation . . . 16

ε Outer cavity damping factor . . . 29

η Fluid viscosity . . . 14

η_c Characteristic fluid viscosity . . . 16

$\bar{\eta}$ Dimensionless fluid viscosity . . . 16

$\dot{\bar{\eta}}$ Lowest order perturbation of the dimensionless fluid viscosity . . . 17

$\ddot{\bar{\eta}}$ First order perturbation of the dimensionless fluid viscosity . . . 17

θ Entrance angle in outer cavity . . . 48

ι Fourier mode number . . . 28

λ_{oc} Outer cavity shape factor . . . 22

ξ Integration variable . . . 28

ρ Fluid density . . . 16

σ Anticipated outer slot back pressure dimensionless group . . . 18

ς Outer cavity damping dimensionless group . . . 27

τ Fluid shear stress . . . 32

ϕ Exit angle in outer cavity . . . 48

Chapter 1

Die Design Fundamentals

In a number of manufacturing processes, extrusion or coating dies are often employed to distribute a uniform, two dimensional liquid film over a solid surface. These films are often formed as an intermediate step in the manufacture of polymeric sheet products, of which several layers may be applied simultaneously. A high degree of thickness uniformity in each of these layers can be extremely important for acceptable quality of the final product. Demanding applications require the film thickness nonuniformity to be as little as one percent across the entire coating surface. Therefore, such stringent requirements necessitate optimized design as well as precision manufacturing.

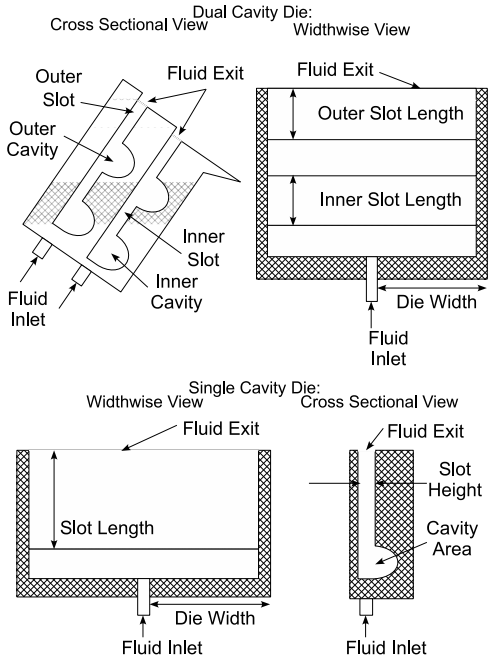

Figure 1.1: Typical Single and Dual Cavity Coating Die Geometry

The simplest possible coating die design consists of a single cavity and slot (Fig. 1.1). Typically, fluid is supplied to the center of the cavity, which acts as a distribution manifold, redistributing fluid from the inlet along the width of the die. A narrow slot joins the cavity, through which fluid is extruded and emerges at the slot exit to form the liquid film. In more complex but often superior designs, a secondary cavity and slot are added to improve flow distribution while increasing the robustness and operating range of the design.

As fluid enters the die through the inlet, flow in the inner cavity is predominantly oriented widthwise along the cavity axis, and thus resembles flow in a duct (Fig. 1.2). To achieve this redistribution of fluid along the widthwise direction, the resistance to flow in the cavity is made low by choosing a relatively large cross sectional area. In contrast, the slot geometry is designed such that the resistance to flow is high, accomplished by choosing a relatively small slot height and long slot length. As a result, fluid entering the inner cavity tends to distribute widthwise, before secondary flows direct the fluid through the slot, where flow consequently becomes oriented primarily along the length of the die toward the slot exit. In a dual cavity coating die design, the functions of the inner cavity and slot are identical to those of the single cavity coating die design. In contrast, significant flow occurs in the cross section of the outer cavity between the exit of the inner slot and entrance to the outer slot, such that the primary flow of the outer cavity is no longer oriented widthwise along the cavity axis but predominantly perpendicular to the axis along the length of the die.

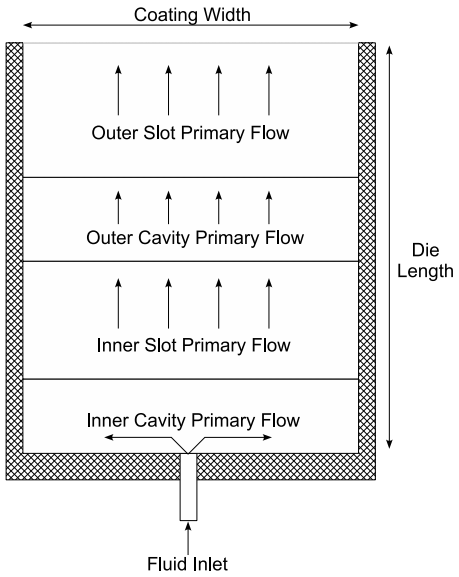

Figure 1.2: Dual Cavity Coating Die Primary Flow Orientation

The objective of coating die design is to achieve uniform flow, which may be accomplished

by maintaining a constant cavity pressure, such that, if the flow is subject to atmospheric conditions at the slot exit, the coating film would be widthwise uniform. It is important to note that a constant cavity pressure cannot be obtained with a finite sized cavity, and so for a coating die with cavity and slot dimensions which are independent of the cavity width, perfect widthwise uniformity cannot be accomplished. In principal this pressure drop cannot be eliminated, as it is required for the redistribution of fluid across the entire width of the die, although it is possible that recoverable pressure from inertia may cancel a portion of the viscous pressure losses.

Geometric adjustments, such as widthwise cavity area and slot length variations, may be chosen to counteract these pressure variations, however, such a design can only ensure perfect flow uniformity for a particular fluid and flow condition. If the cavity and slot dimensions designed to optimize flow uniformity for a particular fluid and flow condition are used to deliver flows of differing fluid rheology, the flow uniformity can deteriorate rapidly and its effect can overcompensate flow profiles (Fig. 1.3). It is important to note that this pressure variance is necessary for the redistribution of flow across the entire width of the die; therefore a more practical consideration of die design is to minimize the pressure drop along the cavity with respect to the average cavity pressure, and thus minimize flow nonuniformity.

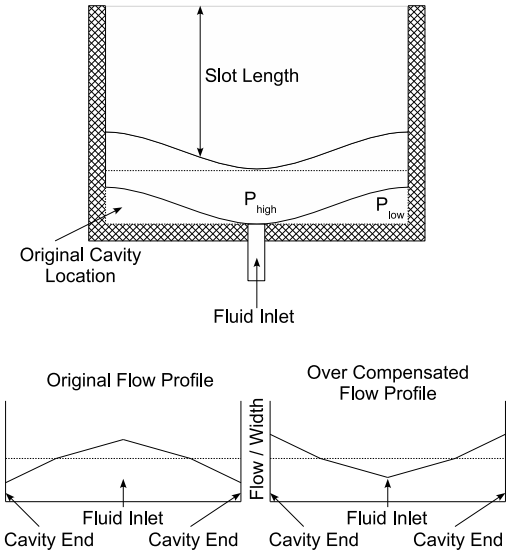

Figure 1.3: Compensation Effects of Geometric Adjustments on Flow Profile

In the coating industries, a single coating die may be utilized to deliver a variety of liquids requiring a high degree of widthwise uniformity. Therefore, one goal of coating die

design is to deliver, with a single die, the largest range of fluids and flow conditions to within specified uniformity limits. To achieve this goal, theoretical models for fluid flow in dies are a valuable tool to identify the impact of geometrical adjustments, as well as allow for the prediction of flow uniformity and design performance. There are two principal techniques used for the prediction of optimal die geometry and the analysis of flow uniformity at the slot exit, full numerical computation of the complete, unsimplified equation set and approximate models.

Full numerical computation utilizes the complete set of three dimensional equations governing fluid flow to extract the precise details of the flow and pressure fields at each node point specified within the cavity and slot geometry. These equations are well known, therefore various commercially available software packages can be used to generate solutions to the equations. However, these governing equations are nonlinear in nature, and with the iterative algorithms used by such packages, there is no guarantee a solution will converge. For the case of coating die design, fine mesh resolution is required to adequately capture the disparate geometrical and flow characteristics in the cavity and slot regions, as well as the rapid changes in flow characteristics as the fluid transitions from one region to another. With each adjustment in the process of dual cavity coating die design through numerical computation, the revised geometry of the current iteration must be remeshed, initialized, and the numerical solution of the flow details recomputed before further analysis and adjustments can be made. Thus, although very accurate, the three dimensional computational solutions are numerically intensive, often requiring long computational times to accurately simulate a single die flow condition, and for this reason it is difficult to optimize coating die design solely through the use of full numerical computation.

In the alternative approximate modeling approach, the complete set of three dimensional equations governing fluid flow are averaged across the cavity cross section. Although the precise knowledge and details of the flow and pressure fields at each node point specified within the cavity and slot geometry are lost, average flow properties such as cavity pressure, widthwise volumetric flow through the cavity, and volumetric flow per width in the slot are readily obtained in exchange. The advantage of these simplified approximate models is that they are much easier to solve, allowing for many flow conditions and geometric parameters to be tested quickly and without redefinition of a computational model and mesh. The shortcoming of the approximate modeling approach is that the governing equations are approximations of the complete three dimensional set, and thus, although quantifiable, there is some incurred error in their use.

The best theoretical approach, based on the previous arguments, would utilize a combination of both the approximate models and numerical computation for the most efficient

coating die design. The modeling approach can be used to determine reasonable designs for a suitable range of flow conditions and fluid rheology, and from these designs the most promising can be scrutinized by the more precise three dimensional numerical computation, identifying adjustments required in the design to correct approximation errors in the modeling approach. The combined use of approximate models and three dimensional numerical computation is advantageous in the reduction of time required to design an coating die.

Chapter 2

Literature Overview

Much of the initial work on theoretical single cavity die design and the approximate modeling approach focused on the viscous dominated analysis of both the cavity and slot regions for a generalized Newtonian fluid obeying a power law dependence of viscosity on shear rate. Such models utilize the common assumption that the cavity volumetric flow, and therefore the axial pressure gradient for designs in which the cavity area does not taper, gradually vary as fluid leaks into the slot. Despite this leakage of flow from the cavity to the slot regions, the pressure drop flow relationship is assumed to have a locally fully developed form, similar to the Poiseuille relationship for Newtonian flow in a pipe. Once flow has transitioned from the cavity to the slot region, the pressure drop flow relationship is assumed to be that of unidirectional flow between parallel plates. Therefore, the initial theoretical single cavity die design and viscous dominated analysis are one dimensional in nature, and the governing equations for fluid flow are spatially dependent upon position along the cavity width only.

For the initial approximate modeling approach and viscous dominated analysis of single cavity coating dies, closed form analytical solutions relating pressure drop to axial position along the cavity for simple geometries of constant circular cross sectional area cavities and straight slots were examined (Carley, 1954). Since this initial work, such viscous dominated analyses have been expanded to incorporate more complex geometries, for which the cavity cross sectional area, slot lengths, and slot heights may vary widthwise along the die (Durst et al., 1994; Leonard, 1985b; Liu et al., 1994; Weinstein and Ruschak, 1996a,b). In all of these analyses, the general form of the pressure drop flow relationship remains that of a locally fully developed form associated with constant geometric dimensions, thus neglecting entrance and end effects at the respective regions of the cavity, to present a one dimensional, closed form analytical solution relating pressure drop to axial position along the cavity.

In the previous viscous dominated analysis of single cavity coating dies, the effects of

inertial and gravitational forces were neglected due to the balance of viscous and pressure forces in the cavity. However, Leonard (1985b) has generalized the viscous dominated model to include these inertial and gravitational effects within the cavity, discussing when these effects become significant in coating die design. In the derivation of his cavity equation, the approximations of the complete set of three dimensional equations governing fluid flow are identical to the approach used by Huang and Yu (1973) to describe flow in porous ducts. It is important to note that from his cavity equation, the aforementioned viscous dominated model may be obtained when such inertial and gravitational effects are neglected.

In most theoretical analyses, the description of flow in the cavity region is treated separately from that of the slot region. However, Vrahopoulou (1991) presents an integrated analysis of die performance, coupling the flow in the cavity and slot regions. It is important to note here that a two dimensional Hele Shaw analysis has been used to examine flows in coating die geometries for which the boundaries of the slot region are considerably sloped, demonstrating good agreement with the one dimensional lubrication approximation in the limit as the die aspect ratio becomes small. Since the purpose of practical coating die design is to obtain a widthwise uniform liquid film at the slot exit, where any design with significant widthwise variation in flow would not be accepted, and the length of the slot is typically greatly exceeded by the width of the coating die, Durst et al. (1994) argues that the one dimensional slot equation of Leonard (1985b) would be reasonable to utilize.

For the approximate, one dimensional modeling approach of single cavity coating dies, numerous forms of the cavity momentum equations have been proposed when inertial effects within the cavity are considered significant to the analysis of flow uniformity. To rectify the differences between the various proposed cavity equation forms, Weinstein and Ruschak (1996b) have formalized the derivation of the cavity equation through asymptotic simplifications, specifically indicating the assumptions essential to their use. The derived cavity equation and differential equation system is found to be identical to that of Leonard (1985b) for single cavity coating dies.

For all of the analyses cited above, shear thinning behavior in the cavity and slot has been characterized as a generalized Newtonian fluid obeying a power law dependence of viscosity on shear rate. The typical rheological curves of polymers may approach a constant Newtonian viscosity at low and high rates of strain, making the power law model inadequate to predict flow nonuniformities for fluids that may be classified as moderately shear thinning. Due to the disparate rates of strain in the cavity and slot of an coating die, flow in portions of the cavity may exhibit Newtonian behavior, while at the same time, flow in the slot may exhibit power law rheology (Yuan, 1995). There are models which do overcome this shortcoming, such as the Carreau viscosity model, however the added mathematical com-

plexity cannot easily be implemented in the one dimensional approximate model approach. Through a linearization of the one dimensional equations, Weinstein and Ruschak (1996a) have demonstrated how derived analytic switching criteria are used to determine whether the flow can effectively be viewed as either Newtonian or power law in both the cavity and slot regions as a whole.

Following the rigorous proof of Weinstein and Ruschak (1996b) to clarify the differences in modeling the inertial effects of the various proposed cavity equation forms, Yu et al. (1997) examine the validity of the different one dimensional approaches through comparison of three dimensional finite element simulations. Their results have indicated that the approximate, one dimensional modeling approach can predict the flow distributions emerging from the slot with reasonable confidence, while the approaches of Yuan (1995) and Weinstein and Ruschak (1996a) can handle both Newtonian and shear thinning behavior of the cavity and should be favorable in the theoretical analysis of single cavity coating die design.

Demanding applications in the photographic industry require the film thickness nonuniformity to be as little as one percent across the entire coating surface; therefore in more complex but often superior designs, a secondary cavity and slot are added to improve flow distribution while increasing the robustness and operating range of the design. In a dual cavity coating die design, the function of the inner cavity and slot is identical to those respective of the single cavity coating die design. Here, the primary flow of the inner cavity is predominantly oriented widthwise along the cavity axis, and thus resembles flow in a duct, before secondary flows direct the fluid through the slot, where flow consequently becomes oriented primarily along the length of the die toward the slot exit (Figure 1.2). In contrast, significant flow occurs in the cross section of the outer cavity between the exit of the inner slot and entrance to the outer slot, such that the primary flow of the outer cavity is no longer oriented widthwise along the cavity axis but predominantly perpendicular to the axis along the length of the die.

For the purely viscous flow of a Newtonian fluid, the equations for flow along the width and cross section of the outer cavity are independent; however, as recognized by Leonard (1985a), nonlinearities occurring due to inertia couple the flow, and the equations for the outer cavity become three dimensional in nature. The inertia of this cross flow impedes widthwise redistribution along the outer cavity, and thus the damping ability of the outer cavity to improve flow uniformity is diminished. Despite this complication of flow in the outer cavity, much of the initial work on theoretical dual cavity design directly applied the established governing equations of flow in the inner cavity to both the inner and outer cavities of the approximate models (Leonard, 1985a; Lee and Liu, 1989; Yuan, 1995).

Ruschak and Weinstein (1997a) obtain a different outer cavity equation for the analysis

of dual cavity coating dies, utilizing a perturbation technique to derive a flow equation which accounts for the three dimensional nature of the outer cavity flow and considers the nonlinearities occurring due to inertia or generalized Newtonian rheology. Since the flow uniformity of practical coating die design cannot vary more than a few percent across the entire coating width, an asymptotic technique is justified and thus linearizes the governing equations of momentum and mass conservation about small deviations in the flow per unit cavity width exiting the inner slot. The components of the momentum equation in the cross section of the outer cavity indicate that the pressure perturbation varies widthwise along the die but is uniform over the outer cavity cross section, and thus the resulting form of the governing equation of flow along the axis of the outer cavity becomes analogous to the convective heat transfer equation with internal heat generation. Furthermore, Ruschak and Weinstein (1997b) have designed a dual cavity coating die analytically through the asymptotic solution of their equations for which the flows in the inner and outer cavities are coupled.

Much of the theoretical single and dual cavity die design and the approximate modeling approach focused on the derivation of the general form of the governing equation and pressure drop flow relationship for more complex geometries where the cavity shape and cross sectional area vary widthwise along the die. Additional parameters, known as shape factors, are necessary inputs to the approximate die design models which incorporate the specific cross sectional shape of the cavity into the pressure drop flow relationship. By approximating the velocity field in the inner cavity as fully developed in any cross section, the viscous and kinetic shape factors explicitly arise (Leonard, 1985b; Weinstein and Ruschak, 1996b).

A similar, yet differing, shape factor for the outer cavity arises (Ruschak and Weinstein, 1997a), which is identical to that of the viscous shape factor for the inner cavity under conditions of creeping flow, relating the pressure drop to fully developed flow in a duct. However, if fluid inertia is present or the rheological model is that of a generalized Newtonian fluid, such as a power law dependence of viscosity on shear rate, the flow across the outer cavity cross section and along the outer cavity axis are coupled. The generalized outer cavity shape factor accounts for the effects of the flow field in the cross section of the outer cavity, specifically those of fluid inertia and a shear rate dependent viscosity, on the redistribution of flow along the outer cavity axis.

The accurate prediction of the pressure drop flow relationship for the laminar flow of generalized Newtonian fluids through ducts of arbitrary yet constant cross section is essential for the determination of the necessary shape factor inputs to approximate die design models. A variational method evolved from an expression of the principal of minimum entropy production has been applied to the steady flow of power law fluids to solve for

the velocity profiles in rectangular ducts, from which the friction factor Reynolds number correlation, or cavity viscous shape factor, has been determined (Schechter, 1961). The velocity profiles of power law fluids in rectangular ducts were also solved through the finite difference method (Wheeler and Wissler, 1965), from which a three parameter expression for the viscous shape factor was correlated through a least squares regression which was then verified experimentally. Since this initial work, the prediction of the pressure drop flow relationship has been expanded to incorporate more complex geometries of arbitrary cross section, where the geometric parameters required in the expression of Wheeler and Wissler (1965) to characterize the duct geometry have been tabulated through the finite element method (Liu, 1983).

A different approach to predict pressure losses has been proposed by Kozicki et al. (1966), through which an expression is derived in terms of two geometric parameter constants characteristic of the shape of the duct cross section, whose determination for more complex geometries requires Newtonian flow data, and a function of shear stress characterizing the fluid. In a much simpler empirical method, Miller (1972) suggests there exists a universal curve relating the average shear rate to the average wall shear stress for the flow of a given generalized Newtonian fluid through ducts of arbitrary cross section. Such a curve is obtained through flow experiments or calculations in a duct of simple geometry, such as that of a circular duct, from which the pressure drop flow relationship is obtained for any duct of arbitrary cross section through the knowledge of the Newtonian viscous shape factor.

Theoretical models for fluid flow in coating dies are a valuable tool to identify the impact of geometrical adjustments, as well as allow for the prediction of flow uniformity and design performance. For the approximate, one dimensional modeling approach of single cavity coating dies, the pressure drop flow relationship for cavity geometries of irregular cross section provides the necessary inputs to analyze flow widthwise distribution and thickness uniformity quickly and effectively. Hanks (1974) and Liu and Hong (1988) examine the analytical basis of Miller's method for estimating the pressure drop flow relationship for a generalized Newtonian rheology, observing several restrictions to the original method, defining limits of applicability, and proposing additional methods to supplement Miller's basic technique.

The final coating die designs obtained through the use of approximate models must be examined experimentally, as this is the ultimate test and validation for any of the theoretical approaches discussed. However, in order to perform a meaningful experimental verification of lateral flow uniformity, the coating die must be built with the proper dimensional aspect ratios and precisely machined. Such a coating die is prohibitively expensive, and academic researchers do not generally posses the funds for its construction. On the other hand, infor-

mation regarding the die flow experiments performed in industry are considered proprietary and seldom released; even there, reliable data is difficult to obtain while conclusive results are often elusive (Ruschak, 2010). For this reason, the validity of theoretical one dimensional approximate die design models and the governing pressure drop flow relationships are examined in academic literature through the use of three dimensional numerical simulation; whereas such an approach is widely accepted within industry as well, when experiments are difficult to quantify.

Fluid flow in single and dual cavity coating dies is three dimensional in nature, and thus the most accurate approach to the analysis of widthwise flow uniformity is to solve the complete set of three dimensional equations governing fluid flow, without simplifications, through numerical computation. This technique extracts the precise details of the flow and pressure fields at each node point specified within the cavity and slot geometry. Three dimensional finite element methods are a valuable tool to identify secondary flows within the cavity and slot flow fields, such as regions of stagnation and vortex formation.

A study of the three dimensional flow fields of generalized Newtonian fluids concerning the entrance region and inlet effects of single cavity coating dies has been examined by Wen and Liu (1994). The center fed and end fed inlet designs have been analyzed for the effects of inertial force, fluid rheology, and inlet geometry on flow uniformity and local vortex formation, while theoretical predictions have been qualitatively confirmed experimentally by the observation of streamlines through a flow visualization technique. For center fed inlet designs, strong jetting effects of increased fluid inertia cause a "fountaining effect" peak in the flow distribution confined to the central region of the coating width. For end fed inlet designs, strong jetting effects of increased fluid inertia cause the appearance of two undesirable vortices near the inlet entrance region, with a peak in flow distribution near the cavity end. Although a number of the theoretical approximate die design models incorporate the effects of fluid inertia in their analysis, three dimensional numerical simulation is necessary for the prediction, and ultimate elimination, of entrance effects and vortex formation at the inlet region.

Similar to the analysis of entrance effects in the inlet regions of single and dual cavity coating dies, three dimensional numerical simulation is a valuable tool for the prediction of vortex formation in the cross flow of the outer cavity regions of a dual cavity coating die. Flow patterns of fluids obeying a power law dependence of viscosity on shear rate within semicircular and tear drop outer cavity cross sections were computed by the finite element method to reveal the formation of vortices with increased fluid inertia. A relationship has been derived for the critical Reynolds number as a function of power law index, above which the vortex formations occur (Lee and Liu, 1989). The effects of cavity shape, particularly

the expansion and contraction angles, as well as the rheological properties of polymeric fluids on vortex formation in the outer cavity of a dual cavity coating die have also been examined by Lee et al. (1990). Again, a relationship for the critical Reynolds number, above which vortex formations are found to occur, has been presented as a function of power law index and expansion angle, and a flow visualization technique was used to observe the flow field patterns in the outer cavity experimentally. While the theoretical approximate die design models allow for the quick and efficient determination of general coating die design geometrical parameters, such as the required cross sectional area of the cavity domain, two and three dimensional numerical simulation is necessary for the detailed analysis of specific cavity shape and ultimate geometrical design.

While much of the complete three dimensional numerical simulation approaches focused on stagnation and vortex formation within the cross section of the outer cavity, general three dimensional finite element codes have also been developed for the purpose of widthwise flow distribution analysis. Wang (1991) has discussed the effects of coating die geometry on film thickness uniformity, concluding that a uniform widthwise flow distribution may be obtained if the contour of the cross section of the slot geometry were to be machined with a "dog bone profile". Several design variations, such as the discharge of coating solutions at the cavity end have been examined to eliminate stagnant regions and reduce flow nonuniformities caused by production variations (Liu et al., 1994).

There are two principal techniques used for the prediction of optimal die geometry and the analysis of flow uniformity at the slot exit, full numerical computation and approximate models. The modeling approach can be used to determine reasonable designs for a suitable range of flow conditions and fluid rheology. From these designs the most promising can be scrutinized by the more precise three dimensional numerical computation, identifying adjustments required in the design to correct approximation errors in the modeling approach (Lee and Liu, 1989; Liu et al., 1994). Such three dimensional computational solutions are numerically intensive, often requiring long computational times to accurately simulate a single die flow condition, and for this reason the most advantageous design approach utilizes a combination of the approximate models and numerical computation for the most efficient coating die design process.

The experimental validation of current theoretical approximate die design models through the verification of lateral flow uniformity is difficult, owing to the fact that the coating die must be built with the proper dimensional aspect ratios and precisely machined, making phenomena occurring within the individual cavities difficult to measure. Computational Fluid Dynamics offers valuable information to the internal flow details, yet such an analysis is difficult due to disparate length scales, and to date an adequate analysis of single and

dual cavity coating die designs has been lacking while the mesh generation for the numerical computations cited has been coarse. The focus of this research is to utilize Computational Fluid Dynamics as idealized experimental data, which is to be used for the improvement and verification of simplified approximate models as well as provide the first numerical computations for the generalized outer cavity shape factor proposed by Ruschak and Weinstein (1997a).

Chapter 3

Derivation of the Outer Cavity Approximate Model

Demanding applications in industry require the film thickness nonuniformity to be as small as one percent across the entire coating surface. Therefore, in more complex but often superior designs, a secondary cavity and slot are added to improve flow distribution. For the purely viscous flow of a Newtonian fluid, the equations for flow along the width and cross section of the outer cavity are independent, however, nonlinearities occurring due to inertia or non-Newtonian rheologies couple the flow, and the equations of motion for the outer cavity become nonlinear. When the flow uniformity of the liquid film exiting the outer slot can vary by no more than a few percent, perturbation methods are applicable and the flow equations are linearized about the limiting case of perfect uniformity.

The derivation of the outer cavity approximate model utilizes the complete set of three dimensional equations of motion that govern the flow in the outer cavity of a dual cavity coating die design. Here, the complete set of three dimensional governing momentum equations are applied for generalized Newtonian rheologies with a power law dependence of viscosity on shear rate, where the viscosity of the fluid may be expressed as a function of the magnitude of the rate of strain tensor.

$$\eta = m|\dot{\gamma}|^{n-1} \tag{3.0.1}$$

where

$$|\dot{\gamma}|^2 = \frac{\mathrm{II}_\Delta}{2} \tag{3.0.2a}$$

$$\mathrm{II}_\Delta = \Delta_{ij}\Delta_{ij} \tag{3.0.2b}$$

$$\Delta_{ij} = \frac{\partial V_i}{\partial R_j} + \frac{\partial V_j}{\partial R_i} \tag{3.0.2c}$$

Disparate length scales typical of coating die design give rise to small parameters, which are summarized below, that enable simplifications to the complete set of three dimensional governing momentum and continuity equations. These simplifications are achieved through scaling each of the components and considering the relative order of magnitude of terms, which is the basis of asymptotic analysis.

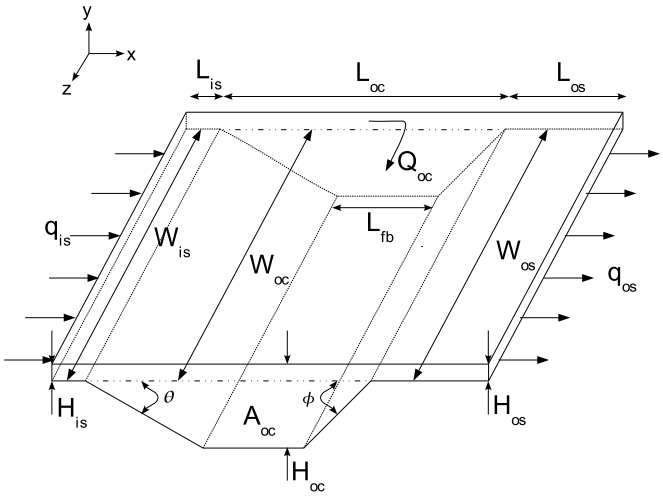

Figure 3.1: Detailed View of the Outer Cavity Geometry Symmetric About the Inlet Plane

For consistency in the final form of the derived approximate model, the characteristic length of the outer cavity cross section (Fig. 3.1) is chosen to be the length of the outer cavity, while the axial characteristic length is chosen to be the width of the outer cavity. As a result of this scaling, a small parameter arises in the derivation of the outer cavity approximate model, defined as the ratio of the outer cavity length to width.

$$\bar{x} = \frac{x}{L_{oc}} \qquad \bar{y} = \frac{y}{L_{oc}} \qquad \bar{z} = \frac{z}{W_{oc}} \tag{3.0.3a}$$

$$\delta = \frac{L_{oc}}{W_{oc}} \tag{3.0.3b}$$

The characteristic flow per unit cavity width in the outer slot is chosen to be the average flow per unit cavity width, and is used to construct the dimensionless velocity components in the governing momentum and continuity equations. The characteristic velocity was defined to be the ratio of this characteristic flow per unit cavity width and the respective dimensional characteristic length.

$$\bar{q}_{os} = \frac{q_{os}}{q_a} \tag{3.0.4a}$$

$$\bar{V}_x = \frac{V_x L_{oc}}{q_a} \qquad \bar{V}_y = \frac{V_y L_{oc}}{q_a} \qquad \bar{V}_z = \frac{V_z W_{oc}}{\epsilon q_a} \tag{3.0.4b}$$

For generalized Newtonian rheologies with a power law dependence of viscosity on shear rate, a characteristic viscosity is defined in the outer cavity such that the characteristic viscosity of the outer cavity is equivalent to the Newtonian viscosity for a power law index of unity.

$$\bar{\eta} = \frac{\eta}{\eta_c} \tag{3.0.5a}$$

$$\eta_c = \frac{m}{\left\{\frac{q_a}{(L_{oc})^2}\right\}^{1-n}} \tag{3.0.5b}$$

The pressure forces in the outer cavity must balance the anticipated axial flow in the outer cavity along the width of the die, and therefore a characteristic pressure in the outer cavity is chosen to balance the leading viscous and pressure terms in the governing equations of motion.

$$\bar{P}_{oc} = \frac{P_{oc}(L_{oc})^2}{\eta_c q_a} \tag{3.0.6}$$

From the preceding scalings, the following form of the Reynolds number arises in the complete set of dimensionless governing equations of motion in the outer cavity.

$$Re = \frac{\rho q_a}{\eta_c} \tag{3.0.7}$$

Introducing the aforementioned dimensionless variables, the derivation of the outer cavity approximate model begins with the dimensionless form of the complete set of three dimensional governing momentum and continuity equations.

Continuity Equation

$$\frac{\partial \bar{V}_x}{\partial \bar{x}} + \frac{\partial \bar{V}_y}{\partial \bar{y}} + \delta^2 \epsilon \frac{\partial \bar{V}_z}{\partial \bar{z}} = 0 \tag{3.0.8a}$$

X-Component of Momentum

$$\begin{aligned} Re\left[\bar{V}_x \frac{\partial \bar{V}_x}{\partial \bar{x}} + \bar{V}_y \frac{\partial \bar{V}_x}{\partial \bar{y}} + \delta^2 \epsilon \bar{V}_z \frac{\partial \bar{V}_x}{\partial \bar{z}}\right] &= -\frac{\partial \bar{P}_{oc}}{\partial \bar{x}} + \frac{\partial}{\partial \bar{x}}\left\{\bar{\eta}\frac{\partial \bar{V}_x}{\partial \bar{x}}\right\} \\ + \frac{\partial \bar{\eta}}{\partial \bar{x}}\frac{\partial \bar{V}_x}{\partial \bar{x}} + \frac{\partial}{\partial \bar{y}}\left\{\bar{\eta}\frac{\partial \bar{V}_x}{\partial \bar{y}}\right\} + \frac{\partial \bar{\eta}}{\partial \bar{y}}\frac{\partial \bar{V}_y}{\partial \bar{x}} + \delta^2 \frac{\partial}{\partial \bar{z}}\left\{\bar{\eta}\frac{\partial \bar{V}_x}{\partial \bar{z}}\right\} + \delta^2 \epsilon \frac{\partial \bar{\eta}}{\partial \bar{z}}\frac{\partial \bar{V}_z}{\partial \bar{x}} \end{aligned} \tag{3.0.8b}$$

Y-Component of Momentum

$$Re\left[\bar{V}_x\frac{\partial\bar{V}_y}{\partial\bar{x}}+\bar{V}_y\frac{\partial\bar{V}_y}{\partial\bar{y}}+\delta^2\epsilon\bar{V}_z\frac{\partial\bar{V}_y}{\partial\bar{z}}\right]=-\frac{\partial\bar{P}_{oc}}{\partial\bar{y}}+\frac{\partial}{\partial\bar{x}}\left\{\bar{\eta}\frac{\partial\bar{V}_y}{\partial\bar{x}}\right\}$$
$$+\frac{\partial\bar{\eta}}{\partial\bar{x}}\frac{\partial\bar{V}_x}{\partial\bar{y}}+\frac{\partial}{\partial\bar{y}}\left\{\bar{\eta}\frac{\partial\bar{V}_y}{\partial\bar{y}}\right\}+\frac{\partial\bar{\eta}}{\partial\bar{y}}\frac{\partial\bar{V}_y}{\partial\bar{y}}+\delta^2\frac{\partial}{\partial\bar{z}}\left\{\bar{\eta}\frac{\partial\bar{V}_y}{\partial\bar{z}}\right\}+\delta^2\epsilon\frac{\partial\bar{\eta}}{\partial\bar{z}}\frac{\partial\bar{V}_z}{\partial\bar{y}} \tag{3.0.8c}$$

Z-Component of Momentum

$$\epsilon Re\left[\bar{V}_x\frac{\partial\bar{V}_z}{\partial\bar{x}}+\bar{V}_y\frac{\partial\bar{V}_z}{\partial\bar{y}}+\delta^2\epsilon\bar{V}_z\frac{\partial\bar{V}_z}{\partial\bar{z}}\right]=-\frac{\partial\bar{P}_{oc}}{\partial\bar{z}}+\epsilon\frac{\partial}{\partial\bar{x}}\left\{\bar{\eta}\frac{\partial\bar{V}_z}{\partial\bar{x}}\right\}$$
$$+\frac{\partial\bar{\eta}}{\partial\bar{x}}\frac{\partial\bar{V}_x}{\partial\bar{z}}+\epsilon\frac{\partial}{\partial\bar{y}}\left\{\bar{\eta}\frac{\partial\bar{V}_z}{\partial\bar{y}}\right\}+\frac{\partial\bar{\eta}}{\partial\bar{y}}\frac{\partial\bar{V}_y}{\partial\bar{z}}+\delta^2\epsilon\frac{\partial}{\partial\bar{z}}\left\{\bar{\eta}\frac{\partial\bar{V}_z}{\partial\bar{z}}\right\}+\delta^2\epsilon\frac{\partial\bar{\eta}}{\partial\bar{z}}\frac{\partial\bar{V}_z}{\partial\bar{z}} \tag{3.0.8d}$$

Viscosity

$$\bar{\eta}^{\frac{2}{n-1}}=2\left[\left\{\frac{\partial\bar{V}_x}{\partial\bar{x}}\right\}^2+\left\{\frac{\partial\bar{V}_y}{\partial\bar{y}}\right\}^2+\delta^4\epsilon^2\left\{\frac{\partial\bar{V}_z}{\partial\bar{z}}\right\}^2\right]+\left\{\frac{\partial\bar{V}_x}{\partial\bar{y}}+\frac{\partial\bar{V}_y}{\partial\bar{x}}\right\}^2$$
$$+\delta^2\left\{\frac{\partial\bar{V}_x}{\partial\bar{z}}+\epsilon\frac{\partial\bar{V}_z}{\partial\bar{x}}\right\}^2+\delta^2\left\{\frac{\partial\bar{V}_y}{\partial\bar{z}}+\epsilon\frac{\partial\bar{V}_z}{\partial\bar{y}}\right\}^2 \tag{3.0.8e}$$

If the flow per unit cavity width exiting the inner cavity and inner slot exhibits perfect widthwise uniformity, there is no damping effect in the outer cavity as flow passes directly through to the outer slot unaffected. In this scenario, flow in the outer cavity is governed by only the cross sectional components of momentum conservation. This two dimensional flow field in the outer cavity cross section, driven by uniform flow in the inner slot, is considered the base flow and the starting point for the perturbation analysis. When there is small widthwise variation in the flow per unit cavity width exiting the inner slot, nonuniformities in the profile are represented as a deviation from the average flow, or perfect widthwise uniformity condition. Considering the necessary requirements for acceptable coating die design, where a significant widthwise variation in the the flow per unit cavity width exiting the outer slot would not be accepted, asymptotic methods are utilized to expand the system about the limiting case of perfect widthwise flow uniformity.

$$\bar{q}_{os}=1+\epsilon\ddot{\bar{q}}_{os}+O(\epsilon^2) \tag{3.0.9a}$$

$$\bar{V}_x=\dot{\bar{V}}_x+\epsilon\ddot{\bar{V}}_x+O(\epsilon^2) \tag{3.0.9b}$$

$$\bar{V}_y=\dot{\bar{V}}_y+\epsilon\ddot{\bar{V}}_y+O(\epsilon^2) \tag{3.0.9c}$$

$$\bar{V}_z=\epsilon\ddot{\bar{V}}_z+O(\epsilon^2) \tag{3.0.9d}$$

$$\bar{\eta}=\dot{\bar{\eta}}+\epsilon\ddot{\bar{\eta}}+O(\epsilon^2) \tag{3.0.9e}$$

Due to the typical aspect ratios demonstrated in a dual cavity coating die design (Fig. 3.1), as the width of the outer cavity generally greatly exceeds the length or height of the outer cavity cross section, it is thus anticipated that the back pressure of the outer slot greatly exceeds pressure variations in the cross section of the outer cavity. Therefore, in the derivation of the outer cavity approximate model, the pressure drop along the length of the outer slot determines a uniform pressure in the cross section of the outer cavity while the pressure distribution in the outer cavity varies axially along the coating die width. It is important to note that the absolute pressure in the outer cavity does not influence the flow field, as it is the pressure gradient along the outer cavity axis which drives the axial flow responsible for damping variations in the flow per unit cavity width exiting the inner slot. Based on this reasoning, the dimensionless perturbed pressure in the outer cavity is constructed in a form which includes the anticipated dominant back pressure of the outer slot.

$$\bar{P}_{oc} = [\sigma\{1 + n\epsilon\ddot{\bar{q}}_{os}\}] + \dot{\bar{P}}_{oc} + \epsilon\ddot{\bar{P}}_{oc} + O(\epsilon^2) \tag{3.0.10a}$$

where

$$\sigma = \frac{2^{1+n}\left\{2 + \frac{1}{n}\right\}^n (L_{oc})^{2n} L_{os}}{(H_{os})^{2n+1}} \tag{3.0.10b}$$

For the typical geometry of a dual cavity coating die design (Fig. 3.1), the characteristic length of the outer cavity cross section is small compared to the axial characteristic length of the outer cavity; consequently, the ratio of these characteristic lengths is much less than order unity. Substituting the asymptotic expansions (Eqs. 3.0.9a to 3.0.9e and 3.0.10a) into the dimensionless form of the complete set of three dimensional governing momentum and continuity equations (Eqs. 3.0.8a to 3.0.8e), the derivation of the outer cavity approximate model considers the simplification to the governing momentum and continuity equations in the limit as the flow perturbation and this ratio of the outer cavity length to width approach zero, holding the Reynolds number of the flow condition fixed.

Lowest Order:

Continuity Equation

$$\frac{\partial \dot{\bar{V}}_x}{\partial \bar{x}} + \frac{\partial \dot{\bar{V}}_y}{\partial \bar{y}} = 0 \tag{3.0.11a}$$

X-Component of Momentum

$$\begin{aligned} Re\left[\dot{\bar{V}}_x \frac{\partial \dot{\bar{V}}_x}{\partial \bar{x}} + \dot{\bar{V}}_y \frac{\partial \dot{\bar{V}}_x}{\partial \bar{y}}\right] &= -\frac{\partial \dot{\bar{P}}_{oc}}{\partial \bar{x}} + \frac{\partial}{\partial \bar{x}}\left\{\dot{\bar{\eta}} \frac{\partial \dot{\bar{V}}_x}{\partial \bar{x}}\right\} \\ &+ \frac{\partial \dot{\bar{\eta}}}{\partial \bar{x}} \frac{\partial \dot{\bar{V}}_x}{\partial \bar{x}} + \frac{\partial}{\partial \bar{y}}\left\{\dot{\bar{\eta}} \frac{\partial \dot{\bar{V}}_x}{\partial \bar{y}}\right\} + \frac{\partial \dot{\bar{\eta}}}{\partial \bar{y}} \frac{\partial \dot{\bar{V}}_y}{\partial \bar{x}} \end{aligned} \tag{3.0.11b}$$

Y-Component of Momentum

$$Re\left[\dot{\bar{V}}_x\frac{\partial\dot{\bar{V}}_y}{\partial\bar{x}}+\dot{\bar{V}}_y\frac{\partial\dot{\bar{V}}_y}{\partial\bar{y}}\right]=-\frac{\partial\dot{\bar{P}}_{oc}}{\partial\bar{y}}+\frac{\partial}{\partial\bar{x}}\left\{\dot{\bar{\eta}}\frac{\partial\dot{\bar{V}}_y}{\partial\bar{x}}\right\}+\frac{\partial\dot{\bar{\eta}}}{\partial\bar{x}}\frac{\partial\dot{\bar{V}}_x}{\partial\bar{y}}+\frac{\partial}{\partial\bar{y}}\left\{\dot{\bar{\eta}}\frac{\partial\dot{\bar{V}}_y}{\partial\bar{y}}\right\}+\frac{\partial\dot{\bar{\eta}}}{\partial\bar{y}}\frac{\partial\dot{\bar{V}}_y}{\partial\bar{y}} \tag{3.0.11c}$$

Z-Component of Momentum

$$\frac{\partial\dot{\bar{P}}_{oc}}{\partial\bar{z}}=0 \tag{3.0.11d}$$

Viscosity

$$\dot{\bar{\eta}}^{\frac{2}{n-1}}=2\left[\left\{\frac{\partial\dot{\bar{V}}_x}{\partial\bar{x}}\right\}^2+\left\{\frac{\partial\dot{\bar{V}}_y}{\partial\bar{y}}\right\}^2\right]+\left\{\frac{\partial\dot{\bar{V}}_x}{\partial\bar{y}}+\frac{\partial\dot{\bar{V}}_y}{\partial\bar{x}}\right\}^2 \tag{3.0.11e}$$

Through a qualitative examination of the lowest order system above, the pressure drop along the width of the coating die in the outer cavity is negligible, and thus there is no redistribution of the flow per unit cavity width along the axis of the outer cavity. Consistent with the definition of the flow per unit cavity width perturbation (Eq. 3.0.9a), this confirms the expectation that in the solution of the lowest order system, the flow per unit cavity width exiting the inner cavity and inner slot exhibits the perfect widthwise uniformity of ideal coating die design. Therefore, there is no damping effect in the outer cavity as the two dimensional flow field in the outer cavity cross section passes directly through to the outer slot unaffected.

If the cavity and slot dimensions designed to optimize flow uniformity for a particular fluid and flow condition are used to deliver flows of differing fluid rheology, the flow uniformity can deteriorate rapidly (Fig. 1.3). Therefore, the primary interest of coating die design is the peak to peak variation in the widthwise distribution of the flow per unit cavity width exiting the outer slot. As evident from the examination of the lowest order system (Eqs. 3.0.11a to 3.0.11e) and the definition of the flow per unit cavity width perturbation (Eq. 3.0.9a), the system equations in the first order contain the nonuniformity information, and the solution of this system is necessary for the determination of the desired peak to peak variation in widthwise flow uniformity.

First Order:

Continuity Equation

$$\frac{\partial\ddot{\bar{V}}_x}{\partial\bar{x}}+\frac{\partial\ddot{\bar{V}}_y}{\partial\bar{y}}=0 \tag{3.0.12a}$$

X-Component of Momentum

$$\begin{aligned} Re\left[\dot{\bar{V}}_x\frac{\partial\ddot{\bar{V}}_x}{\partial\bar{x}}+\ddot{\bar{V}}_x\frac{\partial\dot{\bar{V}}_x}{\partial\bar{x}}+\dot{\bar{V}}_y\frac{\partial\ddot{\bar{V}}_x}{\partial\bar{y}}+\ddot{\bar{V}}_y\frac{\partial\dot{\bar{V}}_x}{\partial\bar{y}}\right] &= -\frac{\partial\ddot{\bar{P}}_{oc}}{\partial\bar{x}} \\ +\frac{\partial}{\partial\bar{x}}\left[\left\{\dot{\bar{\eta}}\frac{\partial\ddot{\bar{V}}_x}{\partial\bar{x}}\right\}+\left\{\ddot{\bar{\eta}}\frac{\partial\dot{\bar{V}}_x}{\partial\bar{x}}\right\}\right]+\frac{\partial\dot{\bar{\eta}}}{\partial\bar{x}}\frac{\partial\ddot{\bar{V}}_x}{\partial\bar{x}}+\frac{\partial\ddot{\bar{\eta}}}{\partial\bar{x}}\frac{\partial\dot{\bar{V}}_x}{\partial\bar{x}} & \quad (3.0.12b) \\ +\frac{\partial}{\partial\bar{y}}\left[\left\{\dot{\bar{\eta}}\frac{\partial\ddot{\bar{V}}_x}{\partial\bar{y}}\right\}+\left\{\ddot{\bar{\eta}}\frac{\partial\dot{\bar{V}}_x}{\partial\bar{y}}\right\}\right]+\frac{\partial\dot{\bar{\eta}}}{\partial\bar{y}}\frac{\partial\ddot{\bar{V}}_y}{\partial\bar{x}}+\frac{\partial\ddot{\bar{\eta}}}{\partial\bar{y}}\frac{\partial\dot{\bar{V}}_y}{\partial\bar{x}} & \end{aligned}$$

Y-Component of Momentum

$$\begin{aligned} Re\left[\dot{\bar{V}}_x\frac{\partial\ddot{\bar{V}}_y}{\partial\bar{x}}+\ddot{\bar{V}}_x\frac{\partial\dot{\bar{V}}_y}{\partial\bar{x}}+\dot{\bar{V}}_y\frac{\partial\ddot{\bar{V}}_y}{\partial\bar{y}}+\ddot{\bar{V}}_y\frac{\partial\dot{\bar{V}}_y}{\partial\bar{y}}\right] &= -\frac{\partial\ddot{\bar{P}}_{oc}}{\partial\bar{y}} \\ +\frac{\partial}{\partial\bar{x}}\left[\left\{\dot{\bar{\eta}}\frac{\partial\ddot{\bar{V}}_y}{\partial\bar{x}}\right\}+\left\{\ddot{\bar{\eta}}\frac{\partial\dot{\bar{V}}_y}{\partial\bar{x}}\right\}\right]+\frac{\partial\dot{\bar{\eta}}}{\partial\bar{x}}\frac{\partial\ddot{\bar{V}}_x}{\partial\bar{y}}+\frac{\partial\ddot{\bar{\eta}}}{\partial\bar{x}}\frac{\partial\dot{\bar{V}}_x}{\partial\bar{y}} & \quad (3.0.12c) \\ +\frac{\partial}{\partial\bar{y}}\left[\left\{\dot{\bar{\eta}}\frac{\partial\ddot{\bar{V}}_y}{\partial\bar{y}}\right\}+\left\{\ddot{\bar{\eta}}\frac{\partial\dot{\bar{V}}_y}{\partial\bar{y}}\right\}\right]+\frac{\partial\dot{\bar{\eta}}}{\partial\bar{y}}\frac{\partial\ddot{\bar{V}}_y}{\partial\bar{y}}+\frac{\partial\ddot{\bar{\eta}}}{\partial\bar{y}}\frac{\partial\dot{\bar{V}}_y}{\partial\bar{y}} & \end{aligned}$$

Z-Component of Momentum

$$\begin{aligned} Re\left[\dot{\bar{V}}_x\frac{\partial\ddot{\bar{V}}_z}{\partial\bar{x}}+\dot{\bar{V}}_y\frac{\partial\ddot{\bar{V}}_z}{\partial\bar{y}}\right] &= -\frac{\partial}{\partial\bar{x}}\left\{\sigma n\ddot{\bar{q}}_{os}\right\}-\frac{\partial\ddot{\bar{P}}_{oc}}{\partial\bar{z}}+\frac{\partial}{\partial\bar{x}}\left\{\dot{\bar{\eta}}\frac{\partial\ddot{\bar{V}}_z}{\partial\bar{x}}\right\} \\ &+\frac{\partial\dot{\bar{\eta}}}{\partial\bar{x}}\frac{\partial\ddot{\bar{V}}_x}{\partial\bar{z}}+\frac{\partial}{\partial\bar{y}}\left\{\dot{\bar{\eta}}\frac{\partial\ddot{\bar{V}}_z}{\partial\bar{y}}\right\}+\frac{\partial\dot{\bar{\eta}}}{\partial\bar{y}}\frac{\partial\ddot{\bar{V}}_y}{\partial\bar{z}} \end{aligned} \quad (3.0.12d)$$

Viscosity

$$\begin{aligned} \ddot{\bar{\eta}} = 2\{n-1\}\dot{\bar{\eta}}^{\frac{n-1}{3-n}}\Bigg[&\left\{\frac{\partial\dot{\bar{V}}_x}{\partial\bar{x}}\frac{\partial\ddot{\bar{V}}_x}{\partial\bar{x}}\right\}+\left\{\frac{\partial\dot{\bar{V}}_y}{\partial\bar{y}}\frac{\partial\ddot{\bar{V}}_y}{\partial\bar{y}}\right\} \\ &+\frac{1}{2}\left\{\frac{\partial\dot{\bar{V}}_x}{\partial\bar{y}}+\frac{\partial\dot{\bar{V}}_y}{\partial\bar{x}}\right\}\left\{\frac{\partial\ddot{\bar{V}}_x}{\partial\bar{y}}+\frac{\partial\ddot{\bar{V}}_y}{\partial\bar{x}}\right\}\Bigg] \end{aligned} \quad (3.0.12e)$$

In the derivation of the outer cavity approximate model, it is anticipated that the back pressure of the outer slot dominates pressure variations in the cross section of the outer cavity, and thus the pressure drop along the length of the outer slot determines a uniform pressure in the cross section of the outer cavity. The pressure distribution in the outer cavity varies axially along the width of the coating die due to variations in the widthwise flow distribution exiting the inner slot, therefore a superposition of the axial component of velocity in the outer cavity is introduced.

$$\ddot{\bar{V}}_z = \dot{\bar{V}}_z + \sigma\ddot{\bar{V}}_z \quad (3.0.13)$$

First Order:

Z-Component of Momentum

$$Re\left[\dot{\bar{V}}_x\frac{\partial\ddot{\bar{V}}_z}{\partial\bar{x}}+\dot{\bar{V}}_y\frac{\partial\ddot{\bar{V}}_z}{\partial\bar{y}}\right]=-\frac{\partial}{\partial\bar{z}}\left\{n\ddot{\bar{q}}_{os}\right\}+\frac{\partial}{\partial\bar{x}}\left\{\dot{\bar{\eta}}\frac{\partial\ddot{\bar{V}}_z}{\partial\bar{x}}\right\}+\frac{\partial}{\partial\bar{y}}\left\{\dot{\bar{\eta}}\frac{\partial\ddot{\bar{V}}_z}{\partial\bar{y}}\right\} \tag{3.0.14}$$

Upon inspection of the first order system of equations (Eqs. 3.0.12a to 3.0.12c, 3.0.12e and 3.0.14), it is important to note that the axial component of velocity is now the only surviving component of the perturbation velocity in the axial component of momentum, while it does not appear in the remaining system equations. In the quasi two dimensional flow field assumed as the base flow in the outer cavity cross section, the components of the flow field scale with a respective increase or decrease in the local flow per unit cavity width entering the outer slot. Along the width of the coating die, the axial pressure gradient drives the flow responsible for damping nonuniformities in the flow per unit cavity width exiting the inner slot, and thus the axial component of velocity scales with the local pressure gradient.

$$\ddot{\bar{V}}_z=\left[-\frac{\partial}{\partial\bar{z}}\left\{n\ddot{\bar{q}}_{os}\right\}\right]\ddot{\bar{V}}_z \tag{3.0.15}$$

First Order:

Z-Component of Momentum

$$Re\left[\dot{\bar{V}}_x\frac{\partial\ddot{\bar{V}}_z}{\partial\bar{x}}+\dot{\bar{V}}_y\frac{\partial\ddot{\bar{V}}_z}{\partial\bar{y}}\right]=1+\frac{\partial}{\partial\bar{x}}\left\{\dot{\bar{\eta}}\frac{\partial\ddot{\bar{V}}_z}{\partial\bar{x}}\right\}+\frac{\partial}{\partial\bar{y}}\left\{\dot{\bar{\eta}}\frac{\partial\ddot{\bar{V}}_z}{\partial\bar{y}}\right\} \tag{3.0.16}$$

For the derivation of the outer cavity approximate model, the perturbed set of three dimensional equations (Eqs. 3.0.11a to 3.0.11c, 3.0.11e and 3.0.16) governing fluid flow in the outer cavity are averaged across the cavity cross section. Although the precise knowledge and details of the flow and pressure fields at each node point specified within the cavity and slot geometry are lost, average flow properties such as cavity pressure, widthwise volumetric flow through the cavity, and volumetric flow per width in the slot are obtained in exchange. Therefore, neglecting entrance and end effects at the respective regions of the cavity, a one dimensional, closed form analytical solution relating pressure drop to axial position along the cavity may be presented.

The solution to the perturbed set of three dimensional equations (Eqs. 3.0.11a to 3.0.11c, 3.0.11e and 3.0.16) governing fluid flow in the outer cavity of a dual cavity coating die may be obtained numerically with no slip boundary conditions imposed at the surfaces of the domain. With the flow field profiles in the outer cavity cross section determined, the postulated form of the axial velocity component, scaled with the local axial pressure gradient, is integrated over the dimensionless area of the outer cavity cross section to provide the desired relationship between the axial pressure gradient and volumetric flow along the outer cavity.

$$\iint_{\bar{A}_{oc}} \ddot{\bar{V}}_z \, d\bar{x}d\bar{y} = -\frac{\partial}{\partial \bar{z}}\left\{ n\ddot{\bar{q}}_{os} \right\} \iint_{\bar{A}_{oc}} \ddot{\bar{V}}_z \, d\bar{x}d\bar{y} \tag{3.0.17}$$

The form of the integrated axial velocity component is similar to that which appears in the derivation of the single cavity approximate model, where the viscous shape factor for one dimensional flow through a duct of arbitrary cross section was defined. In a similar fashion to the derivation of the single cavity approximate model, the pressure at the exit of the outer slot in a dual cavity coating die design is assumed to be at negligible gauge pressure. Therefore, the desired one dimensional approximate model, in dimensional form, relating the axial pressure gradient and volumetric flow along the outer cavity through the outer cavity shape factor is obtained.

$$Q_{oc} = -\left\{ \frac{(A_{oc})^2 \lambda_{oc}}{\eta_c} \right\} \frac{\partial P_{oc}}{\partial z} \tag{3.0.18a}$$

where

$$\lambda_{oc} = \frac{\iint_{\bar{A}_{oc}} \ddot{\bar{V}}_z \, d\bar{x}d\bar{y}}{\left[\iint_{\bar{A}_{oc}} d\bar{x}d\bar{y} \right]^2} \tag{3.0.18b}$$

This additional parameter, the outer cavity shape factor, defines the dimensionless flow along the outer cavity and is a necessary input to the approximate die design models which incorporates the specific cross sectional shape of the cavity domain into the pressure drop flow relationship. This shape factor depends on the Reynolds number and power law index through the solution of the perturbed set of three dimensional equations (Eqs. 3.0.11a to 3.0.11c, 3.0.11e and 3.0.16) governing fluid flow in the outer cavity. Although this parameter is termed the outer cavity shape factor, it is defined to be consistent with the usual definition of the inner cavity viscous shape factor only for the purely viscous flow of a Newtonian fluid, the Stokes flow condition.

The conservation of mass in the outer cavity approximate model needs only to be considered in the surface integral of the mass flux through the volume between any arbitrary outer cavity cross sections, where there is no contribution to the integral over the solid boundaries of the domain. The remaining terms in the integral equation correspond to the widthwise volumetric flow along the outer cavity axis and the perturbed flow per unit cavity width exiting the inner slot and entering the outer slot, leading to the final form of the mass conservation equation utilized in the outer cavity approximate model.

$$\frac{\partial Q_{oc}}{\partial z} = q_{is} - q_{os} \tag{3.0.19}$$

Chapter 3: Derivation of the Outer Cavity Approximate Model

In the derivation of the approximate model, a method for obtaining the flow equations of the outer cavity of a dual cavity coating die has been demonstrated, which accounts for the three dimensional nature of the equations of motion and couples the flow through nonlinearities in the governing equations occurring due to inertia or non-Newtonian rheologies. An expression for the desired relationship between the axial pressure gradient and volumetric flow along the outer cavity axis has been provided, which is a valuable tool for the determination of the desired peak to peak variation in widthwise flow uniformity exiting the outer slot of a dual cavity coating die. The outer cavity shape factor is a necessary input to the approximate die design models which incorporates the specific cross sectional shape of the cavity domain into the pressure drop flow relationship, and the determination of the outer cavity shape factor requires the solution to the perturbed set of three dimensional equations governing fluid flow in the outer cavity domain.

Chapter 4

Solution of the Outer Cavity Approximate Model

The primary interest of coating die design is the peak to peak variation in the widthwise distribution of the flow per unit cavity width exiting the outer slot in the form of a thin, liquid film. Approximate models are essential tools for die design because a meaningful experimental verification of lateral flow uniformity requires expensive hardware which must be built with the proper dimensional aspect ratios and precisely machined, while there are too many geometric and flow parameters for a purely experimental approach to be efficient. Although the flow field within the outer cavity of a dual cavity coating die is three dimensional in nature, full numerical computation of the complete set of three dimensional equations governing fluid flow is numerically intensive, often requiring long computational times to accurately simulate a single die flow condition. The following alternative approximate modeling approach allows for many flow conditions and geometric parameters to be tested quickly, and thus reasonable designs for a suitable range of widthwise flow uniformity may be determined efficiently and effectively.

The derivation of the outer cavity approximate model (Chapter 3) provides an expression for the desired relationship between the axial pressure gradient and volumetric flow along the outer cavity axis. Coupled with a conservation of mass in the outer cavity domain, the solution of these equations (Eqs. 3.0.18a and 3.0.19), based upon a Fourier analysis of the perturbed flow per unit cavity width exiting the inner slot, yields the widthwise distribution of the flow per unit cavity width exiting the outer slot.

Here, the pressure drop along the outer cavity axis is related to the viscous pressure losses through the outer cavity shape factor, incorporating the specific cross sectional shape of the cavity domain into the pressure drop flow relationship (Chapter 3). The inertial term which appears in the pressure drop flow relationship of a single cavity coating die is not

present in the form provided for the outer cavity. Inertia in the outer cavity approximate model is embedded in the outer cavity shape factor, as the primary orientation of flow occurs in the cross section of the outer cavity between the exit of the inner slot and entrance to the outer slot, rather than that of the inner cavity along the die width.

To complete the definition of the one dimensional outer cavity approximate model, the boundary conditions for a well posed system of governing equations specify no flow through the walls at the cavity ends (Fig. 3.1).

$$Q_{oc}\Big|_{z=-W_{oc}} = 0 \qquad \text{and} \qquad Q_{oc}\Big|_{z=W_{oc}} = 0 \tag{4.0.1}$$

For consistency in the final form of the outer cavity approximate model solution, the axial characteristic length of the outer cavity was chosen to be the width of the outer cavity.

$$\bar{z} = \frac{z}{W_{oc}} \tag{4.0.2}$$

The characteristic flow per unit cavity width exiting the inner slot and entering the outer slot was chosen to be the average flow per unit cavity width, and for the volumetric flow along the axis of the outer cavity, the characteristic volumetric flow was defined to be the product of this characteristic flow per unit cavity width and the dimensional cavity width.

$$\bar{q}_{is} = \frac{q_{is}}{q_a} \qquad\qquad \bar{q}_{os} = \frac{q_{os}}{q_a} \tag{4.0.3a}$$

$$\bar{Q}_{oc} = \frac{Q_{oc}}{q_a W_{oc}} \tag{4.0.3b}$$

The pressure forces in the outer cavity must balance the anticipated axial volumetric flow in the outer cavity along the width of the die, and therefore a characteristic pressure in the outer cavity was chosen to balance the leading viscous and pressure terms in the governing equations of motion.

$$\bar{P}_{oc} = \frac{P_{oc}(L_{oc})^2}{\eta_c q_a} \tag{4.0.4}$$

Introducing the aforementioned dimensionless variables of the outer cavity approximate model derivation, the dimensionless form of the system of equations governing the combined inner slot and outer cavity flows is obtained.

$$-\frac{\partial \bar{P}_{oc}}{\partial \bar{z}} = \frac{\bar{Q}_{oc}(W_{oc})^2(L_{oc})^2}{\lambda_{oc}(A_{oc})^2} \tag{4.0.5a}$$

$$\frac{\partial \bar{Q}_{oc}}{\partial \bar{z}} = \bar{q}_{is} - \bar{q}_{os} \tag{4.0.5b}$$

where

$$\bar{Q}_{oc}\Big|_{\bar{z}=-1} = 0 \qquad \text{and} \qquad \bar{Q}_{oc}\Big|_{\bar{z}=1} = 0 \tag{4.0.6}$$

Nonlinearities in the outer cavity pressure, induced by the flow per unit cavity width entering the outer slot, are introduced to the approximate model governing equations through the effects of a generalized Newtonian rheological model. When demanding applications require the film thickness nonuniformity to be as small as one percent across the entire coating surface, perturbation methods are applicable for the solution of the approximate model, and the equations are linearized about the limiting case of perfect widthwise uniformity. Considering the necessary requirements for acceptable coating die design, where a significant widthwise variation in the flow per unit cavity width exiting the outer slot would not be accepted, asymptotic methods are utilized to expand the system in the limit as the perturbation approaches zero. To obtain a closed form analytical solution to the one dimensional approximate model, the flow per unit cavity width exiting the inner slot and entering the outer slot, as well as the volumetric flow along the width of the outer cavity, are linearized about the limiting case of perfect widthwise uniformity, truncating terms of higher order.

$$\bar{q}_{is} = 1 + \epsilon\ddot{\bar{q}}_{is} + O(\epsilon^2) \tag{4.0.7a}$$

$$\bar{q}_{os} = 1 + \epsilon\ddot{\bar{q}}_{os} + O(\epsilon^2) \tag{4.0.7b}$$

$$\bar{Q}_{oc} = \dot{\bar{Q}}_{oc} + \epsilon\ddot{\bar{Q}}_{oc} + O(\epsilon^2) \tag{4.0.7c}$$

In the derivation of the outer cavity approximate model (Chapter 3), the pressure drop along the length of the outer slot determines the pressure level in the cross section of the outer cavity, and thus the pressure distribution in the outer cavity varies axially along the width of the coating die while is taken to be uniform over the entire cross section. Therefore, assuming the pressure at the exit of the outer slot in a dual cavity coating die design to be of negligible gauge pressure in a similar fashion to the solution of the single cavity approximate model, the dimensionless form of the perturbed pressure in the outer cavity expresses the anticipated dominant back pressure of the outer slot.

$$\bar{P}_{oc} = \sigma\{1 + \epsilon n\ddot{\bar{q}}_{os}\} + O(\epsilon^2) \tag{4.0.8}$$

Substituting the asymptotic expansions (Eqs. 4.0.7a to 4.0.7c and 4.0.8) into the dimensionless form of the one dimensional outer cavity approximate model (Eqs. 4.0.5a, 4.0.5b

and 4.0.6), the system is linearized about the condition of perfect widthwise uniformity. The solution of the outer cavity approximate model considers the simplification in the limit as the flow perturbation approaches zero, holding all other parameters fixed.

Lowest Order:

$$\dot{\bar{Q}}_{oc} = 0 \tag{4.0.9a}$$

$$\frac{\partial \dot{\bar{Q}}_{oc}}{\partial \bar{z}} = 0 \tag{4.0.9b}$$

Through a qualitative examination of the lowest order system above, the volumetric flow along the width of the coating die in the outer cavity is negligible, and thus there is no redistribution of flow per unit cavity width along the axis of the outer cavity. Consistent with the definition of the flow per unit cavity width perturbations (Eqs. 4.0.7a and 4.0.7b), this confirms the expectation that in the solution of the lowest order system, the flow per unit cavity width exiting the inner cavity and inner slot exhibits the perfect widthwise uniformity of ideal coating die design. Therefore, there is no damping effect in the outer cavity as the two dimensional flow field in the outer cavity cross section passes directly through to the outer slot unaffected.

When there is small widthwise variation in the flow per unit cavity width exiting the inner slot, as a significant widthwise variation in flow would not be accepted, nonuniformities in the profile are represented as a deviation from the average flow, or perfect widthwise uniformity condition. As evident from the examination of the lowest order system (Eqs. 4.0.9a and 4.0.9b) and the definitions of the flow per unit cavity width perturbations (Eqs. 4.0.7a and 4.0.7b), the solution of the first order system is necessary for the determination of the desired peak to peak variation in widthwise flow uniformity. The system equations in the first order contain the desired nonuniformity information, and the governing equation for volumetric flow along the axis of the outer cavity is obtained by eliminating the flow per unit cavity width entering the outer slot from the approximate model system.

First Order:

$$\frac{\partial^2 \ddot{\bar{Q}}_{oc}}{\partial \bar{z}^2} - \varsigma \ddot{\bar{Q}}_{oc} = \frac{\partial \ddot{\bar{q}}_{is}}{\partial \bar{z}} \tag{4.0.10a}$$

where

$$\varsigma = \frac{\{\frac{H_{os}}{L_{oc}}\}^{2n+1}(L_{oc})^3(W_{oc})^2}{2^{1+n}\{2+\frac{1}{n}\}^n L_{os} n \lambda_{oc} (A_{oc})^2} \tag{4.0.10b}$$

Here, the ratio of flow resistance along the outer cavity axis to that along the outer slot length are quantified through the outer cavity damping dimensionless group, from which the effects of individual geometric parameters on flow uniformity, as well as the degree

of that effect, are determined. It will become apparent that an increased value of this dimensionless group, and thus increased resistance to flow along the outer cavity axis, will result in a decreased effect of outer cavity damping, while in contrast, a decreased value of this dimensionless group, and thus increased resistance to flow along the outer slot length, will result in an increased effect of outer cavity damping and flow uniformity.

If the cavity and slot dimensions designed to optimize flow uniformity for a particular fluid and flow condition are used to deliver flows of various rheology and Reynolds number, the flow uniformity can deteriorate rapidly (Fig. 1.3). Therefore, for the solution of the outer cavity approximate model under numerous geometric parameters and flow conditions, it is convenient to express the perturbed flow distribution in the inner slot as a Fouier series of an unspecified flow distribution function. In this way, it is possible to represent any desired form of the flow per unit cavity width exiting the inner slot in the outer cavity approximate model, producing the final form of the dimensionless differential equation to be solved for the widthwise flow distribution.

$$\ddot{\bar{q}}_{is} = 1 + \sum_{\iota=1}^{\infty} \alpha_\iota \cos(\{\iota\pi\bar{z}\} + \beta_\iota) \tag{4.0.11a}$$

where

$$\alpha_\iota = \sqrt{\left[\int_{-1}^{1} f(\xi)\cos(\iota\pi\xi)\,d\xi\right]^2 + \left[\int_{-1}^{1} f(\xi)\sin(\iota\pi\xi)\,d\xi\right]^2} \tag{4.0.11b}$$

$$\beta_\iota = \tan^{-1}\left(\frac{\int_{-1}^{1} f(\xi)\cos(\iota\pi\xi)\,d\xi}{\int_{-1}^{1} f(\xi)\sin(\iota\pi\xi)\,d\xi}\right) - \frac{\pi}{2} \tag{4.0.11c}$$

First Order:

$$\frac{\partial^2 \ddot{\bar{Q}}_{oc}}{\partial \bar{z}^2} - \varsigma \ddot{\bar{Q}}_{oc} = \sum_{\iota=1}^{\infty} \{-\alpha_\iota \iota\pi\} \sin(\{\iota\pi\bar{z}\} + \beta_\iota) \tag{4.0.12a}$$

with boundary conditions

$$\ddot{\bar{Q}}_{oc}\Big|_{\bar{z}=-1} = 0 \qquad \text{and} \qquad \ddot{\bar{Q}}_{oc}\Big|_{\bar{z}=1} = 0 \tag{4.0.12b}$$

It is important to note that the solution of the differential equation system defined above provides an expression for the dimensionless outer cavity volumetric flow along the coating die width, however, it is the peak to peak variation in the widthwise flow distribution of the flow per unit cavity width exiting the outer slot that is of primary interest in coating die design. Therefore, utilizing the conservation of mass (Eq. 4.0.5b) in the domain of the outer cavity geometry, the desired widthwise flow distribution in the flow per unit cavity width exiting the outer slot is obtained, as well as the ratio of the peak to peak variation in

the flow per unit cavity width entering the outer slot and exiting the inner slot in the outer cavity damping factor.

$$\ddot{\bar{q}}_{os} = 1 + \sum_{\iota=1}^{\infty} \left[\left[\alpha_\iota \left\{ 1 - \frac{\{\iota\pi\}^2}{\{\iota\pi\}^2 + \varsigma} \right\} \right] \cos(\{\iota\pi\bar{z}\} + \beta_\iota) \right. \\ \left. - \left[\frac{\sqrt{\varsigma}\alpha_\iota \{\iota\pi\}\{-1\}^{\iota+1}\sin(\beta_\iota)}{\{\{\iota\pi\}^2 + \varsigma\}\cosh(\sqrt{\varsigma})} \right] \sinh(\sqrt{\varsigma}\bar{z}) \right] \tag{4.0.13}$$

$$\varepsilon = \frac{\ddot{\bar{q}}_{os}\langle max\rangle - \ddot{\bar{q}}_{os}\langle min\rangle}{\ddot{\bar{q}}_{is}\langle max\rangle - \ddot{\bar{q}}_{is}\langle min\rangle} \tag{4.0.14}$$

In the solution of the outer cavity approximate model, a method for obtaining the widthwise distribution of the flow per unit cavity width exiting the outer slot of a dual cavity coating die has been demonstrated, which accounts for the three dimensional nature of the equations of motion governing flow in the outer cavity through the outer cavity shape factor. The system of equations governing the combined inner slot and outer cavity flows has been solved through a Fourier analysis, such that any desired form of the flow per unit cavity width exiting the inner slot may be represented in the outer cavity approximate model, to provide the desired expression for the widthwise uniformity of the final coating film. Although the flow field within the outer cavity of a dual cavity coating die is three dimensional in nature, full numerical computation of the complete set of three dimensional equations governing fluid flow is numerically intensive, often requiring long computational times to accurately simulate a single die flow condition. The alternative approximate modeling approach allows for many flow conditions and geometric parameters to be tested quickly, and thus reasonable designs for a specified range of widthwise flow uniformity limits may be determined efficiently and effectively.

Chapter 5

Computation of the Outer Cavity Shape Factor

Theoretical dual cavity coating die design focuses on the derivation of the general form of the governing pressure drop flow relationship for more complex geometries of arbitrary cross sectional shape. An additional parameter, the outer cavity shape factor, defines the dimensionless flow along the outer cavity axis and is a necessary input to the approximate die design models which incorporates the specific cross sectional shape of the outer cavity into the pressure drop flow relationship. For the purely viscous flow of a Newtonian fluid, flow across the outer cavity cross section and along the outer cavity axis are independent, and the outer cavity shape factor is defined to be consistent with the usual definition of the viscous shape factor for the inner cavity. However, if fluid inertia is present or the rheological model is that of a generalized Newtonian fluid, such as a power law dependence of viscosity on shear rate, the governing equations become nonlinear and the flow across the outer cavity cross section and along the outer cavity axis are coupled. Here, the definition of the outer cavity shape factor is no longer consistent with the usual definition of the inner cavity viscous shape factor, and a numerical study of the three dimensional flow fields within the outer cavity domain is required for the computation of the outer cavity shape factor.

The derivation of the outer cavity approximate model (Chapter 3) provides an expression for the outer cavity shape factor, which incorporates the specific cross sectional shape of the outer cavity domain into the pressure drop flow relationship. The solution of this equation (Eq. 3.0.18b), based upon a numerical analysis of the perturbed set of three dimensional momentum and continuity equations (Eqs. 3.0.11a to 3.0.11c, 3.0.11e and 3.0.16) governing fluid flow in the outer cavity, provides the necessary input for the solution of the outer cavity approximate model (Chapter 4) and ultimate widthwise flow distribution exiting the outer slot.

5.1 Numerical Procedure

Computation of the outer cavity shape factor in more complex geometries of arbitrary cross sectional shape (Fig. 3.1) requires the knowledge of the three dimensional flow field within the outer cavity domain. If the length of the outer cavity significantly exceeds its height, the lubrication theory, small slope approximations, can be used and the perturbed set of equations governing flow in the outer cavity may then be solved directly. However, if this aspect ratio of the outer cavity cross section is of order unity, a numerical approach to the solution of the governing equations of motion is essential, and such three dimensional computational solutions are numerically intensive, often requiring long computational times to accurately simulate a single die flow condition. Through inspection of the three dimensional governing equations of motion, which have been reproduced below, derived in the outer cavity approximate model (Chapter 3), a major simplification arises resulting in the reduction of the computational domain to the two dimensional cross section.

Continuity Equation

$$\frac{\partial \dot{\bar{V}}_x}{\partial \bar{x}} + \frac{\partial \dot{\bar{V}}_y}{\partial \bar{y}} = 0 \tag{5.1.1a}$$

X-Component of Momentum

$$Re\left[\dot{\bar{V}}_x \frac{\partial \dot{\bar{V}}_x}{\partial \bar{x}} + \dot{\bar{V}}_y \frac{\partial \dot{\bar{V}}_x}{\partial \bar{y}}\right] = -\frac{\partial \dot{\bar{P}}_{oc}}{\partial \bar{x}} + \frac{\partial}{\partial \bar{x}}\left\{\dot{\bar{\eta}} \frac{\partial \dot{\bar{V}}_x}{\partial \bar{x}}\right\} + \frac{\partial \dot{\bar{\eta}}}{\partial \bar{x}} \frac{\partial \dot{\bar{V}}_x}{\partial \bar{x}} + \frac{\partial}{\partial \bar{y}}\left\{\dot{\bar{\eta}} \frac{\partial \dot{\bar{V}}_x}{\partial \bar{y}}\right\} + \frac{\partial \dot{\bar{\eta}}}{\partial \bar{y}} \frac{\partial \dot{\bar{V}}_y}{\partial \bar{x}} \tag{5.1.1b}$$

Y-Component of Momentum

$$Re\left[\dot{\bar{V}}_x \frac{\partial \dot{\bar{V}}_y}{\partial \bar{x}} + \dot{\bar{V}}_y \frac{\partial \dot{\bar{V}}_y}{\partial \bar{y}}\right] = -\frac{\partial \dot{\bar{P}}_{oc}}{\partial \bar{y}} + \frac{\partial}{\partial \bar{x}}\left\{\dot{\bar{\eta}} \frac{\partial \dot{\bar{V}}_y}{\partial \bar{x}}\right\} + \frac{\partial \dot{\bar{\eta}}}{\partial \bar{x}} \frac{\partial \dot{\bar{V}}_x}{\partial \bar{y}} + \frac{\partial}{\partial \bar{y}}\left\{\dot{\bar{\eta}} \frac{\partial \dot{\bar{V}}_y}{\partial \bar{y}}\right\} + \frac{\partial \dot{\bar{\eta}}}{\partial \bar{y}} \frac{\partial \dot{\bar{V}}_y}{\partial \bar{y}} \tag{5.1.1c}$$

Z-Component of Momentum

$$Re\left[\dot{\bar{V}}_x \frac{\partial \ddot{\bar{V}}_z}{\partial \bar{x}} + \dot{\bar{V}}_y \frac{\partial \ddot{\bar{V}}_z}{\partial \bar{y}}\right] = 1 + \frac{\partial}{\partial \bar{x}}\left\{\dot{\bar{\eta}} \frac{\partial \ddot{\bar{V}}_z}{\partial \bar{x}}\right\} + \frac{\partial}{\partial \bar{y}}\left\{\dot{\bar{\eta}} \frac{\partial \ddot{\bar{V}}_z}{\partial \bar{y}}\right\} \tag{5.1.1d}$$

Viscosity

$$\dot{\bar{\eta}}^{\frac{2}{n-1}} = 2\left[\left\{\frac{\partial \dot{\bar{V}}_x}{\partial \bar{x}}\right\}^2 + \left\{\frac{\partial \dot{\bar{V}}_y}{\partial \bar{y}}\right\}^2\right] + \left\{\frac{\partial \dot{\bar{V}}_x}{\partial \bar{y}} + \frac{\partial \dot{\bar{V}}_y}{\partial \bar{x}}\right\}^2 \tag{5.1.1e}$$

Boundary Conditions

$$\dot{\bar{V}}_x = \dot{\bar{V}}_y = \ddot{\bar{V}}_z = 0 \quad \text{on all solid surfaces} \tag{5.1.1f}$$

The direct numerical computation of each of the velocity components within the outer cavity geometry with traditional, commercially available software packages would require the full three dimensional domain of the geometry be modeled to invoke the complete three dimensional solver. However, it is important to note that there are no velocity gradients along the axial direction of the outer cavity present in any of the three dimensional equations of motion (Eqs. 5.1.1a to 5.1.1e), derived in the outer cavity approximate model (Chapter 3), in the cross section of the outer cavity geometry. Therefore, the computational domain which must be considered for the numerical integration of the outer cavity shape factor remains solely within the cross section of the outer cavity geometry between the exit of the inner slot and entrance to the outer slot.

To obtain a solution for the axial component of velocity in the two dimensional computational domain of the outer cavity cross section with commercially available software packages, the respective component of the momentum equations (Eq. 5.1.1d) is made analogous to the convective heat transfer equation with internal heat generation. Therefore, the two dimensional flow field in the outer cavity cross section, the base flow, is determined through the traditional methods of the flow field solver, while the final component of the flow field is determined indirectly through the convective heat transfer analogy and the energy equation. In this way, the commercially available software packages must be viewed as a general numerical code for the solution of nonlinear partial differential equations, rather than a blanket flow field visualization solver for the specific geometry and boundary conditions provided.

One such commercially available software package, ANSYS Fluent, is generally accepted in both industrial settings and academic research throughout the world, as it is commonly utilized for its broad physical modeling capabilities of fluid flow simulations. With the intention of manipulating the traditional commercially available ANSYS Fluent software package, a thorough investigation of the internal momentum and energy equations implemented within each segment of the solver is required.

Continuity Equation

$$\frac{\partial \rho}{\partial t} + \nabla \cdot \{\rho \vec{V}\} = S_M \tag{5.1.2}$$

Momentum Equation

$$\frac{\partial}{\partial t}\left\{\rho \vec{V}\right\} + \nabla \cdot \left[\left\{\rho \vec{V}\right\}\vec{V}\right] = -\nabla P + \nabla \cdot \tau + \rho \vec{G} + \vec{F} \tag{5.1.3a}$$

where

$$\tau = \eta \left[\left\{\nabla \vec{V} + \nabla \vec{V}^T\right\} - \tfrac{2}{3}\nabla \cdot \{\vec{V} I\}\right] \tag{5.1.3b}$$

Energy Equation

$$\frac{\partial}{\partial t}\Big\{\rho E_t\Big\} + \nabla\cdot\Big[\vec{V}\left\{\rho E_t + P\right\}\Big] = \nabla\cdot\left[k\nabla T - \sum_{J} h_J \vec{J}_J + \tau\cdot\vec{V}\right] + S_E \tag{5.1.4a}$$

where

$$E_t = \sum_{J} Y_J \left[\int_{T_r}^{T} c_p\, dT\right]_J + \frac{{V_a}^2}{2} \tag{5.1.4b}$$

For the dimensionless forms of the perturbed outer cavity cross flow continuity and momentum equations (Eqs. 5.1.1a to 5.1.1c) to be determined directly through the traditional methods of the ANSYS Fluent flow field solver, several assumptions related to the general form of the governing continuity and momentum equations (Eqs. 5.1.2, 5.1.3a and 5.1.3b) are required. Neglecting any error incurred through the numerical computation of the continuity equation, the laminar, steady flow of an incompressible, generalized Newtonian fluid through a two dimensional computational domain where no external body forces are imposed reduces the dimensional components of the governing continuity and momentum equations provided in ANSYS Fluent to a form analogous to the dimensionless perturbed outer cavity cross flow momentum equations derived in the outer cavity approximate model (Chapter 3).

Continuity Equation

$$\frac{\partial V_x}{\partial x} + \frac{\partial V_y}{\partial y} = 0 \tag{5.1.5a}$$

X-Component of Momentum

$$\begin{aligned}\rho\left[V_x\frac{\partial V_x}{\partial x} + V_y\frac{\partial V_x}{\partial y}\right] &= -\frac{\partial P}{\partial x} + \frac{\partial}{\partial x}\left\{\eta\frac{\partial V_x}{\partial x}\right\} + \frac{\partial \eta}{\partial x}\frac{\partial V_x}{\partial x} \\ &+ \frac{\partial}{\partial y}\left\{\eta\frac{\partial V_x}{\partial y}\right\} + \frac{\partial \eta}{\partial y}\frac{\partial V_y}{\partial x}\end{aligned} \tag{5.1.5b}$$

Y-Component of Momentum

$$\begin{aligned}\rho\left[V_x\frac{\partial V_y}{\partial x} + V_y\frac{\partial V_y}{\partial y}\right] &= -\frac{\partial P}{\partial y} + \frac{\partial}{\partial x}\left\{\eta\frac{\partial V_y}{\partial x}\right\} + \frac{\partial \eta}{\partial x}\frac{\partial V_x}{\partial y} \\ &+ \frac{\partial}{\partial y}\left\{\eta\frac{\partial V_y}{\partial y}\right\} + \frac{\partial \eta}{\partial y}\frac{\partial V_y}{\partial y}\end{aligned} \tag{5.1.5c}$$

For the dimensionless form of the perturbed outer cavity axial momentum equation (Eq. 5.1.1d) to be determined indirectly through the convective heat transfer analogy using the ANSYS Fluent flow field solver, several additional assumptions related to the general form of the energy equation (Eqs. 5.1.4a and 5.1.4b) are required. In addition to the requirements of the base flow solution, a single species model is imposed where a constant specific heat is specified, while the internal reference temperature, which is utilized as the lower limit in the integration of the fluid cell enthalpy calculations, is set to zero. Furthermore,

through the text user interface (Fluent User's Guide, 2006), the effects of viscous energy dissipation, flow work, and kinetic energy must be neglected. Therefore, the general dimensional form of the energy equation provided in ANSYS Fluent becomes analogous to the perturbed outer cavity axial momentum equation derived in the outer cavity approximate model (Chapter 3).

Energy Equation

$$\rho c_p \left[V_x \frac{\partial T}{\partial x} + V_y \frac{\partial T}{\partial y} \right] = \frac{\partial}{\partial x} \left\{ k \frac{\partial T}{\partial x} \right\} + \frac{\partial}{\partial y} \left\{ k \frac{\partial T}{\partial y} \right\} + S_E \tag{5.1.6}$$

The computation of the outer cavity shape factor utilizes the internal momentum and energy equations implemented within each segment of the ANSYS Fluent solver (Eqs. 5.1.5a to 5.1.5c and 5.1.6) as an analogous form of the perturbed set of three dimensional governing momentum equations (Eqs. 5.1.1a to 5.1.1d) from the derivation of the outer cavity approximate model (Chapter 3). For the purely viscous flow of a Newtonian fluid, the equations for flow along the width and cross section of the outer cavity are independent, however nonlinearities occurring due to inertia of generalized Newtonian rheologies couple the flow. Here, the complete set of analogous momentum and energy equations implemented within each segment of the ANSYS Fluent solver is considered valid for generalized Newtonian rheologies, of which the power law model is a specific case. For generalized Newtonian fluids with a power law dependence of viscosity on shear rate, the apparent viscosity of the fluid is provided in ANSYS Fluent through the non-Newtonian power law model as a function of the apparent shear rate.

$$\eta = m|\dot{\gamma}|^{n-1} e^{\frac{T_r}{T}} \tag{5.1.7}$$

To obtain a solution for the outer cavity shape factor, an analogy must be developed between the perturbed set of three dimensional governing continuity and momentum equations (Eqs. 5.1.1a to 5.1.1d) from the derivation of the outer cavity approximate model (Chapter 3) and the reduced forms of the governing continuity, momentum, and energy equations (Eqs. 5.1.5a to 5.1.5c and 5.1.6) from ANSYS Fluent. A direct qualitative comparison of the perturbed set of governing continuity and momentum equations and the analogous set of ANSYS Fluent governing continuity, momentum, and energy equations provides the necessary correlation of variables for the computation of the outer cavity shape factor in the two dimensional cross section.

The two dimensional flow field in the outer cavity cross section, the base flow, is determined through the traditional methods of the flow field solver, and thus the respective cross flow components of the perturbed set of governing momentum equations (Eqs. 5.1.1a to 5.1.1c) and the analogous set of ANSYS Fluent governing momentum equa-

tions (Eqs. 5.1.5a to 5.1.5c) are correlated to determine the proper definition of the solver variables in the context of a general numerical code. Considering the dimensional forms of the velocity components, pressure, viscosity, and spatial coordinates in ANSYS Fluent to be analogous to the respective dimensionless forms of the approximate model, it becomes apparent that the density in the material property specification must be equivalent to the Reynolds number of the desired flow condition. In this way, the base flow required for the computation of the outer cavity shape factor in the dimensionless form of the outer cavity approximate model derivation is solved through a manipulation of the traditional dimensional methods of commercially available software packages.

The axial component of momentum, determined in the two dimensional cross section of the outer cavity geometry, is solved through the heat equation analogy, and thus the axial component of the perturbed set of governing momentum equations (Eq. 5.1.1d) and the analogous energy equation of ANSYS Fluent (Eq. 5.1.6) are correlated to determine the proper definition of the solver variables in the context of a general numerical code. In a similar fashion to the two dimensional base flow, the spatial coordinates and velocity components of the reduced energy equation are considered to be analogous to the dimensionless forms of the approximate model, while the temperature in the reduced form of the energy equation is considered equivalent to the axial component of velocity in the dimensionless form of the approximate model. With the previous restriction that the density of the material property specification must be equivalent to the Reynolds number of the desired flow condition, it becomes apparent that the specific heat of the material property specification must be equivalent to unity. In addition to the material property specification of the fluid density and specific heat, the dimensionless viscosity of the fluid within each computational cell must be replicated in the material property specification of the fluid thermal conductivity, thus simulating the characteristics of the momentum equation within the convective heat transfer analogy. Furthermore, an energy source within the outer cavity domain must be imposed to correspond with the unitary constant appearing in the dimensionless form of the axial component of momentum in the outer cavity approximate model derivation due to the postulated form of the axial component of velocity. In this way, the axial component of velocity in the dimensionless form of the outer cavity approximate model derivation (Chapter 3), which is required for the computation of the outer cavity shape factor, is solved through a manipulation of the traditional dimensional methods of commercially available software packages.

The internal momentum and energy equations (Eqs. 5.1.5a to 5.1.5c and 5.1.6) implemented within each segment of the ANSYS Fluent solver have been manipulated to express an analogous form of the perturbed set of three dimensional governing momentum equa-

tions (Eqs. 5.1.1a to 5.1.1d) from the derivation of the outer cavity approximate model (Chapter 3). With the intention of manipulating traditional, commercially available software packages as a general numerical code, an analogy has been developed to correlate the explicit specification of appropriate fluid properties and available solver models. Any remaining parameters of the model which have not been explicitly defined in the correlation of the analogous ANSYS Fluent momentum and energy equations do not require specification which is unique to the computation of the outer cavity shape factor. However, a set of relationships between these remaining parameters, specifically the fluid consistency, characteristic viscosity, average flow per unit cavity width, and length of the outer cavity, is introduced as a result of the dimensionless scales (Eqs. 3.0.5b and 3.0.7) defined in the derivation of the outer cavity approximate model.

In the correlation of the analogous ANSYS Fluent momentum equations (Eqs. 5.1.5a to 5.1.5c) utilized in the computation of the outer cavity base flow, the density in the material property specification must be equivalent to the Reynolds number of the desired flow condition. This explicit specification of the appropriate fluid density, coupled with the definition of the Reynolds number (Eq. 3.0.7) in the derivation of the outer cavity approximate model (Chapter 3), further requires the average flow per unit cavity width in the inner slot to be equivalent to the characteristic viscosity in the outer cavity cross section. An additional relationship is obtained from the definition of the characteristic viscosity (Eq. 3.0.5b) in the derivation of the outer cavity approximate model, where the average flow per unit cavity width couples with the length of the outer cavity and the consistency of the fluid.

These relationships constitute an underdetermined algebraic set, where there is an infinite number of solutions for the remaining parameters of the model which have not been explicitly defined in the correlation of the analogous ANSYS Fluent momentum and energy equations (Eqs. 5.1.5a to 5.1.5c and 5.1.6). Due to the presence of shear thinning in a generalized Newtonian fluid with a power law dependence of viscosity on shear rate, the relationship coupling the length of the outer cavity and the consistency of the fluid with the average flow per unit cavity width is nonlinear. Here, a variation in fluid rheology would require an adjustment to the previously determined characteristics of the model and subsequent redefinition of material properties, inlet boundary condition, or cavity geometry.

In the most convenient form of the solution of the outer cavity shape factor, the remaining parameters of the model would be kept constant for all flow conditions and fluid rheologies simulated within a given outer cavity shape. Upon inspection of the definition of the characteristic viscosity (Eq. 3.0.5b) from the derivation of the outer cavity approximate model (Chapter 3), it becomes apparent that restricting the average flow per unit

cavity width in the outer slot to be equivalent to the length of the outer cavity maintains constant parameter values for all fluid rheologies. As a result of this additional restriction, the arbitrary choice of any one of these parameters of the model would explicitly constrain the remaining parameters, and thus any superfluous increase in the required computational time, due to a redefinition of material properties or cavity geometry with a variation in fluid rheology, is eliminated.

$$q_a = \eta_c \tag{5.1.8a}$$

$$m = \eta_c \left\{ \frac{q_a}{{L_{oc}}^2} \right\}^{1-n} \tag{5.1.8b}$$

$$L_{oc} = q_a \tag{5.1.8c}$$

The set of relationships above, introduced as a result of the dimensionless scales (Eqs. 3.0.5b and 3.0.7) defined in the derivation of the outer cavity approximate model (Chapter 3), has been obtained to determine the remaining physical properties of the ANSYS Fluent model, valid for all flow conditions and fluid rheologies. These relationships constitute an underdetermined algebraic set, which is satisfied only when the average flow per unit cavity width, characteristic viscosity in the outer cavity cross section, length of the outer cavity, and consistency of the fluid are numerically equivalent. A particularly convenient form of the numerical model utilized in the determination of the outer cavity shape factor arises when the aforementioned physical properties are defined to be numerically equivalent to unity. This specific choice leads to a condition where the spatial coordinates, velocity components, cavity pressure, fluid viscosity, and flow per unit cavity width scale such that the dimensional forms of the ANSYS Fluent model are numerically equivalent to the dimensionless forms of the derivation of the outer cavity approximate model.

General Simulation Parameters	
ρ	Re
m	1.0
k	η
c_p	1.0
L_{oc}	1.000
q_a	1.0

Table 5.1: Simulation Parameters General for All Cross Sections in the Computation of the Outer Cavity Shape Factor

The internal continuity, momentum, and energy equations (Eqs. 5.1.5a to 5.1.5c and 5.1.6) implemented within each segment of the ANSYS Fluent solver have been manipulated to express an analogous form of the perturbed set of three dimensional governing continuity and momentum equations (Eqs. 5.1.1a to 5.1.1d) from the derivation of the outer cavity approximate model (Chapter 3) which is valid for all flow conditions and fluid rheologies. To complete the definition of the ANSYS Fluent model as a general numerical code for the solution of nonlinear partial differential equations, appropriate boundary conditions for the uncoupled base flow and convective heat transfer analogy are required to create a well posed, solvable system.

To ensure consistent mesh generation and material property specification for all flow conditions and fluid rheologies of a given outer cavity cross sectional shape, a unitary definition of the average flow per unit cavity width exiting the inner slot has been imposed for the computation of the outer cavity base flow. This assumed form of the inlet boundary condition demonstrates a fully developed profile, which is consistent with the analysis of single cavity coating dies where the length of the inner slot greatly exceeds the height of the inner slot. To specify an influx of internal, incompressible flow into the system, ANSYS Fluent offers several available inlet boundary conditions: the velocity inlet, pressure inlet, and mass flow inlet. The velocity inlet boundary condition is chosen for the computation of the outer cavity shape factor to control the necessary influx of mass prescribed through the average flow per unit cavity width entering the system as well as the ability to define the desired fully developed form of the velocity profile.

In contrast to the definition of the inlet boundary condition, the details of the flow field at the outlet boundary of the outer cavity geometry are not explicitly known prior to the solution of the two dimensional base flow problem. Although ANSYS Fluent offers a variety of boundary conditions to specify such details at the respective surface of the domain, the outflow boundary condition does not require this information a priori. In this way, the details of the flow field information at the outlet boundary of the computational domain are extrapolated from the interior nodes; assuming the flow field near this boundary has achieved a fully developed condition, consistent with the assumption that the length of the outer slot greatly exceeds the height of the outer slot.

An important characteristic associated with the velocity inlet and outflow boundary conditions imposed in the computation of the base flow problem is the assumed fully developed profile of the flow per unit cavity width exiting the inner slot and entering the outer slot. The expansion of the two dimensional cross section of the outer cavity geometry (Fig. 3.1) induces a region near the exit of the inner slot where the velocity distribution deviates from the assumed fully developed profile. At the entrance of the outer slot, there exists an in-

termediate region due to the contraction of the two dimensional outer cavity cross section where the velocity distribution has not achieved the fully developed profile necessary for the outflow boundary condition. To ensure the fully developed character of the velocity distribution associated with the boundary conditions required in the computational domain of the ANSYS Fluent model, small portions of the inner and outer slot regions must be included with the two dimensional cross section of the outer cavity geometry.

Due to the constructed form of the axial component of velocity (Eq. 3.0.15) in the derivation of the outer cavity approximate model (Chapter 3), a unitary energy source within the outer cavity domain is imposed for the axial flow of the convective heat transfer analogy (Eq. 5.1.6). This energy source drives the secondary flow along the width of the outer cavity and is responsible for the widthwise redistribution and damping of nonuniformities in the flow per unit cavity width exiting the inner slot due to pressure variations in the inner cavity. Although the one dimensional outer cavity approximate model assumes that no widthwise redistribution of the flow per unit cavity width occurs in the regions of the inner and outer slots, this energy source is applied to all three regions of the computational domain to prevent a discontinuity in the numerical solution process.

The velocity perturbation vanishes at the cavity walls, thus the standard no slip boundary condition (Eq. 5.1.1f) is imposed to bound the fluid along the solid surfaces of the computational domain. The wall boundary condition in ANSYS Fluent enforces the no slip condition in the viscous flow model by default, setting the two dimensional components of velocity to zero at the respective surfaces. For the axial component of velocity, which is determined in the computation of the outer cavity shape factor through the energy equation and convective heat transfer analogy (Eq. 5.1.6), the temperature at the solid surfaces of the computational domain must also be specified as zero.

Appropriate physical properties and boundary conditions have been specified to create a well posed, solvable system in the definition of the ANSYS Fluent model as a general numerical code for the solution of the perturbed set of governing continuity and momentum equations (Eqs. 5.1.1a to 5.1.1d) and the computation of the outer cavity shape factor. It is important to note that several of the factors constrained in the correlation of the analogous ANSYS Fluent momentum and energy equations cannot be implemented directly within the ANSYS Fluent graphical user interface. Therefore, user defined functions are required to specify the fully developed velocity distribution imposed at the velocity inlet boundary condition, determined from the prescribed average flow per unit cavity width, as well as the replication of the fluid viscosity, determined in the computation of the base flow problem, as the thermal conductivity in the convective heat transfer analogy. The most convenient application of user defined functions allows for model specific parameters, such as the power

law index and Reynolds number, to be passed through a single ANSYS Fluent case file to determine the appropriate physical properties and boundary conditions relevant to the desired flow condition and fluid rheology in the computation of the outer cavity shape factor.

A major simplification arises in the determination of the outer cavity shape factor which allows for the solution of the perturbed set of governing continuity and momentum equations (Eqs. 5.1.1a to 5.1.1d) from the derivation of the outer cavity approximate model (Chapter 3) in the two dimensional cross section. For the axial component of velocity, which is determined in the computation of the outer cavity shape factor through the energy equation and convective heat transfer analogy (Eq. 5.1.6), the temperature at the solid surfaces of the computational domain is specified as zero. By default, ANSYS Fluent utilizes an absolute temperature scale which bounds the solution of temperature from the energy equation with a lower limit of unity, thus the specification of the no slip boundary condition through the convective heat transfer analogy generates a discontinuity near the cavity wall surfaces. This bounded limit of the absolute temperature in the solution process of the ANSYS Fluent energy equation must be adjusted to properly implement the boundary conditions required in the computation of the outer cavity shape factor through the convective heat transfer analogy.

Viewing ANSYS Fluent as a general numerical code for the solution of nonlinear partial differential equations, rather than a blanket flow field visualization solver for the specific geometry and boundary conditions provided, selecting an appropriate solver model is critical to solution convergence. Computational errors may arise with the improper selection of solver models, resulting in inefficient convergence which requires more computational time than is necessary, misguided convergence to an erroneous solution, or a divergent solution with no convergence at all.

Upon launching the ANSYS Fluent software, both the single precision and double precision versions of the two dimensional solver are available, and although the single precision solver is sufficiently accurate for most cases, specific simulations benefit from the utilization of the double precision version. Double precision calculations are necessary to resolve the pressure variations, required to drive the axial flow responsible for damping nonuniformities in the flow per unit cavity width exiting the inner slot, which are greatly exceeded by the anticipated dominant back pressure of the outer slot (Chapter 3). For models involving high aspect ratio grids, convergence or accuracy may be impaired with the single precision calculation due to the inefficient transfer of boundary information. With the disparate length scales of the modeled outer cavity cross section (Fig. 3.1), where the height and length of the outer cavity greatly exceeds the height of the outer slot, the double precision solver is advantageous in the computation of the outer cavity shape factor.

ANSYS Fluent offers the pressure based solver and density based solver, as well as a multitude of subsequent specialized submodels, for the numerical solution of the Navier Stokes equations and the precise details of the flow and pressure fields at each node point specified within the cavity and slot geometry."Historically speaking, the pressure based approach was developed for low speed incompressible flows, while the density based approach was mainly used for high speed compressible flow. However, recently both methods have been extended and reformulated to solve and operate for a wide range of flow conditions beyond their traditional or original intent" (Fluent User's Guide, 2006). With the restriction of the density to be equivalent to the Reynolds number of the desired flow condition in the correlation of the analogous ANSYS Fluent continuity, momentum, and energy equations (Eqs. 5.1.5a to 5.1.5c and 5.1.6), the computation of the outer cavity shape factor utilizes the pressure based solver.

Within the pressure based solver, the numerical solution of the flow, pressure, and temperature fields at each node point specified within the cavity and slot geometry is obtained through an implicit linearization of the governing momentum, continuity, and energy equations (Fluent User's Guide, 2006). The solution of the resulting linear system is accomplished either through the segregated algorithm, where each of the components of momentum are solved independently, or through the coupled algorithm (Fig. 5.1), which computes each of the components of momentum simultaneously. Regardless of the chosen algorithm, the energy equation (Eq. 5.1.6) and additional scaler quantities are subsequently computed independent of the system of continuity and momentum equations (Eqs. 5.1.5a to 5.1.5c), demonstrating a single iteration of the complete solution loop which repeats continuously until a specified level of convergence is achieved. Although the segregated algorithm requires minimal computational power, the determination of the outer cavity shape factor in the two dimensional cross section is not computationally intensive, and thus the coupled algorithm of the implicit linearization through the pressure based solver is preferred to improve the rate of solution convergence.

At the inlet boundary condition of the ANSYS Fluent numerical model, the components of the prescribed velocity profile may be specified in either an absolute or relative reference frame. The absolute velocity formulation is appropriate in applications where the flow field throughout the majority of the domain is irrotational, while in contrast, the relative velocity formulation is intended for simulations where rotational flow dominates the flow field throughout the majority of the domain. The Fluent User's Guide (2006) recommends that the appropriate velocity formulation be applied such that the bulk of the flow field exhibits the smallest possible velocity magnitudes in that frame, thereby reducing numerical diffusion and producing a more accurate solution. With the absence of rotational flow in

the computational domain of the two dimensional outer cavity cross section, the absolute velocity formulation is specified in the solution of the perturbed set of three dimensional equations governing flow in the outer cavity and the computation of the outer cavity shape factor.

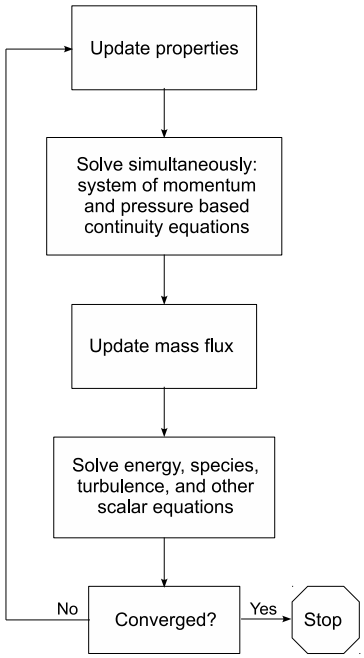

Figure 5.1: ANSYS Fluent Pressure Based Coupled Algorithm Solution Process Flowchart Fluent User's Guide (2006)

ANSYS Fluent stores the discrete values of computed scaler quantities, such as temperature in the solution of the energy equation (Eq. 5.1.6), at the center of each mesh cell, while the scaler quantities at the surrounding mesh cell faces are interpolated through an upwind scheme derived from quantities in the neighboring mesh cell centers which are upstream relative to the direction of the normal velocity. With the default first order upwind scheme, flow field variables computed at the mesh cell center represent an average quantity which is considered valid throughout the entire mesh cell, and the flow field variables determined at the surrounding mesh cell faces directly reflect the corresponding quantities at the upstream mesh cell center. This approximation is sufficient for the computation of the outer cavity shape factor in the two dimensional cross section where minimal variation of the computed flow field components within the individual mesh cells is anticipated due to the fine mesh required by the aspect ratios demonstrated in the two dimensional cross section of a dual cavity coating die (Fig. 3.1).

Each of the analogous ANSYS Fluent continuity, momentum, and energy equations

(Eqs. 5.1.5a to 5.1.5c and 5.1.6) is implicitly linearized through a relationship involving both existing and unknown quantities of the flow field variables, resulting in a system of linear equations which is iteratively solved until convergence is determined (Fluent User's Guide, 2006). The default residual of the ANSYS Fluent pressure based solver defines the imbalance demonstrated in the respective conservation equations, which is summed over each mesh cell in the computational domain, utilizing a scaling factor which is representative of the largest absolute value of the residuals determined during the first several iterations.

The scaled residuals of the pressure based solver may fall below the specified convergence criteria, offering a useful indication of solution convergence, however this result does not sufficiently determine an acceptable solution of the perturbed set of three dimensional equations (Eqs. 5.1.1a to 5.1.1f) governing flow in the outer cavity alone. This method of convergence represents an imbalance in the conservation equations over the entire computational domain as a specified order of magnitude less than the corresponding bulk component of the system, which may remain in decline although the predetermined criteria indicates the solution has converged. A more complete identification of solution convergence occurs as the traditional residual plot demonstrates a flattened, unchanging profile, although this approach increases the required computational time and may be beyond the requisite needs of the outer cavity approximate model. To determine if an acceptable solution is converged, a check must be conducted to ensure a conservation of mass within the computational domain, as well as a constant result in the integration of temperature over the outer cavity cross section, which is the desired result of the computation for the determination of the shape factor.

Due to nonlinearity in the perturbed set of governing momentum equations (Eqs. 5.1.1b to 5.1.1e) from the derivation of the outer cavity approximate model (Chapter 3) with the introduction of a generalized Newtonian rheology, it is necessary to control the change of the velocity components within the iteration loop for stable convergence. This is typically achieved through under relaxation, also referred to as explicit relaxation, which reduces the adjustment produced in the initialized quantity of the proceeding iteration by a factor of the relaxation parameter. The choice of successively smaller under relaxation factors with a respective increase in the shear thinning of fluids with a power law dependence of viscosity on shear rate is essential to prevent the associated oscillations in the numerical solution of the momentum conservation equations.

Once the solution of the perturbed set of three dimensional equations (Eqs. 5.1.1a to 5.1.1f) governing flow in the outer cavity is converged, additional post processing is required to determine the necessary input for the solution of the approximate model. The integral of the perturbed axial component of velocity in the outer cavity as well as the

dimensionless area, which is also available as the spatial integral over the cross sectional domain, are necessary for the calculation of the outer cavity shape factor. In the ANSYS Fluent post processor, a surface integral is computed through the summation of the product of the mesh facet area and the selected field variable, while the volume integral is computed through the summation of the product the mesh cell volume and the selected field variable. It is important to note that in the cross sectional flow problem of the two dimensional outer cavity domain, the mesh cell volume is considered the product of the planer area of the mesh element and an integer unit depth, while the mesh facet area is considered along the perimeter of the element (Fig. 5.2). With a specified unit depth of unity, the volume integral of the ANSYS Fluent post processor provides the required data for the computation of the outer cavity shape factor.

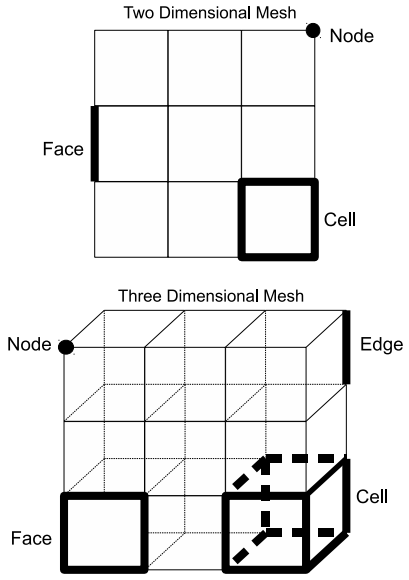

Figure 5.2: Illustration of ANSYS Fluent Mesh Terminology

The outer cavity shape factor incorporates the specific cross sectional shape of the domain into the pressure drop flow relationship, and the computation of this additional parameter requires the knowledge of the three dimensional flow field within the outer cavity domain. Through inspection of the governing equations of motion derived in the outer cavity approximate model, a major simplification arises for the reduction of the computational domain to the two dimensional cross section. A method for obtaining the outer cavity shape factor, utilizing commercially available software, has been established to correlate the perturbed equations of the approximate model with those implemented within the ANSYS Fluent package. This numerical procedure for the computation of the outer cavity shape factor has

been generalized in a form which is valid for the design of more complex geometries of any arbitrary, yet constant, cross sectional shape.

5.2 Mesh Generation

The design of the outer cavity requires a more complex shape than that of the inner cavity to prevent regions of stagnation and recirculation due to the orientation and relative fluid inertia of the primary flow exiting the inner slot of a dual cavity coating die (Fig. 5.3). These effects not only diminish the ability of the outer cavity to improve widthwise flow uniformity, but also result in gelation, due to a cross linking agent or flocculated rheology, as well as the sedimentation of pigments. Optimum outer cavity design utilizes a streamlined shape such that the expansion and contraction angles of the cross sectional geometry may be determined to minimize or eliminate the undesirable effects of vortex formation and fluid stagnation for a range of fluids and flow conditions. Three specific triangular outer cavity designs, which include fifteen-fifteen, thirty-thirty, and thirty-sixty degree expansion and contraction angles respectively, are considered in the computation of the outer cavity shape factor.

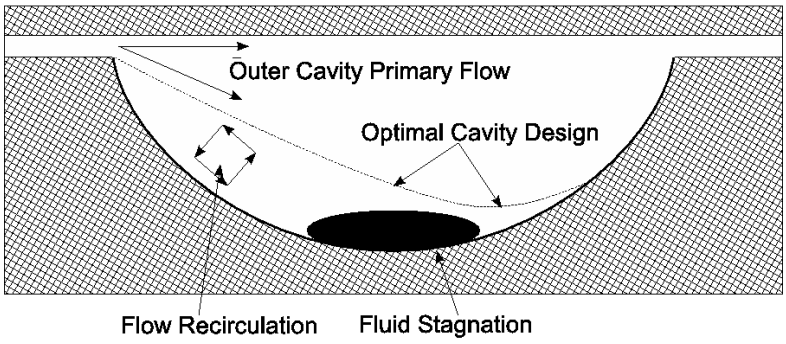

Figure 5.3: Streamlined Outer Cavity Cross Sectional Design

To achieve a redistribution of fluid along the widthwise direction (Fig. 1.1), the resistance to flow along the axis of the outer cavity is made low by choosing a relatively large cross sectional area (Fig. 3.1). In contrast, the slot geometry is designed such that the resistance to flow is high, accomplished by choosing a relatively small slot height and long slot length. In the correlation of the analogous ANSYS Fluent governing momentum and energy equations (Eqs. 5.1.5b, 5.1.5c and 5.1.6), the length of the outer cavity has been constrained, therefore the choice of expansion and contraction angles determines the cross sectional area of the outer cavity domain. The gross partitioning of flow resistances which drives the axial flow

responsible for damping nonuniformities in the flow per unit cavity width is thus achieved in the definition of the height of the outer slot. For the specific cases considered in the computation of the outer cavity shape factor, the height of the outer slot is specified to be ten percent of the respective height of the outer cavity.

The expansion of the two dimensional cross section of the outer cavity geometry (Fig. 3.1) induces a region near the exit of the inner slot where the velocity distribution deviates from the assumed fully developed profile. At the entrance of the outer slot, there exists an intermediate region, due to the contraction of the two dimensional outer cavity cross section, where the velocity distribution has not achieved the fully developed profile assumed by the outflow condition. The development of plane channel flows from a preassigned velocity distribution requires a certain axial distance, and the dependence of this development length on Reynolds number has received considerable attention. An asymptotic combination of the creeping flow and boundary layer solutions has provided a quantitative correlation to express the entry length of channel flows as a function of the Reynolds number for the laminar, stead flow of Newtonian fluids (Atkinson et al., 1969; Durst et al., 2005). For generalized Newtonian fluids with a power law dependence of viscosity on shear rate, the fully developed profile of shear thinning fluids between parallel plates resembles plug flow, and thus the entry length is expected to be less than that of Newtonian fluids. From these relationships provided in the literature to express the entry length of channel flows, an inner slot length which is two times greater than the inner slot height, as well as an outer slot length which is ten times greater that the outer slot height, is found to be sufficient for the calculation of the outer cavity shape factor in the two dimensional computational domain.

Selecting an appropriate mesh for the modeled geometry is critical to solution convergence, as computational errors or an increase in the required computational time can arise as a result of an inadequate meshing scheme. To mesh the two dimensional cross section of the computational domain, Gambit offers several available element options and meshing algorithms, such as the map, submap, pave, tri primitive, and wedge primitive schemes utilizing either quadrilateral or triangular elements. The quadrilateral map meshing scheme is applicable primarily to faces which are bounded by four edges and applies a structured grid of quadrilateral face elements which is preferred in the rectangular portions of the modeled inner and outer slot geometries. Remaining consistent with the quadrilateral element option, the irregular domain of the outer cavity cross section is meshed with the quadrilateral pave scheme, creating an unstructured grid of quadrilateral face elements which may be applied to any face which consists of closed loop edges.

A sufficient number of nodes perpendicular to the direction of flow in the two dimensional cross section (Fig. 3.1) is required to accurately represent the velocity distribution of shear

thinning fluids with rapidly changing characteristics at the wall surface. To determine the appropriate mesh density for a converged solution which is consistent among the cases considered in the computation of the outer cavity shape factor, a characteristic mesh size is defined as the number of cell elements across the height of the outer slot. The corresponding mesh interval size determined from this parameter serves as the basis for the implemented size functions, which gradually decreases the mesh density normal to the surface boundaries as the velocity gradients diminish.

The appropriate number of elements across the height of the inner slot (Fig. 3.1) required for acceptable solution convergence is determined through a mesh refinement series, where the corresponding outer cavity shape factors are investigated as the characteristic mesh size is gradually increased. A sparse number of elements inadequately represents the velocity distribution at the inlet boundary condition as well as the gradients necessary in the determination of the viscosity of generalized Newtonian fluids. In contrast, a dense number of elements requires long computational times while producing a divergent solution for the outer cavity shape factor under flow conditions of increased Reynolds number. Therefore, a characteristic mesh size of fifteen elements across the height of the inner slot is selected as an adequate mesh for the computation of the outer cavity shape factor in the two dimensional cross section.

Model Specific Simulation Parameters	
θ	15.0
ϕ	15.0
H_{is}	0.015
H_{oc}	0.150
H_{os}	0.015
L_{is}	0.030
L_{os}	0.150
M_c	0.0010

Table 5.2: Simulation Parameters Specific to the Triangular 15.0-15.0 Cross Section in the Computation of the Outer Cavity Shape Factor

Figure 5.4: Triangular 15.0-15.0 Final Mesh

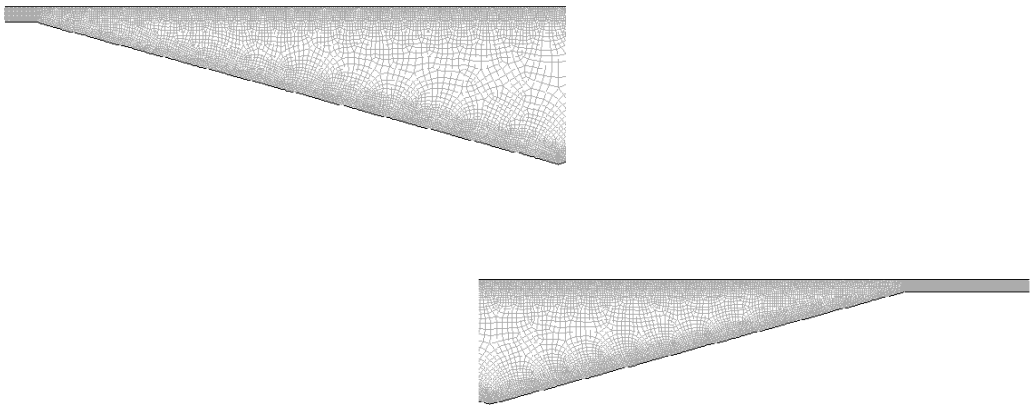

Figure 5.5: Triangular 15.0-15.0 Final Mesh Magnified

Model Specific Simulation Parameters	
θ	30.0
ϕ	30.0
H_{is}	0.030
H_{oc}	0.300
H_{os}	0.060
L_{is}	0.030
L_{os}	0.300
M_c	0.0020

Table 5.3: Simulation Parameters Specific to the Triangular 30.0-30.0 Cross Section in the Computation of the Outer Cavity Shape Factor

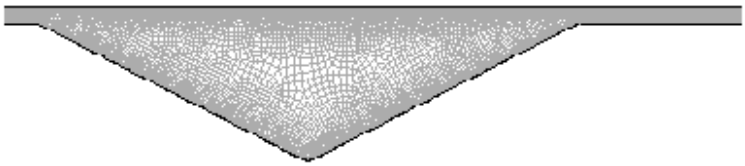

Figure 5.6: Triangular 30.0-30.0 Final Mesh

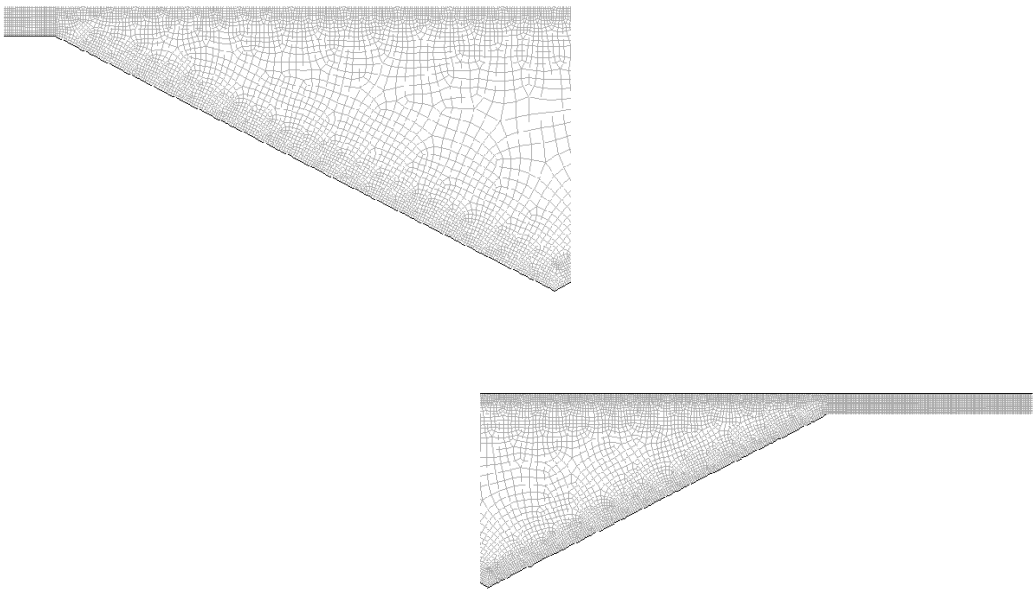

Figure 5.7: Triangular 30.0-30.0 Final Mesh Magnified

Model Specific Simulation Parameters	
θ	30.0
ϕ	60.0
H_{is}	0.048
H_{oc}	0.480
H_{os}	0.048
L_{is}	0.096
L_{os}	0.480
M_c	0.0032

Table 5.4: Simulation Parameters Specific to the Triangular 30.0-60.0 Cross Section in the Computation of the Outer Cavity Shape Factor

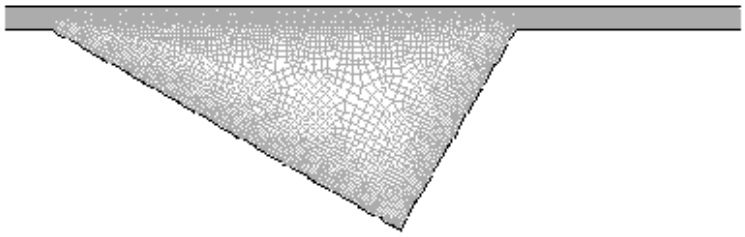

Figure 5.8: Triangular 30.0-60.0 Final Mesh

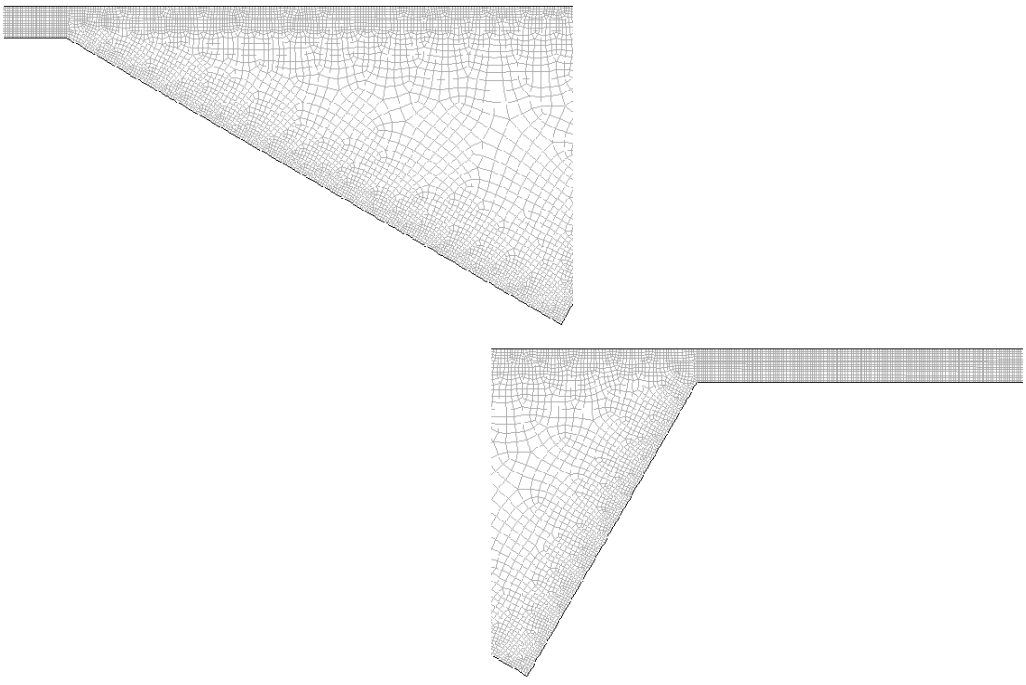

Figure 5.9: Triangular 30.0-60.0 Final Mesh Magnified

The design of the outer cavity requires a more complex shape than that of the inner cavity to prevent regions of stagnation and recirculation, and three specific triangular outer cavity designs are considered in the computation of the outer cavity shape factor. Due to the expansion and contraction of the two dimensional cross section in the outer cavity geometry, intermediate regions of the inner and outer slots are included in the numerical model to satisfy the required boundary conditions. Through a mesh refinement process, the appropriate number of elements across the height of the inner slot is determined for the final mesh of the numerical model implemented within Fluent for the computation of the outer cavity shape factor.

5.3 Results

Utilizing the commercially available ANSYS Fluent software, the solution of the perturbed set of three dimensional continuity and momentum equations (Eqs. 5.1.1a to 5.1.1f) governing flow in the outer cavity is performed through the Rochester Institute of Technology's Research Computing Systems. The Large Memory Computer offers a symmetric multiprocessor, providing a quad core machine which is targeted to run interactive and single threaded jobs which are bound on the researcher's office workstation and connected through a high performance file server. Therefore, the computational resources which are available through Research Computing Systems is well suited for the volume of simulations required to determine the outer cavity shape factor of the specific triangular outer cavity cross sections considered for a suitable range of flow conditions and fluid rheologies.

The outer cavity shape factor defines the dimensionless flow along the width of the outer cavity and incorporates the specific cross sectional shape of the cavity domain into the pressure drop flow relationship (Chapter 3). Once the solution of the perturbed set of three dimensional equations (Eqs. 5.1.1a to 5.1.1f) governing flow in the outer cavity is converged, additional post processing is required to determine this necessary input for the solution of the outer cavity approximate die design model (Chapter 4). The integral of the perturbed axial component of velocity in the outer cavity as well as the dimensionless area, which are available through the volume integral of the ANSYS Fluent post processor, provide the necessary data for the computation of the outer cavity shape factor.

A particularly convenient representation of the outer cavity shape factor for a given cross sectional design characterizes the numerically determined data over the entire range of fluid rheologies and flow conditions considered through a bipartite series of fitted curves. The first of the required curve fits represents the initial set of necessary fitting constants, determined as the predicted outer cavity shape factor for a given fluid rheology at zero Reynolds number

which could not be achieved through the definition of the correlated momentum and energy equations implemented within ANSYS Fluent, as a function of the power law index. This first set of fitting constants is specific to the given shape of the outer cavity cross section as well as the power law index of the generalized Newtonian rheological model, utilized to scale the numerically determined data for all fluid rheologies within an identical range. The second of the required curve fits represents the outer cavity shape factor, which is now scaled with the predicted outer cavity shape factor at zero Reynolds number for a given fluid rheology, as a function of the scaled Reynolds number, which is suggested through an approximate analysis. Similar to the intention of the previous curve fit, this scaled Reynolds number is utilized to compress the numerically determined outer cavity shape factor data along the independent axis, creating a plot on which the outer cavity shape factor for all fluid rheologies and flow conditions may be expressed through a single curve. In this way, the outer cavity shape factor for a given cross sectional design may be extracted for any given fluid rheology and flow condition, within the limits of the plotted data, as input to the outer cavity approximate die design model.

$$\frac{\lambda_{oc}}{c_1} = \frac{e^{-c_5 \bar{Re}} + c_6 e^{-c_7 \bar{Re}^{c_8}}}{1 + c_6} \tag{5.3.1a}$$

where

$$c_1 = c_2 e^{c_3(1-n)} \tag{5.3.1b}$$

$$\bar{Re} = \left\{ \frac{1}{n^{c_4}} \right\} \left\{ \frac{(2 + \frac{1}{n})^{1-n}}{(3 + \frac{2}{n}) 2^n} \right\} Re \tag{5.3.1c}$$

Outer Cavity Shape Factor							
$n = 1.0$		$n = 0.9$		$n = 0.8$		$n = 0.7$	
Re	Fluent λ_{oc}	Re	Fluent λ_{oc}	Re	Fluent λ_{oc}	Re	Fluent λ_{oc}
0.10	0.010849	0.10	0.019449	0.10	0.035002	0.10	0.063273
1.00	0.010802	1.00	0.019259	1.00	0.034212	1.00	0.059925
5.00	0.010195	5.00	0.017016	2.00	0.032545	2.00	0.053787
10.0	0.009148	10.0	0.014043	3.00	0.030570	3.00	0.047757
15.0	0.008179	15.0	0.011800	4.00	0.028585	4.00	0.042561
20.0	0.007359	20.0	0.010141	5.00	0.026718	5.00	0.038215
25.0	0.006677	25.0	0.008884	10.0	0.019703	7.50	0.030162
30.0	0.006106	30.0	0.007903	15.0	0.015449	10.0	0.024606
40.0	0.005213	35.0	0.007115	20.0	0.012630	12.5	0.020632
50.0	0.004550	40.0	0.006467	25.0	0.010603	15.0	0.017689

$n = 0.6$		$n = 0.5$		$n = 0.4$	
Re	Fluent λ_{oc}	Re	Fluent λ_{oc}	Re	Fluent λ_{oc}
0.10	0.114936	0.10	0.209877	0.10	0.379330
1.00	0.101008	0.50	0.189534	0.50	0.296572
2.00	0.081886	1.00	0.157195	1.00	0.210710
3.00	0.067252	1.50	0.130541	1.50	0.157575
4.00	0.056306	2.00	0.109535		
5.00	0.047882	2.50	0.093127		
6.00	0.041484	3.00	0.080180		
7.00	0.036459				

Table 5.5: Triangular 15.0-15.0 ANSYS Fluent Outer Cavity Shape Factor Data Summary

Fitting Constants			
Rheological and Model Specific		Model Specific	
n	c_1		
1.0	0.011344	c_2	0.010704
0.9	0.019444	c_3	5.932035
0.8	0.033382	c_4	2.919321
0.7	0.060103	c_5	0.016073
0.6	0.109240	c_6	2.906562
0.5	0.208570	c_7	0.226532
0.4	0.398297	c_8	1.235717

Table 5.6: Triangular 15.0-15.0 Curve Fitting Constants Summary

Outer Cavity Shape Factor

$n = 1.0$				$n = 0.9$			
Re	Fitted λ_{oc}	Percent Error λ_{oc}	Percent Error ε	Re	Fitted λ_{oc}	Percent Error λ_{oc}	Percent Error ε
0.10	0.010698	1.4	1.4	0.10	0.019352	0.5	0.5
1.00	0.010595	1.9	1.9	1.00	0.019034	1.2	1.2
5.00	0.009952	2.4	2.4	5.00	0.017092	0.4	0.4
10.0	0.009046	1.1	1.1	10.0	0.014560	3.7	3.5
15.0	0.008154	0.3	0.3	15.0	0.012304	4.3	4.1
20.0	0.007325	0.5	0.5	20.0	0.010421	2.8	2.7
25.0	0.006576	1.5	1.5	25.0	0.008908	0.3	0.3
30.0	0.005913	3.2	3.3	30.0	0.007721	2.3	2.3
40.0	0.004837	7.2	7.8	35.0	0.006806	4.3	4.5
50.0	0.004050	11.0	12.3	40.0	0.006110	5.5	5.8
$n = 0.8$				$n = 0.7$			
Re	Fitted λ_{oc}	Percent Error λ_{oc}	Percent Error ε	Re	Fitted λ_{oc}	Percent Error λ_{oc}	Percent Error ε
0.10	0.034992	0.0	0.0	0.10	0.063218	0.1	0.1
1.00	0.033960	0.7	0.7	1.00	0.059706	0.4	0.4
2.00	0.032554	0.0	0.0	2.00	0.055116	2.5	2.4
3.00	0.031058	1.6	1.6	3.00	0.050495	5.7	5.4
4.00	0.029543	3.4	3.2	4.00	0.046084	8.3	7.6
5.00	0.028045	5.0	4.7	5.00	0.041994	9.9	9.0
10.0	0.021373	8.5	7.8	7.50	0.033402	10.7	9.7
15.0	0.016453	6.5	6.1	10.0	0.027065	10.0	9.0
20.0	0.013111	3.8	3.7	12.5	0.022586	9.5	8.6
25.0	0.010940	3.2	3.1	15.0	0.019502	10.3	9.2
$n = 0.6$				$n = 0.5$			
Re	Fitted λ_{oc}	Percent Error λ_{oc}	Percent Error ε	Re	Fitted λ_{oc}	Percent Error λ_{oc}	Percent Error ε
0.10	0.113970	0.8	0.8	0.10	0.204282	2.7	2.7
1.00	0.101382	0.4	0.4	0.50	0.183977	2.9	3.0
2.00	0.086434	5.6	5.2	1.00	0.157365	0.1	0.1
3.00	0.073096	8.7	8.0	1.50	0.133496	2.3	2.2
4.00	0.061952	10.0	9.1	2.00	0.113441	3.6	3.4
5.00	0.052981	10.6	9.6	2.50	0.097198	4.4	4.1
6.00	0.045934	10.7	9.6	3.00	0.084362	5.2	4.9
7.00	0.040495	11.1	9.9				

$n = 0.4$			
Re	Fitted λ_{oc}	Percent Error λ_{oc}	Percent Error ε
0.10	0.359408	5.3	5.5
0.50	0.274849	7.3	7.8
1.00	0.191684	9.0	9.7
1.50	0.140362	10.9	11.9

Table 5.7: Triangular 15.0-15.0 Fitted Curve Outer Cavity Shape Factor Data Summary

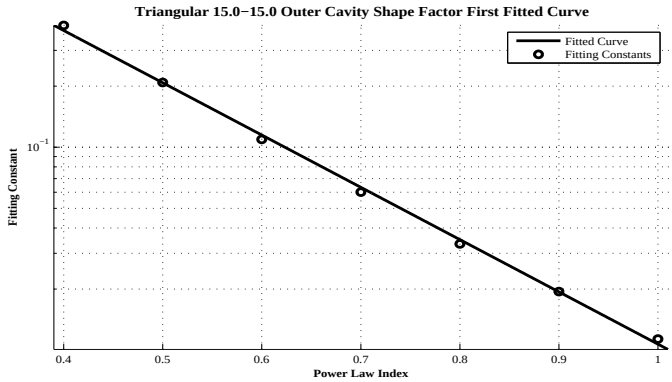

Figure 5.10: Triangular 15.0-15.0 Outer Cavity Shape Factor First Fitted Curve Plotted Results

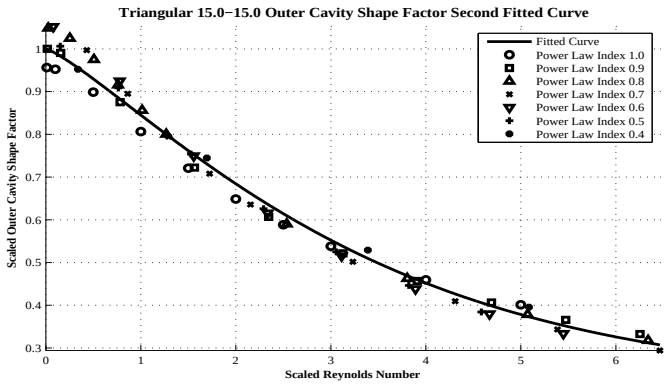

Figure 5.11: Triangular 15.0-15.0 Outer Cavity Shape Factor Second Fitted Curve Plotted Results

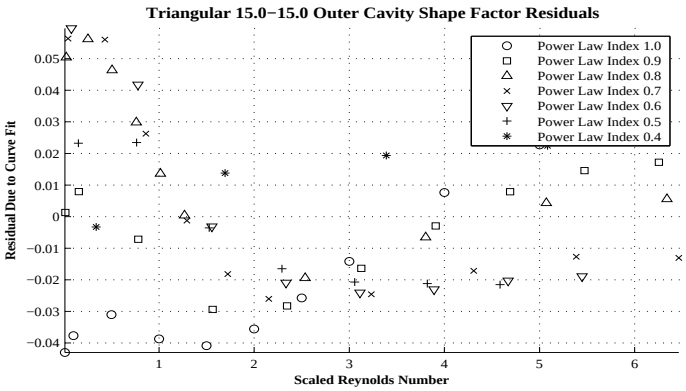

Figure 5.12: Triangular 15.0-15.0 Outer Cavity Shape Factor Second Fitted Curve Plotted Residuals

Outer Cavity Shape Factor

$n = 1.0$		$n = 0.9$		$n = 0.8$		$n = 0.7$	
Re	Fluent λ_{oc}	Re	Fluent λ_{oc}	Re	Fluent λ_{oc}	Re	Fluent λ_{oc}
0.10	0.018338	0.10	0.029181	0.10	0.046613	0.10	0.074755
1.00	0.018192	1.00	0.028717	1.00	0.045106	1.00	0.069838
5.00	0.016249	5.00	0.023454	2.00	0.041925	2.00	0.061034
10.0	0.013490	10.0	0.017851	3.00	0.038371	3.00	0.052886
15.0	0.011381	15.0	0.014280	4.00	0.035029	4.00	0.046213
20.0	0.009822	20.0	0.011891	5.00	0.032066	5.00	0.040840
25.0	0.008641	25.0	0.010186	10.0	0.022104	7.50	0.031186
30.0	0.007721	30.0	0.008911	15.0	0.016617	10.0	0.024285
40.0	0.006390	35.0	0.007986				
50.0	0.005479						

$n = 0.6$		$n = 0.5$		$n = 0.4$	
Re	Fluent λ_{oc}	Re	Fluent λ_{oc}	Re	Fluent λ_{oc}
0.10	0.120400	0.10	0.194688	0.10	0.314947
1.00	0.104742	0.50	0.177486	0.50	0.257179
2.00	0.083365	1.00	0.148216	1.00	0.189868
3.00	0.067378	1.50	0.123150	1.50	0.143009
4.00	0.055605	2.00	0.103376		
5.00	0.046520	2.50	0.087944		
		3.00	0.073496		

Table 5.8: Triangular 30.0-30.0 ANSYS Fluent Outer Cavity Shape Factor Data Summary

Fitting Constants

Rheological and Model Specific		Model Specific	
n	c_1		
1.0	0.019241	c_2	0.018285
0.9	0.029732	c_3	4.740214
0.8	0.046524	c_4	2.246542
0.7	0.072214	c_5	0.000000
0.6	0.117646	c_6	2.920488
0.5	0.193771	c_7	0.439885
0.4	0.330694	c_8	1.254134

Table 5.9: Triangular 30.0-30.0 Curve Fitting Constants Summary

Outer Cavity Shape Factor

$n = 1.0$				$n = 0.9$			
Re	Fitted λ_{oc}	Percent Error λ_{oc}	Percent Error ε	Re	Fitted λ_{oc}	Percent Error λ_{oc}	Percent Error ε
0.10	0.018266	0.4	0.4	0.10	0.029326	0.5	0.5
1.00	0.017955	1.3	1.3	1.00	0.028531	0.6	0.7
5.00	0.015991	1.6	1.6	5.00	0.023775	1.4	1.3
10.0	0.013437	0.4	0.4	10.0	0.018305	2.5	2.5
15.0	0.011219	1.4	1.4	15.0	0.014269	0.1	0.1
20.0	0.009434	3.9	4.1	20.0	0.011565	2.8	2.8
25.0	0.008063	6.7	7.2	25.0	0.009858	3.2	3.3
30.0	0.007044	8.8	9.6	30.0	0.008829	0.9	0.9
40.0	0.005779	9.6	10.6	35.0	0.008828	3.0	2.9
50.0	0.005161	5.8	6.2				

$n = 0.8$				$n = 0.7$			
Re	Fitted λ_{oc}	Percent Error λ_{oc}	Percent Error ε	Re	Fitted λ_{oc}	Percent Error λ_{oc}	Percent Error ε
0.10	0.047060	1.0	0.9	0.10	0.075448	0.9	0.9
1.00	0.044969	0.3	0.3	1.00	0.069757	0.1	0.1
2.00	0.042125	0.5	0.5	2.00	0.062436	2.3	2.2
3.00	0.039178	2.1	2.1	3.00	0.055371	4.7	4.5
4.00	0.036294	3.6	6.2	4.00	0.048982	6.0	5.6
5.00	0.033555	4.6	4.4	5.00	0.043412	6.3	5.9
10.0	0.022940	3.8	3.6	7.50	0.033020	5.9	5.5
15.0	0.017056	2.6	2.6	10.0	0.026728	10.1	9.1

$n = 0.6$				$n = 0.5$			
Re	Fitted λ_{oc}	Percent Error λ_{oc}	Percent Error ε	Re	Fitted λ_{oc}	Percent Error λ_{oc}	Percent Error ε
0.10	0.120725	0.3	0.3	0.10	0.192275	1.2	1.2
1.00	0.104685	0.1	0.1	0.50	0.172237	3.0	3.0
2.00	0.086198	3.4	3.3	1.00	0.145911	1.6	1.6
3.00	0.070701	4.9	4.7	1.50	0.122714	0.4	0.4
4.00	0.058726	5.6	5.3	2.00	0.103765	0.4	0.4
5.00	0.049914	7.3	6.7	2.50	0.088959	1.2	1.1
				3.00	0.077749	5.8	5.4

$n = 0.4$			
Re	Fitted λ_{oc}	Percent Error λ_{oc}	Percent Error ε
0.10	0.302333	4.0	4.1
0.50	0.238107	7.4	7.9
1.00	0.171739	9.6	10.3
1.50	0.129322	9.6	10.3

Table 5.10: Triangular 30.0-30.0 Fitted Curve Outer Cavity Shape Factor Data Summary

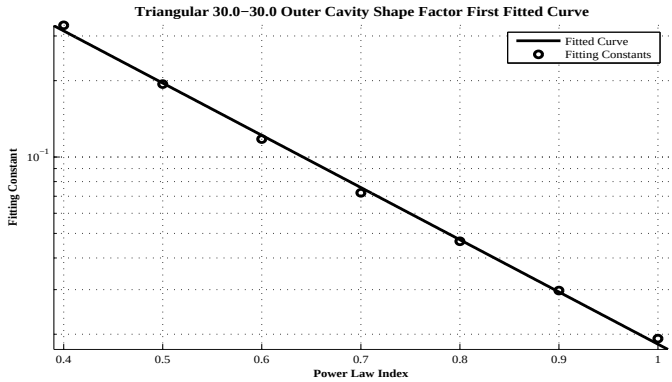

Figure 5.13: Triangular 30.0-30.0 Outer Cavity Shape Factor First Fitted Curve Plotted Results

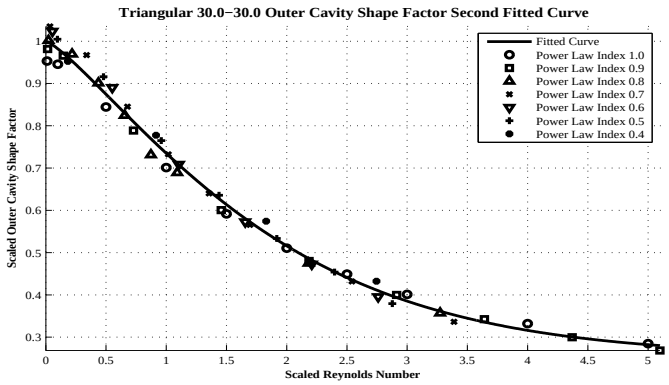

Figure 5.14: Triangular 30.0-30.0 Outer Cavity Shape Factor Second Fitted Curve Plotted Results

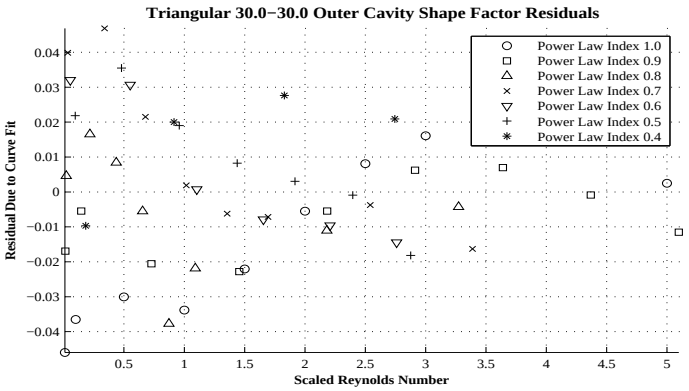

Figure 5.15: Triangular 30.0-30.0 Outer Cavity Shape Factor Second Fitted Curve Plotted Residuals

Outer Cavity Shape Factor

$n = 1.0$		$n = 0.9$		$n = 0.8$		$n = 0.7$	
Re	Fluent λ_{oc}	Re	Fluent λ_{oc}	Re	Fluent λ_{oc}	Re	Fluent λ_{oc}
0.10	0.024230	0.10	0.035314	0.10	0.051674	0.10	0.075896
1.00	0.023949	1.00	0.034563	1.00	0.049632	1.00	0.070395
5.00	0.020403	5.00	0.026725	2.00	0.045463	2.00	0.060925
10.0	0.016101	10.0	0.019560	3.00	0.041031	3.00	0.052437
15.0	0.013209	15.0	0.015399	4.00	0.037039	4.00	0.045621
20.0	0.011232	20.0	0.012754	5.00	0.033612	5.00	0.040194
25.0	0.009811	25.0	0.010954	10.0	0.022670	7.50	0.030561
30.0	0.008747	30.0	0.009632	15.0	0.016935	10.0	0.024008
40.0	0.007272						
50.0	0.006312						

$n = 0.6$		$n = 0.5$		$n = 0.4$	
Re	Fluent λ_{oc}	Re	Fluent λ_{oc}	Re	Fluent λ_{oc}
0.10	0.111941	0.10	0.165749	0.10	0.245383
1.00	0.097493	0.50	0.151958	0.50	0.209366
2.00	0.078042	1.00	0.129482	1.00	0.161679
3.00	0.063363	1.50	0.109794	1.50	0.125960
4.00	0.052603	2.00	0.093530	2.00	0.099497
5.00	0.044218	2.50	0.079805	2.50	0.078485
6.00	0.037457	3.00	0.069056		
7.00	0.033791	4.00	0.051835		

Table 5.11: Triangular 30.0-60.0 ANSYS Fluent Outer Cavity Shape Factor Data Summary

Fitting Constants

Rheological and Model Specific		Model Specific	
n	c_1		
1.0	0.024555	c_2	0.023628
0.9	0.035181	c_3	3.917966
0.8	0.051429	c_4	1.890189
0.7	0.074584	c_5	0.000000
0.6	0.109716	c_6	3.119995
0.5	0.161475	c_7	0.525238
0.4	0.257652	c_8	1.246416

Table 5.12: Triangular 30.0-60.0 Curve Fitting Constants Summary

Outer Cavity Shape Factor

$n = 1.0$				$n = 0.9$			
Re	Fitted λ_{oc}	Percent Error		Re	Fitted λ_{oc}	Percent Error	
		λ_{oc}	ε			λ_{oc}	ε
0.10	0.023598	2.6	2.7	0.10	0.034893	1.2	1.2
1.00	0.023102	3.5	3.7	1.00	0.033784	2.3	2.3
5.00	0.020070	1.6	1.7	5.00	0.027366	2.4	2.3
10.0	0.016308	1.3	1.3	10.0	0.020352	4.1	3.9
15.0	0.013213	0.0	0.0	15.0	0.015476	0.5	0.5
20.0	0.010863	3.3	3.4	20.0	0.012407	2.7	2.8
25.0	0.009163	6.6	7.1	25.0	0.010591	3.3	3.4
30.0	0.007975	8.8	9.7	30.0	0.009564	0.7	0.7
40.0	0.006629	8.8	9.7				
50.0	0.006050	4.2	4.3				

$n = 0.8$				$n = 0.7$			
Re	Fitted λ_{oc}	Percent Error		Re	Fitted λ_{oc}	Percent Error	
		λ_{oc}	ε			λ_{oc}	ε
0.10	0.051571	0.2	0.2	0.10	0.076158	0.3	0.3
1.00	0.049028	1.2	1.2	1.00	0.070164	0.3	0.3
2.00	0.045622	0.4	0.3	2.00	0.062538	2.6	2.6
3.00	0.042134	2.7	2.6	3.00	0.055227	5.3	5.0
4.00	0.038758	4.6	4.4	4.00	0.048648	6.6	6.2
5.00	0.035587	5.9	5.5	5.00	0.042935	6.8	6.4
10.0	0.023648	4.3	4.1	7.50	0.032326	5.8	5.4
15.0	0.017362	2.5	2.5	10.0	0.025932	8.0	7.4

$n = 0.6$				$n = 0.5$			
Re	Fitted λ_{oc}	Percent Error		Re	Fitted λ_{oc}	Percent Error	
		λ_{oc}	ε			λ_{oc}	ε
0.10	0.112285	0.3	0.3	0.10	0.164959	0.5	0.5
1.00	0.097717	0.2	0.2	0.50	0.149393	1.7	1.7
2.00	0.080867	3.6	6.5	1.00	0.128603	0.7	0.7
3.00	0.066555	5.0	4.8	1.50	0.109746	0.0	0.0
4.00	0.055300	5.1	4.8	2.00	0.093792	0.3	0.3
5.00	0.046844	5.9	5.6	2.50	0.080825	1.3	1.2
6.00	0.040693	8.6	7.9	3.00	0.070577	2.2	2.1
7.00	0.036330	7.5	6.9	4.00	0.056624	9.2	8.3

$n = 0.4$			
Re	Fitted λ_{oc}	Percent Error	
		λ_{oc}	ε
0.10	0.240193	2.1	2.1
0.50	0.197428	5.7	6.0
1.00	0.149418	7.6	8.0
1.50	0.114833	8.8	9.4
2.00	0.092183	7.4	7.7
2.50	0.078200	0.4	0.3

Table 5.13: Triangular 30.0-60.0 Fitted Curve Outer Cavity Shape Factor Data Summary

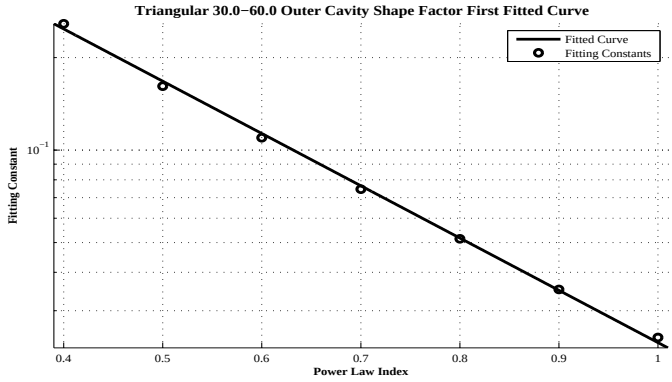

Figure 5.16: Triangular 30.0-60.0 Outer Cavity Shape Factor First Fitted Curve Plotted Results

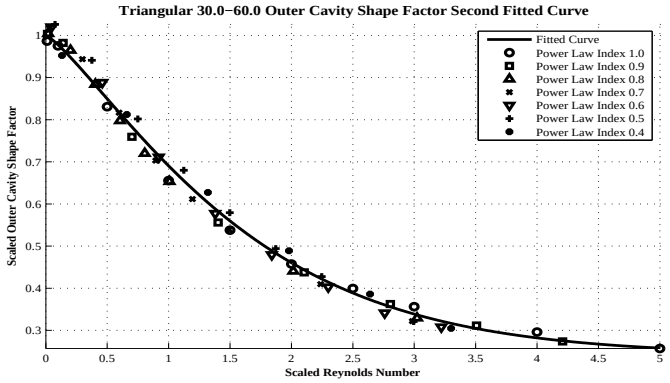

Figure 5.17: Triangular 30.0-60.0 Outer Cavity Shape Factor Second Fitted Curve Plotted Results

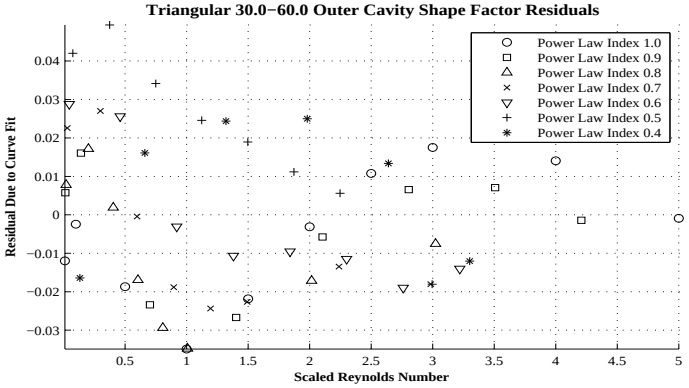

Figure 5.18: Triangular 30.0-60.0 Outer Cavity Shape Factor Second Fitted Curve Plotted Residuals

For each of the cases considered in the computation of the outer cavity shape factor, the triangular fifteen-fifteen, thirty-thirty, and thirty-sixty degree expansion and contraction angles respectively, cognitive results for the outer cavity shape factor were obtained for shear thinning fluids of generalized Newtonian rheology, ranging in power law index as low as $n = 0.4$ to the Newtonian case of $n = 1.0$, with numerous flow conditions. Owing to the velocity distribution of shear thinning fluids with rapidly changing characteristics at the wall surface, difficulty in obtaining a convergent solution of the perturbed equations of the outer cavity approximate model prevent the computation of the outer cavity shape factor beyond a power law index of $n = 0.4$. The numerically obtained data in the tabulated results (Tables 5.5, 5.7, 5.8, 5.10, 5.11 and 5.13) as well as the presentation of the fitted curve plots (Figs. 5.10, 5.11, 5.13, 5.14, 5.16 and 5.17) illustrate three key features of the outer cavity shape factor as inputs to the approximate die design models. First, a relative decrease of the outer cavity shape factor is demonstrated with a corresponding increase in the Reynolds number for a given fluid rheology. As expected, the orientation and relative fluid inertia of the primary flow (Fig. 1.2) exiting the inner slot of a dual cavity die impedes the widthwise redistribution of flow along the axis of the outer cavity, thus diminishing the ability of the outer cavity to improve flow uniformity. Second, a relative increase of the outer cavity shape factor is demonstrated with a corresponding decrease of the power law index for a given flow condition. However, it is important to note that although shear thinning behavior promotes the widthwise redistribution of flow along the width of a dual cavity coating die (Fig. 1.1) by reducing the resistance to flow along the outer cavity, this effect is amplified in the cross section of the outer slot, thus hindering the overall performance of the outer cavity. Third, a relative increase of the outer cavity shape factor is demonstrated with a corresponding increase of the expansion and contraction angles, and thus an enlarged cross sectional area, for a given flow condition and fluid rheology. Similar to the function of the inner cavity, the presence of these disparate resistances to flow in the outer cavity geometry can effectively reduce nonuniformities in the flow per unit cavity width exiting the inner slot due to pressure variations in the inner cavity. These observations of the numerically obtained outer cavity shape factor are consistent with the fundamental physics observed in the outer cavity of a dual cavity coating die, providing confidence as a necessary input to the outer cavity approximate die design models.

While a particularly convenient representation of the outer cavity shape factor characterizes the numerically determined data through a bipartite series of fitted curves (Figs. 5.10, 5.11, 5.13, 5.14, 5.16 and 5.17), it is important to consider the error incurred through such an approximation. Each of the fitted curves is exclusively applicable to the specific cross sectional design from which the outer cavity shape factor data was utilized to gener-

ate the appropriate fitting constants, and thus not valid outside of the range provided in the corresponding figures. It appears that the largest scatter in the numerically obtained outer cavity shape factor data from the plotted residual curves provided (Figs. 5.12, 5.15 and 5.18) occurs in the region of negligible Reynolds number, however due to the relative magnitude of the data, the largest incurred error occurs in the region of high Reynolds number, yet diminishes with an enlarged cross sectional area. Therefore, the determination of the outer cavity shape factor through the approximation of the provided fitted curves results in a maximum incurred error of 11.1, 10.0, and 9.2 percent for the respective triangular fifteen-fifteen, thirty-thirty, and thirty-sixty degree expansion and contraction angle designs considered. This deviation in the determination of the outer cavity shape factor corresponds to a maximum incurred error of 12.3, 10.6, and 9.7 percent for the ratio of the peak to peak variation in the flow per unit cavity width entering the outer slot and exiting the inner slot. The minimal incurred error associated with the determination of the outer cavity shape factor through the approximation of the provided fitted curves is sufficient and consistent with the intended nature of the alternative approximate modeling approach.

5.4 Shape Factor Estimation

The outer cavity shape factor for the triangular fifteen-fifteen, thirty-thirty, and thirty-sixty degree expansion and contraction angles has also been determined through an approximate method, as reported by Weinstein (2010). Here, a velocity distribution is assumed in the two dimensional cross section of the outer cavity, which maintains the fully developed form of shear thinning flow between parallel plates along the length of the outer cavity while varying in magnitude with a corresponding increase or decrease in the respective expansion or contraction of the geometry. With the imposed definition of the cross sectional velocity distribution, the perturbed equations of the outer cavity approximate model may then be integrated across the height of the cross section, resulting in a linear, nonconstant coefficient ordinary differential equation for the solution of the axial component of velocity. The technique applied is similar to the Von Kármán-Pohlhausen approximation to the boundary layer problem (Schlichting, 1979); however, rather than an investigation of the wall shear stress distribution, the integral approach provides the net resistance perpendicular to the primary orientation of flow in the two dimensional cross section and ultimately an approximation of the outer cavity shape factor.

Outer Cavity Shape Factor Estimation

$n = 1.0$		$n = 0.8$		$n = 0.6$		$n = 0.4$	
Re	Approximate λ_{oc}	Re	Approximate λ_{oc}	Re	Approximate λ_{oc}	Re	Approximate λ_{oc}
0.00	0.010499	0.00	0.035150	0.00	0.119488	0.00	0.428013
5.00	0.010152	2.91	0.032352	1.70	0.097487	0.99	0.260499
10.0	0.009435	5.82	0.027793	3.39	0.073094	1.98	0.169594
15.0	0.008670	8.74	0.023846	5.09	0.057316	2.96	0.125546
20.0	0.007961	11.7	0.020717	6.78	0.046846	3.95	0.099943
25.0	0.007332	14.6	0.018253	8.48	0.039492	4.94	0.083271
30.0	0.006781	17.5	0.016283	10.2	0.034070	5.93	0.071560
35.0	0.006298	20.4	0.014683	11.9	0.029919	6.91	0.062887
40.0	0.005875	23.3	0.013361	13.4	0.026639	7.90	0.056214
45.0	0.005502	26.2	0.012253	15.3	0.023986	8.89	0.050913
50.0	0.005171	29.1	0.011311	17.0	0.021796	9.88	0.046608
55.0	0.004877	32.0	0.010502	18.7	0.019958	10.9	0.043039
60.0	0.004613	34.9	0.009800	20.4	0.018395	11.9	0.040033
65.0	0.004375	37.9	0.009184	22.1	0.017048	12.8	0.037467
70.0	0.004161	40.8	0.008641	23.7	0.015876	13.8	0.035250
75.0	0.003966	43.7	0.008158	25.4	0.014848	14.8	0.033317
80.0	0.003788	46.6	0.007726	27.1	0.013937	15.8	0.031615
85.0	0.003625	49.5	0.007337	28.8	0.013126	16.8	0.030106
90.0	0.003475	52.4	0.006985	30.5	0.012398	17.8	0.028759
95.0	0.003338	55.3	0.006665	32.2	0.011742	18.8	0.027549
100.0	0.003210	58.2	0.006373	33.9	0.011147	19.8	0.026455

Table 5.14: Triangular 15.0-15.0 Approximated Outer Cavity Shape Factor Data Summary

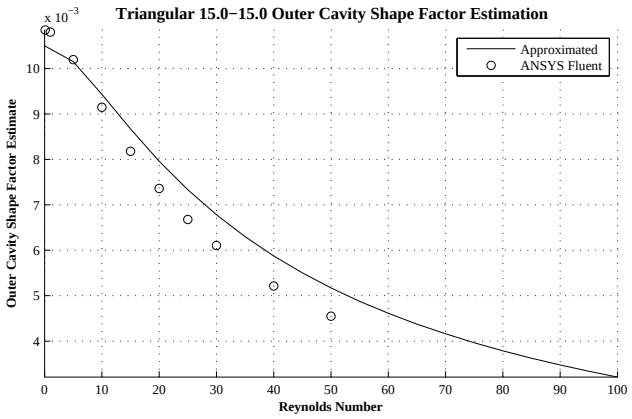

Figure 5.19: Triangular 15.0-15.0 Newtonian Approximated Outer Cavity Shape Factor Plotted Results

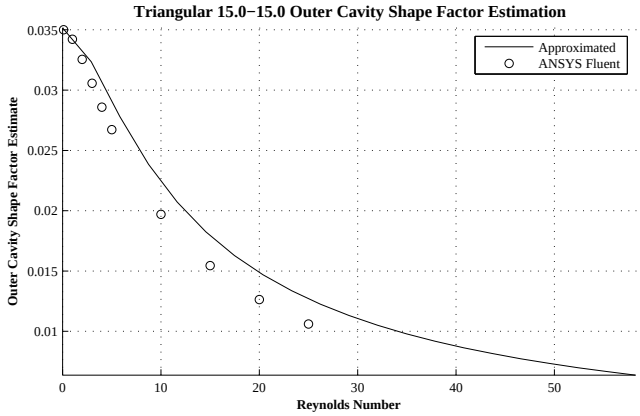

(a) $n = 0.8$

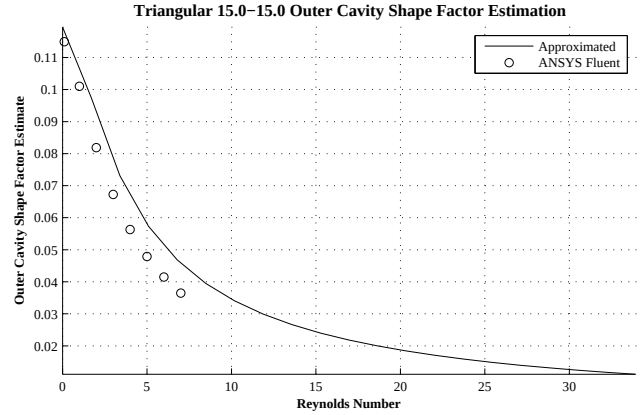

(b) $n = 0.6$

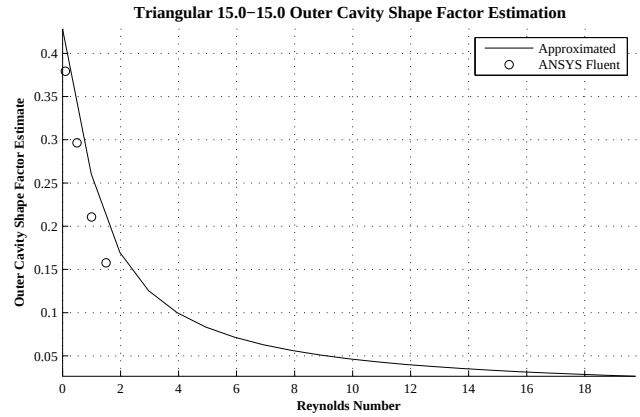

(c) $n = 0.4$

Figure 5.20: Triangular 15.0-15.0 Non-Newtonian Approximated Outer Cavity Shape Factor Plotted Results

Outer Cavity Shape Factor Estimation

$n = 1.0$		$n = 0.8$		$n = 0.6$		$n = 0.4$	
Re	Approximate λ_{oc}	Re	Approximate λ_{oc}	Re	Approximate λ_{oc}	Re	Approximate λ_{oc}
0.00	0.018916	0.00	0.047104	0.00	0.118322	0.00	0.325944
2.00	0.018665	1.36	0.045753	0.46	0.116229	0.31	0.304478
4.00	0.018006	2.72	0.042559	0.92	0.110876	0.63	0.266109
6.00	0.017125	4.07	0.038839	1.38	0.103895	0.94	0.230531
8.00	0.016172	5.43	0.035293	1.84	0.096507	1.25	0.201473
10.0	0.015234	6.79	0.032138	2.31	0.089389	1.57	0.178212
12.0	0.014248	8.15	0.029399	2.77	0.082830	1.88	0.159471
14.0	0.013529	9.51	0.027033	3.23	0.076913	2.19	0.144161
16.0	0.012779	10.9	0.024989	3.69	0.071629	2.50	0.131473
18.0	0.012096	12.2	0.023212	4.15	0.066921	2.82	0.120814
20.0	0.011473	13.6	0.021658	4.61	0.062726	3.13	0.111742
24.0	0.010388	16.3	0.019081	5.53	0.055620	3.44	0.103939
28.0	0.009479	19.0	0.017037	6.45	0.049875	3.76	0.097157
32.0	0.008709	21.7	0.015280	7.38	0.045153	4.07	0.091213
36.0	0.008052	24.4	0.014013	8.30	0.041219	4.38	0.085964
40.0	0.007485	27.2	0.012866	9.22	0.037894	4.70	0.081291
46.0	0.006767	29.9	0.011891	10.1	0.035052	5.01	0.077110
52.0	0.006172	32.6	0.011053	11.1	0.032595	5.32	0.073347
58.0	0.005673	35.3	0.010324	12.0	0.030454	5.64	0.069942
64.0	0.005248	40.7	0.009119	12.9	0.028569	5.95	0.066843
70.0	0.004881	46.2	0.008165	13.8	0.026901	6.26	0.064016
78.0	0.004465	51.6	0.007391	15.7	0.024075	6.57	0.061426
86.0	0.004114	57.0	0.006751	17.5	0.021776	7.20	0.056842
94.0	0.003814	62.5	0.006212	19.4	0.019869	7.83	0.052913
100.0	0.003616	67.9	0.005753	21.2	0.018263	8.45	0.049511

Table 5.15: Triangular 30.0-30.0 Approximated Outer Cavity Shape Factor Data Summary

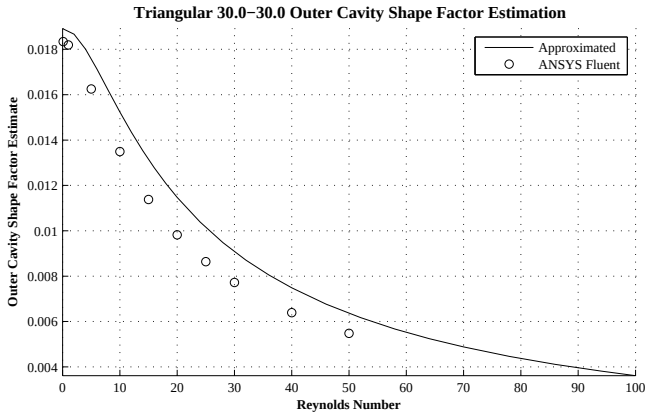

Figure 5.21: Triangular 30.0-30.0 Newtonian Approximated Outer Cavity Shape Factor Plotted Results

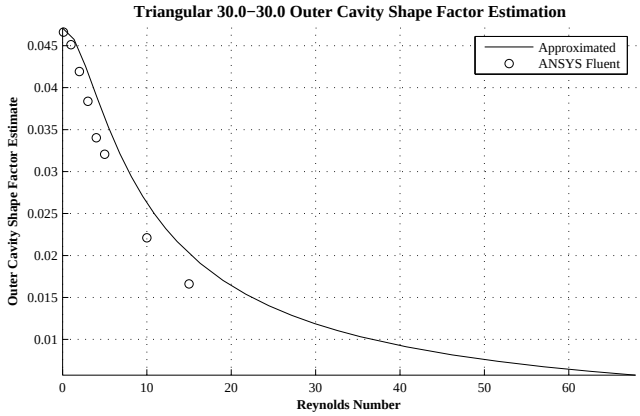

(a) $n = 0.8$

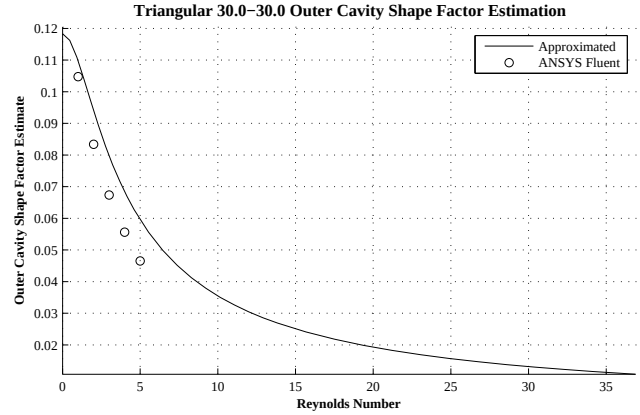

(b) $n = 0.6$

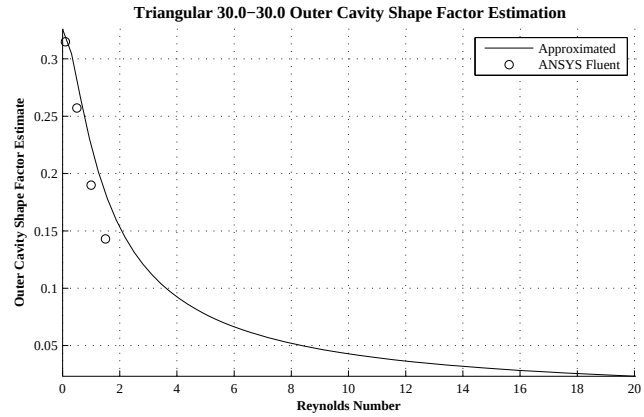

(c) $n = 0.4$

Figure 5.22: Triangular 30.0-30.0 Non-Newtonian Approximated Outer Cavity Shape Factor Plotted Results

Outer Cavity Shape Factor Estimation

$n = 1.0$		$n = 0.8$		$n = 0.6$		$n = 0.4$	
Re	Approximate λ_{oc}	Re	Approximate λ_{oc}	Re	Approximate λ_{oc}	Re	Approximate λ_{oc}
0.00	0.022060	0.00	0.043975	0.00	0.099547	0.00	0.260216
2.00	0.021785	1.47	0.045704	0.54	0.098003	0.40	0.238081
4.00	0.020916	2.95	0.042410	1.08	0.093978	0.80	0.207178
6.00	0.019727	4.42	0.038500	1.63	0.088594	1.20	0.179348
8.00	0.018451	5.89	0.034772	2.17	0.082748	1.60	0.156760
10.0	0.017215	7.36	0.031480	2.71	0.076979	2.00	0.138708
12.0	0.016070	8.84	0.028646	3.25	0.071559	2.40	0.124162
14.0	0.015032	10.3	0.026221	3.80	0.066596	2.79	0.112273
16.0	0.014098	11.8	0.024142	4.34	0.062110	3.19	0.102416
18.0	0.013259	13.3	0.022346	4.88	0.058080	3.59	0.094126
20.0	0.012506	14.7	0.020789	5.42	0.054463	3.99	0.087071
24.0	0.011215	17.7	0.018223	6.51	0.048300	4.79	0.075715
28.0	0.010154	20.6	0.016207	7.59	0.043287	5.59	0.066992
32.0	0.009271	23.6	0.014585	8.68	0.039158	6.39	0.060087
36.0	0.008526	26.5	0.013255	9.76	0.035713	7.19	0.054492
40.0	0.007890	29.5	0.012144	10.8	0.032801	7.99	0.049867
46.0	0.007093	30.9	0.011655	11.9	0.030312	8.78	0.045980
52.0	0.006441	32.4	0.011204	13.0	0.028163	9.58	0.042671
58.0	0.005898	33.9	0.010786	14.1	0.026289	10.8	0.038534
64.0	0.005439	35.4	0.010398	15.2	0.024642	12.0	0.035148
70.0	0.005046	39.8	0.009383	16.3	0.023185	13.2	0.032330
78.0	0.004602	44.2	0.008548	17.9	0.021288	14.4	0.029944
86.0	0.004229	48.6	0.007849	19.5	0.019670	15.6	0.027902
94.0	0.003912	53.0	0.007256	21.2	0.018275	16.8	0.026132
100.0	0.003704	58.9	0.006591	22.8	0.017060	18.4	0.024109

Table 5.16: Triangular 30.0-60.0 Approximated Outer Cavity Shape Factor Data Summary

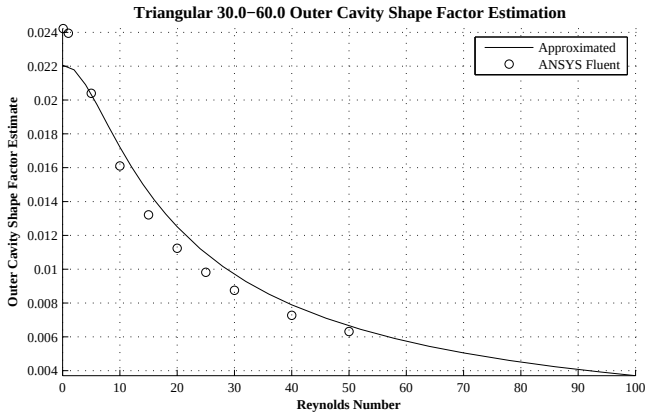

Figure 5.23: Triangular 30.0-60.0 Newtonian Approximated Outer Cavity Shape Factor Plotted Results

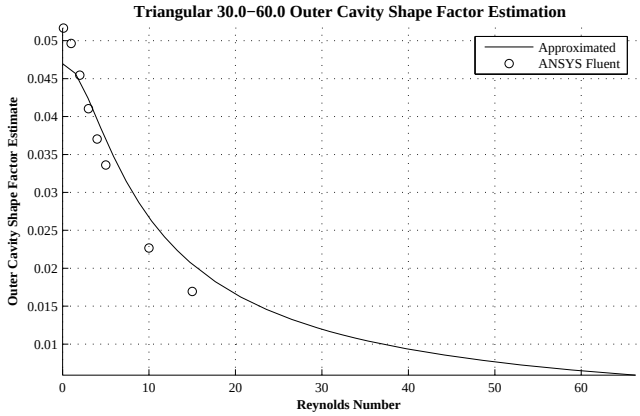

(a) $n = 0.8$

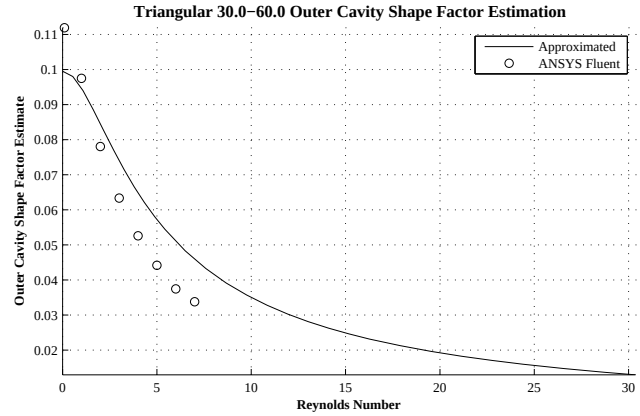

(b) $n = 0.6$

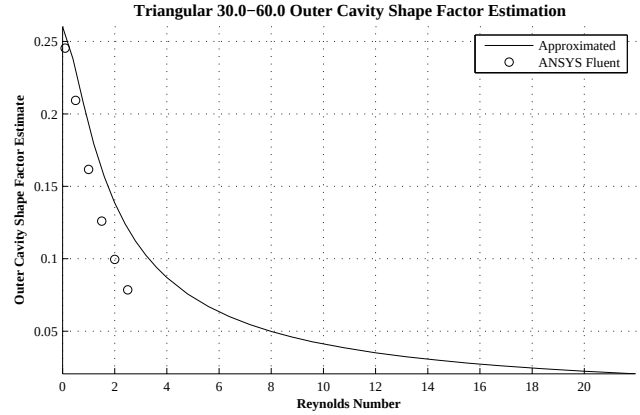

(c) $n = 0.4$

Figure 5.24: Triangular 30.0-60.0 Non-Newtonian Approximated Outer Cavity Shape Factor Plotted Results

There are two important features to note in the comparison of the approximated outer cavity shape factor with those which are numerically obtained through the commercially available ANSYS Fluent software package, evident in the presentation of the plotted results (Figs. 5.19 to 5.24). First, an increased error in the determination of the outer cavity shape factor is incurred through the approximate approach with a corresponding increase in the flow condition Reynolds number. As expected, fluid inertia inhibits the development of unidirectional flow, and thus error is induced into the approximation of the outer cavity shape factor due to the assumption of the locally fully developed form of the velocity distribution in the cross section of the outer cavity. Second, an approximation of the outer cavity shape factor for a given cross sectional design and fluid rheology may be obtained for flow conditions of Reynolds numbers which are beyond the solution capabilities of the method utilizing the commercially available ANSYS Fluent software package. Owing to the characteristics of shear thinning fluids with a power law dependence of viscosity on shear rate, a fine resolution of nodes perpendicular to the direction of flow in the two dimensional cross section of the outer cavity is required to accurately represent the rapidly changing velocity profile at the wall surface. It is important to note that this approximation method provides results for the outer cavity shape factor in a minimal fraction of the time required by the numerical computation of the perturbed set of three dimensional governing momentum equations from the derivation of the outer cavity approximate model through commercially available software. Therefore, an improvement to the assumed form of the velocity distribution in the cross section of the outer cavity, or perhaps one which is adaptive with regards to the corresponding Reynolds number of the given flow condition, would provide an effective and efficient process for the estimation of the outer cavity shape factor as input to the approximate die design model. Velocity profiles extracted from the solution of the base flow in the numerical computation of the outer cavity shape factor could provide suggestion for a more appropriate form of the assumed velocity distribution; however, this is beyond the objectives of the current work yet offers an area for future research.

5.5 Summary

The outer cavity shape factor incorporates the specific cross sectional shape of the domain into the pressure drop flow relationship, and the computation of this additional parameter requires the knowledge of the three dimensional flow field within the outer cavity domain. A method for obtaining the outer cavity shape factor, utilizing commercially available software, has been established to correlate the perturbed equations of the outer cavity approximate model with those implemented within the ANSYS Fluent package. The design of the outer

cavity requires a more complex shape than that of the inner cavity to prevent regions of stagnation and recirculation, thus three specific triangular outer cavity designs are considered in the computation of the outer cavity shape factor. For each of the cases considered in the computation of the outer cavity shape factor, the triangular fifteen-fifteen, thirty-thirty, and thirty-sixty degree expansion and contraction angles respectively, cognitive results for the outer cavity shape factor were obtained for shear thinning fluids of generalized Newtonian rheology, ranging in power law index as low as $n = 0.4$ to the Newtonian case of $n = 1.0$, with numerous flow conditions. A particularly convenient representation of the outer cavity shape factor for a given cross sectional design characterizes the numerically determined data over the entire range of fluid rheologies and flow conditions considered through a bipartite series of fitted curves. In this way, the outer cavity shape factor for a given cross sectional design may be extracted for any given fluid rheology and flow condition, within the limits of the plotted data, as input to the outer cavity approximate die design model.

Chapter 6

Validation of the Outer Cavity Approximate Model

The derivation of the outer cavity approximate model (Chapter 3) provides an expression for the desired relationship between the axial pressure gradient and volumetric flow along the outer cavity axis, the solution of which (Chapter 4) yields the widthwise flow distribution, as well as the peak to peak variation of primary interest, of the flow per unit cavity width exiting the outer slot. There, the complete set of three dimensional equations (Eqs. 3.0.8a to 3.0.8e) governing flow in the outer cavity are averaged across the cavity cross section, and although the precise knowledge and details of the flow and pressure fields at each node point specified within the cavity and slot geometry are lost, average flow properties such as cavity pressure, widthwise volumetric flow through the cavity, and volumetric flow per width in the slot are obtained in exchange. The outer cavity approximate model is an essential tool for the design of dual cavity coating dies, which allows for numerous flow conditions and geometric parameters to be tested such that reasonable designs for a suitable range of widthwise flow uniformity may be determined efficiently and effectively. However, the shortcoming of the approximate modeling approach is that the governing equations are approximations of the complete three dimensional set, and thus, although quantifiable, there is some incurred error in their use. For this reason, the validity of the theoretical one dimensional approximate die design model and the pressure drop flow relationship governing flow in the outer cavity domain must be examined.

Although a complete three dimensional analysis and ultimate experimental validation are necessary to define the applicability and accuracy of the theoretical approximate modeling approach, the assumptions utilized in the derivation of the outer cavity approximate model (Chapter 3) may be verified to further provide confidence. Three key assumptions are employed in the derivation of the outer cavity approximate die design model which state

that the magnitude of the perturbation in the flow per unit cavity width exiting the inner slot is of order much less than unity, the width of the outer cavity greatly exceeds the length of the outer cavity, and the back pressure due to the outer slot geometry dominates pressure variations within the outer cavity cross section. While the majority of these assumptions may be qualitatively assessed, the limit identifying when these assumptions are no longer valid in the context of the outer cavity approximate model may not be defined without the numerical simulation of the complete three dimensional set of governing equations or experimental verification. However, the validity of the assumption which expresses the dominant back pressure of the outer slot due to the typical aspect ratios demonstrated in the geometry of dual cavity coating die design can be investigated through the computation of the flow field in the two dimensional cross section of the outer cavity domain.

The experimental validation of current theoretical approximate die design models through the verification of lateral flow uniformity is difficult, owing to the fact that the coating die must be built with the proper dimensional aspect ratios and precisely machined, making phenomena occurring within the individual cavities difficult to measure. Three dimensional computational solutions are numerically intensive, often requiring long computational times to accurately simulate a single die flow condition with no guarantee a solution will converge, and for this reason it is difficult to optimize coating die design solely through the use of full numerical computation. Much of the published three dimensional numerical simulation approaches have focused on the effects of fluid inertia and rheological properties on the regions of stagnation and vortex formation within specific inlet and outer cavity geometries of the coating die; however, general three dimensional finite element codes have also been developed for the purpose of widthwise flow distribution analysis (Chapter 2). Computational Fluid Dynamics offers valuable information to the internal flow details, yet such analyses are difficult due to disparate length scales, and to date an adequate analysis of single and dual cavity coating die designs has been lacking while the mesh generation for the numerical computations cited has been coarse.

6.1 Two Dimensional Validation

Due to the typical aspect ratios demonstrated in the geometry of dual cavity coating die design (Fig. 3.1), as the ratio of the length of the outer slot to the height of the outer slot greatly exceeds the ratio of the length of the outer cavity to the height of the outer cavity, it is anticipated that the back pressure of the outer slot greatly exceeds pressure variations in the outer cavity cross section (Chapter 3). Therefore, in the derivation of the outer cavity approximate model, the pressure drop along the length of the outer slot determines the

pressure level in the cross section of the outer cavity, and thus the pressure distribution in the outer cavity varies axially along the width of the coating die. It is important to note that the absolute pressure in the outer cavity does not influence the flow field, rather it is the pressure gradient along the width of the outer cavity which drives the axial flow responsible for damping nonuniformities in the flow per unit cavity width exiting the outer slot.

In the derivation of the outer cavity approximate model (Chapter 3), a quasi two dimensional flow field is assumed as the base flow in the cross section of the outer cavity, where the components of the flow field scale with a respective increase or decrease in the local flow per unit cavity width entering the outer slot. From the correlation of the analogous ANSYS Fluent momentum and energy equations (Chapter 5), the spatial coordinates, velocity components, and pressure in the base flow of the outer cavity two dimensional cross section scale such that the dimensional forms of the ANSYS Fluent model are numerically equivalent to the dimensionless forms of the derivation of the outer cavity approximate model. Therefore, the validation of the anticipated dominant back pressure of the outer slot directly corresponds to the simulation of the two dimensional base flow in the computation of the outer cavity shape factor and may be investigated in the two dimensional cross section of the outer cavity.

A method for obtaining the outer cavity shape factor utilizing commercially available software as a general numerical code for the solution of nonlinear partial differential equations has been established to correlate the perturbed equations of the approximate model to those implemented within ANSYS Fluent (Chapter 5). In the computation of the outer cavity shape factor, the two dimensional flow field in the outer cavity cross section, the base flow, is determined through the traditional methods of the flow field solver, while the final component of the flow field is determined indirectly through the convective heat transfer analogy and the energy equation. Validation of the dominant back pressure of the outer slot, anticipated to greatly exceed pressure variations in the cross section of the outer cavity, directly corresponds to the simulation of the two dimensional base flow in the computation of the outer cavity shape factor. Therefore, with the exception of noted revisions, identical considerations in mesh generation as well as the specification of material properties, boundary conditions, and solver models for the computation of the outer cavity shape factor are utilized in the validation of the anticipated dominant back pressure.

The pressure at the exit of the outer slot in a dual cavity coating die design is assumed to be of negligible gauge pressure in a similar fashion to the solution of the single cavity approximate model (Chapter 3), thus the dimensionless form of the perturbed pressure in the outer cavity expresses the anticipated dominant back pressure of the outer slot. Although ANSYS Fluent offers a variety of boundary conditions to specify the details of the flow field

at the outlet of the domain, the pressure outlet boundary condition of ANSYS Fluent is chosen for the validation of the anticipated dominant back pressure to define the negligible static pressure at the respective surface, consistent with the derivation of the outer cavity shape factor.

Pressure velocity coupling of the perturbed set of two dimensional governing continuity and momentum equations (Eqs. 5.1.1a to 5.1.1c) in the cross section of the outer cavity is achieved through the equation for mass flux through the center of each cell face, deriving an additional condition for pressure by reformatting the continuity equation. The ANSYS Fluent commercially available software package provides several pressure velocity coupling algorithms, such as the SIMPLE, SIMPLEC, PISO, coupled, and fractional step method, all of which, with the exception of the coupled scheme, incorporate the predictor corrector approach. Chosen for the validation of the anticipated dominant back pressure, the default SIMPLE algorithm utilizes a relationship between the velocity and pressure corrections, substituting the flux correction equations into the discrete continuity equation to obtain a discrete equation for the pressure correction within each cell, to enforce mass conservation and obtain the pressure field (Fluent User's Guide, 2006).

The design of the outer cavity requires a more complex shape (Fig. 5.3) than that of the inner cavity to prevent regions of stagnation and recirculation due to the orientation and relative fluid inertia of the primary flow exiting the inner slot of a dual cavity coating die. Demanding applications require the film thickness nonuniformity to be as little as one percent across the entire coating surface. Therefore, the triangular outer cavity cross section, which includes the thirty-sixty degree expansion and contraction angles respectively, is considered in the validation of the anticipated dominant back pressure in the derivation of the outer cavity approximate model.

The pressure drop along the length of the outer slot determines the pressure level in the cross section of the outer cavity (Chapter 3), and thus the pressure distribution in the outer cavity varies axially along the width of the coating die due to nonuniformities in the widthwise flow distribution exiting the inner slot. As the ratio of the length of the outer slot to the height of the outer slot greatly exceeds the ratio of the length of the outer cavity to the height of the outer cavity (Fig. 3.1), it is thus anticipated that the back pressure of the outer slot greatly exceeds pressure variations in the outer cavity cross section. For the specific case considered in the validation of the anticipated dominant back pressure, the height of the outer slot is specified to be one percent of the respective length of the outer slot, while the height of the outer cavity is specified to be forty-eight percent of the length of the outer cavity.

Once the solution for the perturbed set of two dimensional continuity and momentum

equations (Eqs. 5.1.1a to 5.1.1c) governing flow in the cross section of the outer cavity is converged, no additional post processing is required to determine the magnitude of pressure variations in the outer cavity cross section relative to the outer cavity pressure statistical mean. From the relationships between the analogous ANSYS Fluent momentum and energy equations (Chapter 5), the spatial coordinates, velocity components, and pressure scale such that the dimensional forms of the ANSYS Fluent model are numerically equivalent to the dimensionless forms of the derivation of the outer cavity approximate model. Therefore, the pressure distribution throughout the outer cavity cross section is extracted directly from the ANSYS Fluent post processor, from which the statistical mean and standard deviation are determined and examined as a ratio of the relative magnitudes.

Model Specific Simulation Parameters	
θ	30.0
ϕ	60.0
H_{is}	0.048
H_{oc}	0.480
H_{os}	0.048
L_{is}	0.096
L_{os}	4.800
M_c	0.0032

Table 6.1: Simulation Parameters Specific to the Triangular 30.0-60.0 Long Slot Cross Section in the Computation of the Outer Cavity Shape Factor

Figure 6.1: Triangular 30.0-60.0 Long Slot Final Mesh

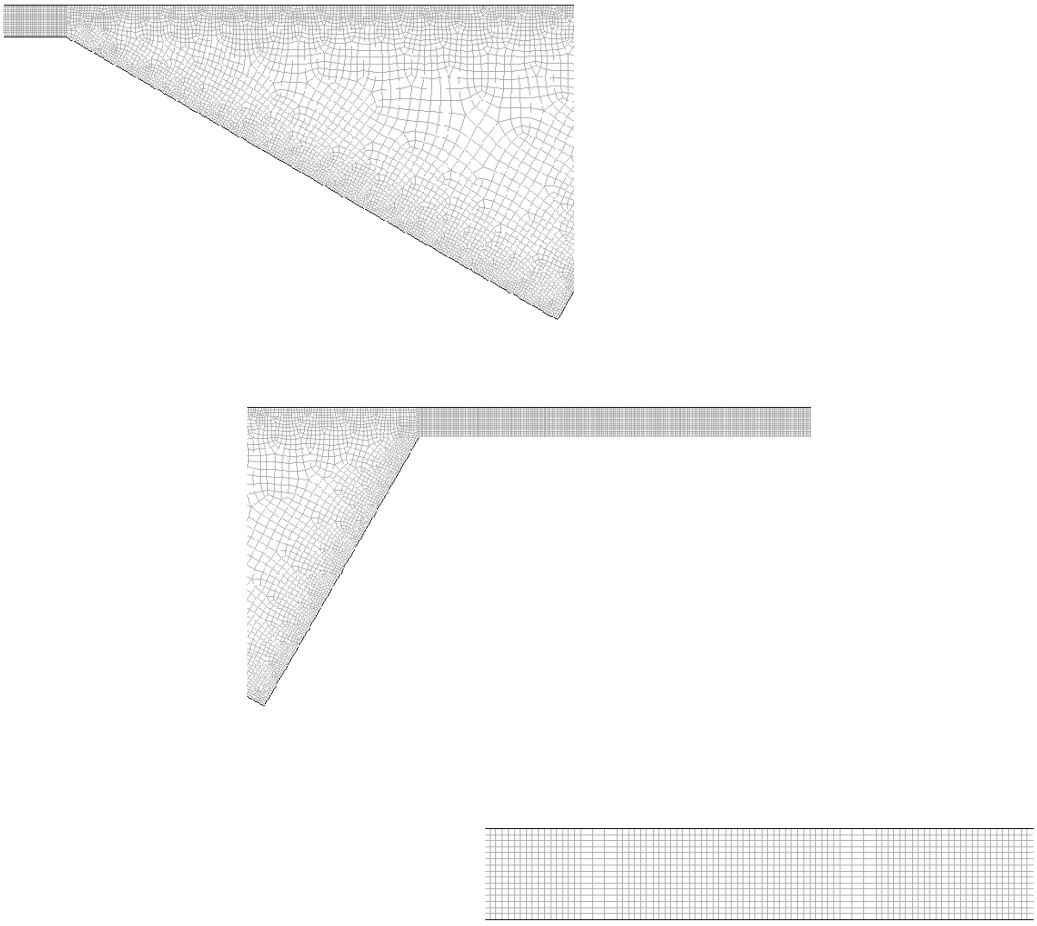

Figure 6.2: Triangular 30.0-60.0 Long Slot Final Mesh Magnified

Outer Cavity Pressure

Re	$n = 1.0$ P_{oc} Statistical Mean	Standard Deviation	Relative Percent of Mean	Re	$n = 0.9$ P_{oc} Statistical Mean	Standard Deviation	Relative Percent of Mean
0.10	522,243.816	727.015	0.139	0.10	246,773.907	396.664	0.161
1.00	522,588.266	709.774	0.136	1.00	246.141.926	378.767	0.154
5.00	524,153.461	660.743	0.126	5.00	247,401.349	359.808	0.145
10.0	526,166.833	671.662	0.128	10.0	249,177.547	457.300	0.184
15.0	528,215.820	758.305	0.144	15.0	250,970.556	626.799	0.250
20.0	530,288.839	898.629	0.169	20.0	252,808.657	822.588	0.325
25.0	532,338.389	1,070.657	0.201	25.0	254,553.792	1,016.377	0.399
30.0	534,394.456	1,261.606	0.236	30.0	256,314.813	1,196.682	0.467
40.0	538,429.248	1,670.401	0.310				
50.0	542,382.460	2,088.022	0.385				

Re	$n = 0.8$ P_{oc} Statistical Mean	Standard Deviation	Relative Percent of Mean	Re	$n = 0.7$ P_{oc} Statistical Mean	Standard Deviation	Relative Percent of Mean
0.10	116,691.195	218.952	0.188	0.10	55,233.889	122.309	0.221
1.00	117,062.664	205.373	0.175	1.00	55,662.164	112.393	0.202
2.00	117,458.531	198.835	0.169	2.00	56.067.124	116.860	0.208
3.00	117,850.642	202.349	0.172	3.00	56,421.700	136.336	0.242
4.00	118,261.483	215.339	0.182	4.00	56,897.317	165.778	0.291
5.00	118,678.895	236.383	0.199	5.00	57,249.858	200.814	0.351
10.0	120,680.106	405.837	0.336	7.50	58,185.898	298.246	0.513
15.0	122,562.406	608.282	0.496	10.0	59,057.459	398.580	0.675

Re	$n = 0.6$ P_{oc} Statistical Mean	Standard Deviation	Relative Percent of Mean	Re	$n = 0.5$ P_{oc} Statistical Mean	Standard Deviation	Relative Percent of Mean
0.10	26,248.605	69.069	0.263	0.10	12,580.376	39.404	0.313
1.00	26,665.311	65.198	0.245	0.50	12,805.844	37.387	0.292
2.00	27,124.709	84.718	0.312	1.00	13,067.056	44.507	0.341
3.00	27,501.865	117.927	0.429	1.50	13,268.693	58.895	0.444
4.00	27,820.064	155.852	0.560	2.00	13,510.823	76.467	0.566
5.00	28,138.841	195.044	0.693	2.50	13,785.394	95.263	0.691
6.00	28,546.282	234.394	0.821	3.00	13,812.376	114.543	0.829
7.00	28,823.341	271.690	0.943	4.00	14,159.722	151.531	1.070

Re	$n = 0.4$ P_{oc} Statistical Mean	Standard Deviation	Relative Percent of Mean
0.10	6,160.491	22.719	0.369
0.50	6,727.974	24.242	0.360
1.00	6,723.771	37.812	0.563
1.50	7,298.790	55.822	0.765
2.00	8,245.195	74.780	0.907
2.50	8,694.343	93.372	1.074

Table 6.2: Triangular 30.0-60.0 Long Slot ANSYS Fluent Pressure Statistical Data Summary

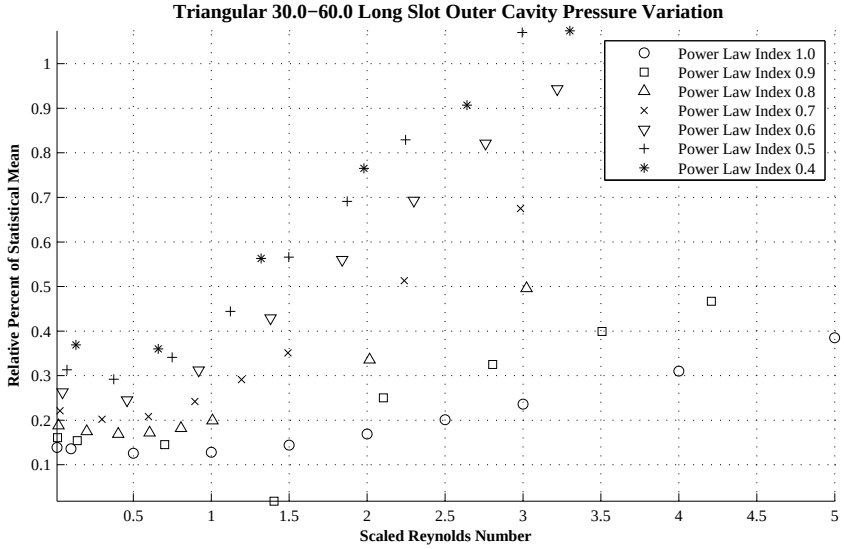

Figure 6.3: Triangular 30.0-60.0 Long Slot Outer Cavity Pressure Variation Plotted Results

For the specific case considered in the validation of the anticipated dominant back pressure, the triangular thirty-sixty degree expansion and contraction angles with an outer slot length equivalent to one hundred times that of the outer slot height, cognitive results were obtained for shear thinning fluids of generalized Newtonian rheology ranging in power law index as low as $n = 0.4$ to the Newtonian case of $n = 1.0$, with numerous flow conditions. The numerically obtained data in the tabulated results (Table 6.2) as well as the presentation of the plotted curve (Fig. 6.3) illustrate three important effects of the typical aspect ratios in the geometry of dual cavity coating die design on pressure variations in the cross section of the outer cavity. First, the standard deviation of pressure in the outer cavity, which represents the pressure variations throughout the two dimensional cross section of the outer cavity, demonstrates a maximum relative magnitude of 1.075 percent of the respective outer cavity pressure statistical mean. As expected, the pressure drop along the length of the outer slot determines the pressure level in the cross section of the outer cavity (Chapter 3), and thus the pressure distribution in the outer cavity varies axially along the width of the coating die while is uniform over the entire cross section. Second, the pressure variations in the cross section of the outer cavity represent a more significant portion of the outer cavity pressure statistical mean with a corresponding relative increase of the Reynolds number for a given power law index of the generalized Newtonian rheology. In accordance with Bernoulli's principal, the recoverable pressure of the fluid momentum associated with the contraction of the triangular outer cavity cross section, coupled with the jetting effect of

increased fluid inertia, shifts the statistical mean of the pressure distribution along the length of the outer cavity, thus inducing a relative broader range of pressure variation. Third, the pressure variations in the cross section of the outer cavity also represent a more significant portion of the outer cavity pressure statistical mean with a corresponding relative decrease of the power law index for a given flow flow condition. Although shear thinning behavior promotes the widthwise redistribution of flow along the width of a dual cavity coating die by reducing the resistance to flow along the outer cavity, this effect is amplified in the cross section of the outer slot, thus hindering the overall performance of the outer cavity. These observations of the numerically obtained pressure variations in the cross section of the outer cavity are consistent with the fundamental physics expected in the outer cavity of a dual cavity coating die, providing validation of the anticipated dominant back pressure of the outer slot assumed in the derivation of the outer cavity approximate model.

The validation of the anticipated dominant back pressure of the outer slot directly corresponds to the simulation of the two dimensional base flow in the computation of the outer cavity shape factor and may be investigated in the two dimensional cross section of the outer cavity. In the derivation of the outer cavity approximate model, it is anticipated that the back pressure of the outer slot greatly exceeds pressure variations in the outer cavity cross section, due to the typical aspect ratios demonstrated in the geometry of dual cavity coating die design as the ratio of the length of the outer slot to the height of the outer slot greatly exceeds the ratio of the length of the outer cavity to the height of the outer cavity. Observations of the numerically obtained pressure variations in the cross section of the outer cavity provide validation of the anticipated dominant back pressure of the outer slot assumed in the derivation of the outer cavity approximate model; however, a complete three dimensional analysis and ultimate experimental validation are necessary to define the applicability and accuracy of the theoretical approximate modeling approach.

6.2 Three Dimensional Validation

The experimental validation of current theoretical approximate die design models through the verification of lateral flow uniformity is difficult, owing to the fact that the coating die must be built with the proper dimensional aspect ratios and precisely machined, making phenomena occurring within the individual cavities difficult to measure. Validation of the outer cavity approximate die design model to predict the peak to peak variation in flow nonuniformity exiting the outer slot of a dual cavity coating die through the application of Computational Fluid Dynamics as idealized experimental data requires the complete three dimensional simulation of the equations (Eqs. 3.0.8a to 3.0.8e) governing flow within the

outer cavity domain. While Computational Fluid Dynamics offers valuable information to the internal flow details, such an analysis is difficult due to disparate length scales, often requiring long computational times to accurately simulate a single die flow condition with no guarantee a solution will converge. Much of the published three dimensional numerical simulation approaches have focused on the effects of fluid inertia and rheological properties on the regions of stagnation and vortex formation; however, an adequate analysis of dual cavity coating die designs has been lacking while the mesh generation for the numerical computations cited has been coarse (Chapter 2).

Fluid flow in dual cavity coating dies is three dimensional in nature, and thus the most realistic approach to the analysis of widthwise flow uniformity and ultimate geometrical design is to solve the complete set of three dimensional equations governing flow in the outer cavity, without simplifications, through numerical computation. In the solution of the outer cavity approximate model (Chapter 4), a method for obtaining the widthwise distribution of the flow per unit cavity width exiting the outer slot of a dual cavity coating die has been demonstrated, which accounts for the three dimensional nature of the equations of motion governing flow in the outer cavity through the outer cavity shape factor. The corresponding flow per unit cavity width, extracted from the numerical solution of the complete set of three dimensional equations governing flow in the outer cavity, serves as the basis for comparison, providing further confidence in the ability of the outer cavity approximate die design model to predict the peak to peak variation in flow nonuniformity exiting the outer slot of a dual cavity coating die.

A method for obtaining the two dimensional flow field in the cross section of the outer cavity through the use of the ANSYS Fluent commercially available software package has been established in the validation of the anticipated dominant back pressure of the outer slot. Here, in the validation of the outer cavity approximate die design model, the commercially available software package of ANSYS Fluent is now viewed in the traditional sense as a general numerical code for the solution of the Navier Stokes equations. However, with the exception of noted revisions, identical considerations in mesh generation as well as the specification of material properties, boundary conditions, and solver models for the validation of the anticipated dominant back pressure of the outer slot may be utilized in the validation of the outer cavity approximate die design model.

In the derivation of the outer cavity approximate model (Chapter 3), the assumed form of the inlet boundary velocity distribution demonstrates a fully developed profile, which is consistent with the flow per unit cavity width exiting the inner slot in the analysis of single cavity coating dies where the length of the inner slot greatly exceeds the height of the inner slot (Fig. 3.1). For the validation of the outer cavity approximate die design model,

the inlet boundary velocity distribution is specified with a fully developed parabolic profile across the height of the inner slot, while a sinusoidal function scales this profile along the coating width in representation of nonuniformities due to pressure variations present in the inner cavity. Therefore, the velocity inlet boundary condition is chosen for the validation of the outer cavity approximate model to control the necessary influx of mass prescribed through the average flow per unit cavity width entering the system as well as the ability to define the perturbed fully developed form of the velocity profile.

To complete the definition of the one dimensional outer cavity approximate model, the boundary conditions (Eq. 4.0.6) for a well posed system of governing equations specify no flow through the walls at the cavity ends, neglecting the entrance and end effects at the respective regions of the outer cavity. These wall surfaces at the ends of the outer cavity width must be specified to confine the flow within the computational domain, while the standard no slip boundary condition is only imposed on the remaining wall surfaces which bound the two dimensional cross section utilized in the computation of the outer cavity shape factor (Chapter 5). The wall boundary condition in ANSYS Fluent enforces the no slip condition in the viscous flow model by default, setting the three dimensional components of velocity to zero at the respective surfaces. Therefore, the cavity walls which bound the computational domain along the width of the coating die must be redefined to specify a zero shear condition, thus confining the flow within the domain of the outer cavity while neglecting entrance and end effects.

In the derivation of the outer cavity approximate model (Chapter 3), the width of the outer cavity (Fig. 3.1) which is utilized in the definition of the dimensionless variables represents one half of the overall coating width of the final liquid film exiting the outer slot. The three dimensional ANSYS Fluent model developed in the validation of the theoretical outer cavity approximate die design model subsequently represents this half width of the dual cavity coating die, symmetrically dividing the geometry along the plane parallel to the fluid inlet corresponding to a center fed coating die. Along the symmetry boundary condition, ANSYS Fluent forces a zero normal velocity component as well as a zero normal velocity gradient to the corresponding planer cross section, which may in turn be interpreted as a slip wall condition when utilized in viscous flow applications. For the validation of the outer cavity approximate die design model, the inlet boundary velocity distribution is specified with a fully developed parabolic profile across the height of the inner slot, while an inherently symmetrical cosine function scales this profile along the coating width in representation of nonuniformities due to pressure variations present in the inner cavity. Therefore, defining the planar cross section parallel to the fluid inlet as a zero shear wall boundary condition similar to the cavity ends, any desired form of the flow per unit cavity width exiting the inner

slot may be prescribed to control and represent the effects of various inlet flow conditions associated with the center fed dual cavity coating die geometry.

In the commercially available ANSYS Fluent software package, gradients are required for constructing the values of scalers at the cell faces as well as computing the secondary diffusion terms and velocity derivatives used to discritize the convection and diffusion terms within the flow conservation equations. ANSYS Fluent offers several available methods for the evaluation of gradients, which include the Green Gauss cell based, the Green Gauss node based, and the least squares cell based. The Green Gauss node based gradient evaluation is utilized for the validation of the outer cavity approximate model through the numerical simulation of the complete three dimensional governing equation set, where the values of scalers at the cell faces are computed through an arithmetic average of the nodal values associated with the respective cell face.

ANSYS Fluent stores the discrete values of computed scaler quantities, such as pressure in the solution of the continuity equation, at the center of each mesh cell, while the scaler quantities at the surrounding mesh cell faces are interpolated through an upwind scheme derived from quantities in the neighboring mesh cell centers which are upstream relative to the direction of the normal velocity. With the default first order upwind scheme, flow field variables computed at the mesh cell center represent an average quantity which is considered valid throughout the entire mesh cell, and the flow field variables determined at the surrounding mesh cell faces directly reflect the corresponding quantities at the upstream mesh cell center. When higher order accuracy is desired, flow field variables in the second order upwind scheme are computed utilizing a multidimensional linear reconstruction method, achieved through a Taylor series expansion of the solution at each mesh cell center about the centroid of the respective mesh cell. This higher order accuracy is required for the validation of the outer cavity approximate model where significant variation of the computed flow field components within the individual mesh cells is anticipated due to the coarser mesh required by the aspect ratios demonstrated in the three dimensional model of a dual cavity coating die.

The scaled residuals of the pressure based solver may fall below the specified convergence criteria, offering a useful indication of solution convergence; however this result does not sufficiently determine an acceptable solution of the complete set of three dimensional equations governing flow in the outer cavity alone. This method of convergence represents an imbalance in the conservation equations over the entire computational domain as a specified order of magnitude less than the corresponding bulk component of the system, which may remain in decline although the predetermined criteria indicates the solution has converged. A more complete identification of solution convergence occurs as the traditional residual plot

demonstrates a flattened, unchanging profile, although this approach increases the required computational time and may be beyond the requisite needs of the validation of the outer cavity approximate die design model. To determine if an acceptable solution is converged, a check must be conducted to ensure a conservation of mass within the computational domain, integrating the normal component of velocity at the entrance and exit of each of the inner slot, outer cavity, and outer slot regions.

In the three dimensional validation of the outer cavity approximate model, the corresponding flow per unit cavity width extracted from the numerical solution of the complete set of three dimensional equations (Eqs. 3.0.8a to 3.0.8e) governing flow in the outer cavity serves as the basis for comparison of the theoretical approximate modeling approach. A method for obtaining the predicted widthwise distribution of the flow per unit cavity width exiting the outer slot of a dual cavity coating die has been demonstrated in the solution of the outer cavity approximate model (Chapter 4). Here, the flow per unit cavity width defines the integral of the two dimensional velocity field across the height of the inner and outer slots, however this result is not explicitly available in the ANSYS Fluent post processor. Therefore, additional external post processing is required to determine the flow per unit cavity width exiting the outer slot, obtained from the numerical solution of the complete set of three dimensional equations governing flow in the outer cavity.

The derivation of the outer cavity approximate model (Chapter 3) assumes that the length of the outer cavity is greatly exceeded by the width of the outer cavity (Fig. 3.1); therefore, in the three dimensional computation of the outer cavity flow field, the length of the outer cavity is defined to be approximately two percent of the overall coating width. Remaining consistent with the two dimensional validation of the anticipated dominant back pressure, the three dimensional validation of the outer cavity approximate model utilizes an identical outer cavity cross section, the triangular thirty-sixty degree expansion and contraction angles respectively, which is uniformly extruded along the specified half width of the dual cavity coating die.

A mesh refinement series in the computation of the outer cavity shape factor (Chapter 5) determines that the appropriate number of elements required for acceptable solution convergence corresponds to a characteristic mesh size of fifteen elements across the height of the outer slot. Due to the aspect ratios demonstrated in the modeled geometry of the outer cavity domain, an adequate mesh for the validation of the outer cavity approximate die design model cannot be generated for such a characteristic mesh size with the computational resources available through the Rochester Institute of Technologys Research Computing Large Memory Computer. To avoid stretching the aspect ratio of the elements along the width of the outer cavity, which negatively impacts the rate of solution convergence as well as the

accuracy of the converged solution itself, the characteristic mesh size utilized in the validation of the outer cavity approximate model is reduced to ten elements across the height of the outer slot. The corresponding mesh interval size determined from this parameter serves as the basis for the implemented size functions, which gradually decreases the mesh density normal to the surface boundaries of the outer cavity as well as along the length of the outer slot as the velocity gradients diminish and the flow field profile becomes fully developed.

To integrate the velocity distribution, which is required to determine the flow per unit cavity width in validation of the outer cavity approximate die design model, a cooper mesh scheme is utilized to extrude the mesh faces of the two dimensional cross section along the width of the die. When the cooper meshing scheme is applied to the modeled geometry, the node patterns of the two dimensional cross section of the outer cavity, denoted as the source face, are projected throughout the volume of the outer cavity domain along the remaining non-source faces at the specified interval spacing. Here, the lowest attainable aspect ratio of the three dimensional grid within the outer cavity domain, limited by the computational resources available through the Rochester Institute of Technologys Research Computing Large Memory Computer, stretches the width of the element volume along the outer cavity axis equivalent to one and a half times the length and height of the corresponding element. The resulting mesh of the outer cavity domain in the three dimensional validation of the outer cavity approximate model comprises of approximately twenty million mesh cell element volumes, which greatly increases the computational time of each associated simulation, requiring over three hundred fifty hours of continuous run time.

Once the numerical solution of the complete set of three dimensional equations (Eqs. 3.0.8a to 3.0.8e) governing flow in the outer cavity is converged, additional post processing is required for the validation of the theoretical outer cavity approximate die design model. While the solution of the outer cavity approximate model (Chapter 4) provides a method for obtaining the widthwise distribution of the flow per unit cavity width exiting the outer slot of a dual cavity coating die, this result is not explicitly available in the ANSYS Fluent post processor. Here, the flow per unit cavity width defines the integral of the two dimensional velocity field across the height of the inner and outer slots; therefore, a data file containing the velocity distribution at the respective cross sections of the computational domain is exported from the ANSYS Fluent solver, where a trapezoidal integration is employed externally to determine the numerically obtained flow per unit cavity width.

Model Specific Simulation Parameters	
θ	30.0
ϕ	60.0
H_{is}	0.048
H_{oc}	0.480
H_{os}	0.048
L_{is}	0.096
L_{os}	2.000
W_{is}	24.0
W_{oc}	24.0
W_{os}	24.0
M_c	0.0032

Table 6.3: Simulation Parameters Specific to the Triangular 30.0-60.0 Three Dimensional ANSYS Fluent Model

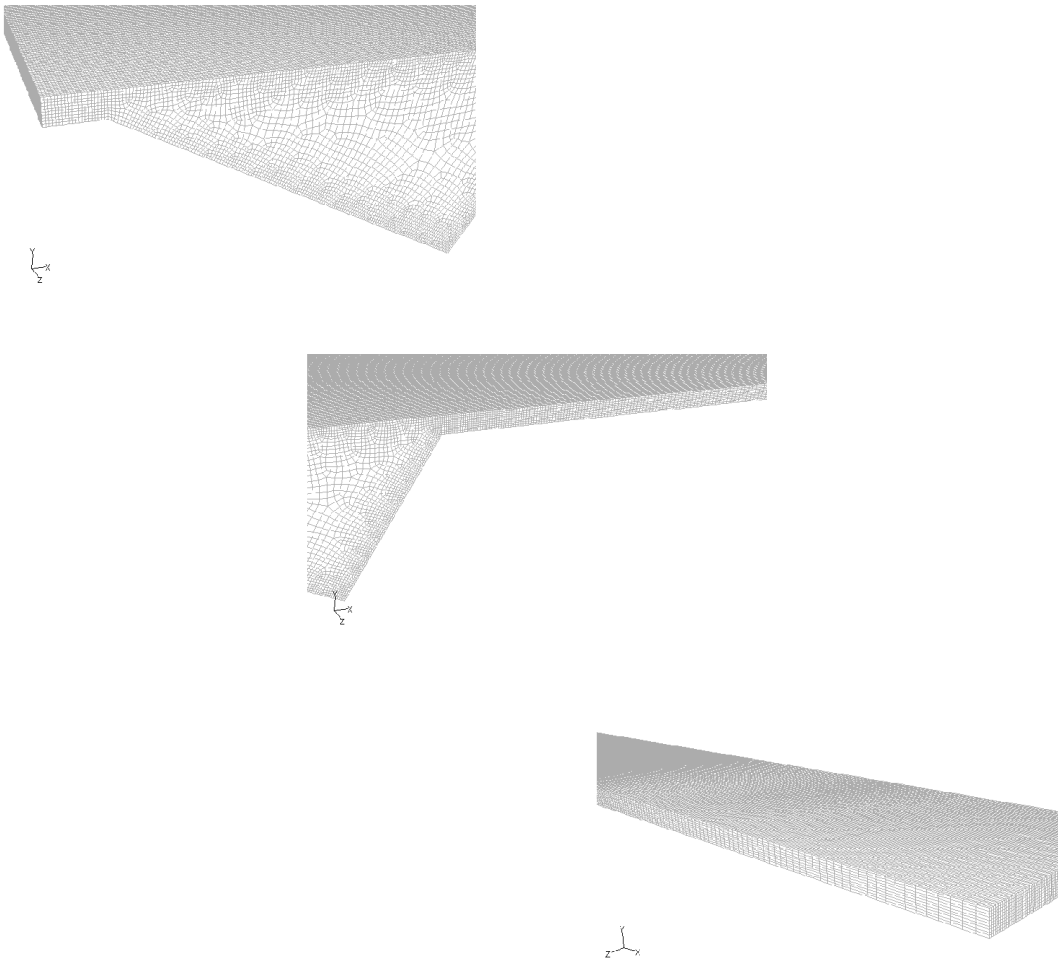

Figure 6.4: Triangular 30.0-60.0 Three Dimensional Final Mesh Magnified

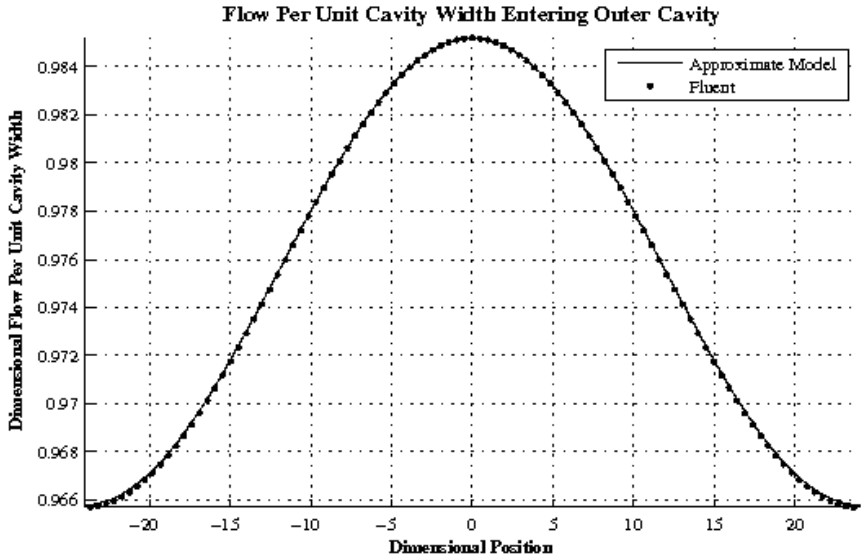

Figure 6.5: Triangular 30.0-60.0 Three Dimensional Newtonian Inlet Flow Profile $n = 1.0$ and $Re = 0.1$

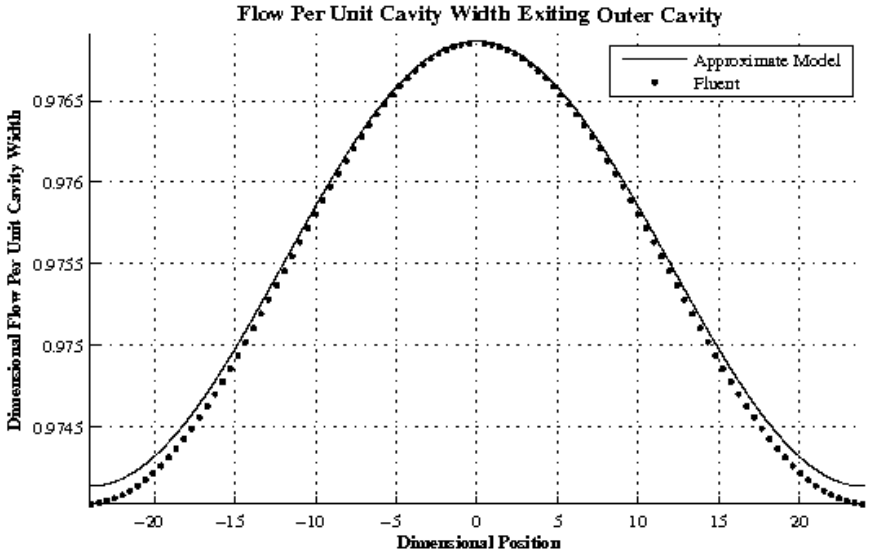

Figure 6.6: Triangular 30.0-60.0 Three Dimensional Newtonian Outlet Flow Profile $n = 1.0$ and $Re = 0.1$

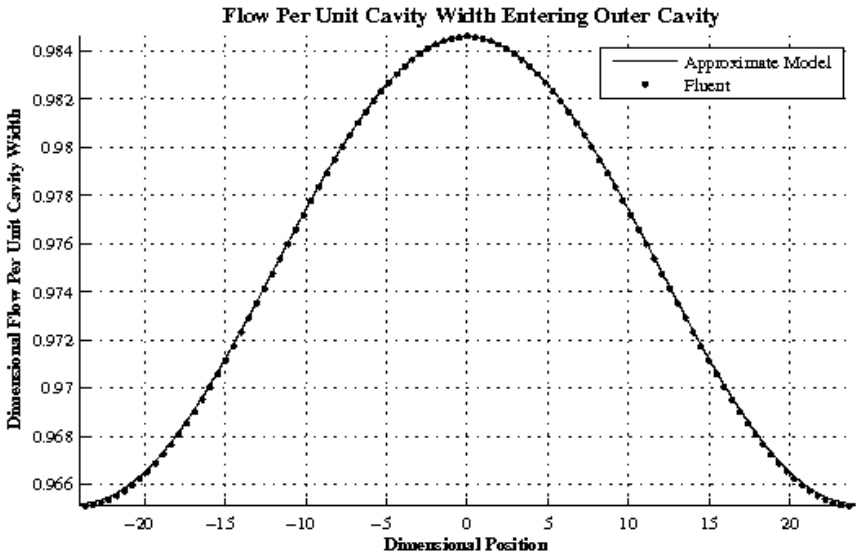

Figure 6.7: Triangular 30.0-60.0 Three Dimensional Non-Newtonian Inlet Flow Profile $n = 0.9$ and $Re = 0.1$

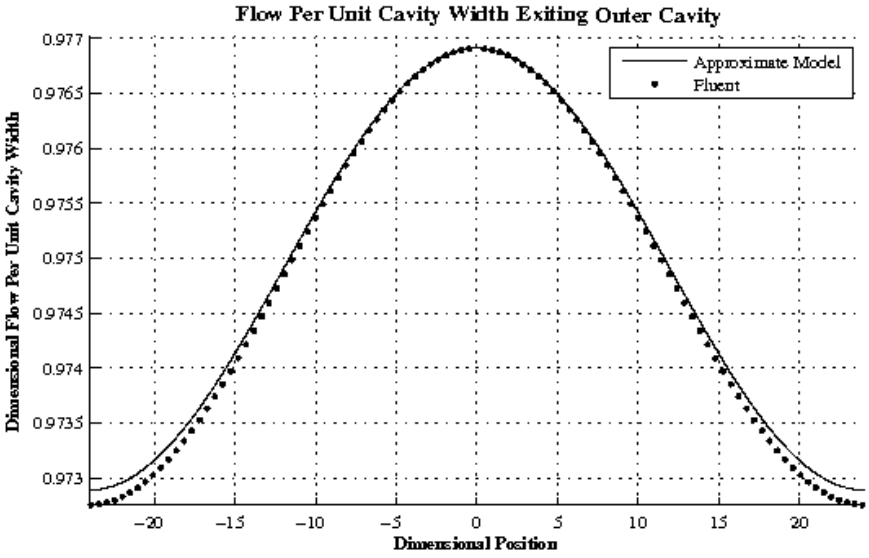

Figure 6.8: Triangular 30.0-60.0 Three Dimensional Non-Newtonian Outlet Flow Profile $n = 0.9$ and $Re = 0.1$

For the specific case considered in the three dimensional validation of the outer cavity approximate model, the triangular thirty-sixty degree expansion and contraction angles with an outer cavity width equivalent to twenty four times that of the outer cavity length, results for the peak to peak variation in the widthwise flow distribution exiting the outer cavity were obtained for shear thinning fluids of generalized Newtonian rheology with a power law index of $n = 1.0$ and $n = 0.9$ at negligible Reynolds number. The numerically obtained data in the presentation of the plotted flow per unit cavity width exiting the outer slot (Figs. 6.5 to 6.8) illustrates three key observations associated with the three dimensional validation of the theoretical approximate modeling approach. First, the theoretically predicted profile of the flow per unit cavity width exiting the outer cavity demonstrates a maximum error of 0.011 and 0.014 percent in the predicted flow per unit cavity width and 4.719 and 5.228 percent in the predicted peak to peak variation, for the Newtonian and non-Newtonian cases respectively, with the numerically obtained profile of the ANSYS Fluent computational model. This excellent agreement provides further confidence in the ability of the approximate modeling approach to predict the peak to peak variation in flow uniformity exiting the outer slot of a dual cavity coating die. Second, the largest deviation of the predicted flow per unit cavity width exiting the outer cavity from that obtained numerically through the ANSYS Fluent model, most evident in the plotted results of the Newtonian case, occurs in the regions of the cavity ends. As expected from the derivation of the one dimensional outer cavity approximate model (Chapter 3), the boundary conditions for a well posed system of governing equations specify no flow through the walls at the cavity ends, neglecting the entrance and end effects at the respective regions of the outer cavity. These observations of the numerically obtained flow per unit cavity width, as idealized experimental data, are consistent with the fundamental assumptions of the outer cavity approximate model, providing good agreement and confidence in the validity of the theoretical approximate modeling approach.

In the practical design of dual cavity coating dies which are utilized in industrial applications, an outer cavity damping factor which reduces the amplitude of the flow per unit cavity width exiting the outer slot to approximately one tenth of that which enters the outer cavity is required to justify the inclusion of the secondary cavity (Ruschak, 2010). The cases considered in the three dimensional validation of the outer cavity approximate die design model, however, demonstrate an outer cavity damping factor which exhibits an approximate $176,905.753$ and $101,969.307$ percent increase in the peak to peak variation as compared with those typically introduced in industry. This effect also becomes evident upon examination of the outer cavity damping dimensionless group, of which an approximate increase

of $5,987.164$ and $3,668.223$ percent is demonstrated in the geometry of the ANSYS Fluent model in comparison with that of industrial dual cavity coating die design. Therefore, the unacceptable level of damping demonstrated in the three dimensional validation of the outer cavity approximate model is attributable to the unrealistic dimensions of the modeled geometry (Fig. 3.1), where a height of the outer slot which is ten percent of the height of the outer cavity is utilized in contrast to the typical designs which incorporate an outer slot height which is only one percent of the height of the outer cavity.

6.3 Summary

The experimental validation of current theoretical approximate die design models through the verification of lateral flow uniformity is difficult, owing to the fact that the coating die must be built with the proper dimensional aspect ratios and precisely machined, making phenomena occurring within the individual cavities difficult to measure. Fluid flow in dual cavity coating die designs is three dimensional in nature, and thus the most realistic approach to the analysis of widthwise flow uniformity and ultimate geometrical designs is to solve the complete set of three dimensional equations governing flow, without simplifications, through numerical computation. While observations of the numerically obtained flow per unit cavity width exiting the outer cavity provide good agreement and confidence in the validity of the theoretical approximate modeling approach, these simulations are numerically intensive, requiring over three hundred fifty hours of continuous run time to accurately simulate a single die flow condition with no guarantee a solution will converge. In the three dimensional validation of the outer cavity approximate model, the realistic aspect ratios demonstrated in dual cavity coating die designs utilized in typical industrial applications, specifically the coating width and slot height, could not be obtained with the available resources of the Rochester Institute of Technologys Research Computing Large Memory Computer. Therefore, the limitations of the validity of the outer cavity approximate model can not be identified, however, the attempts of the complete, three dimensional numerical simulation of the outer cavity further demonstrate the utility and importance of the theoretical approximate die design models.

Chapter 7

Design of the Outer Cavity Cross Section

The design of the outer cavity requires a more complex shape (Fig. 5.3) than that of the inner cavity to prevent regions of stagnation and recirculation due to the orientation and relative fluid inertia of the primary flow exiting the inner slot of a dual cavity coating die. To achieve a redistribution of fluid along the widthwise direction, the resistance to flow along the width of the cavity is made low by choosing a relatively large cross sectional area. In contrast, the slot geometry is designed such that the resistance to flow is high, accomplished by choosing a relatively small slot height and long slot length. Similar to the function of the inner cavity, the presence of these disparate resistances to flow in the outer cavity can effectively reduce nonuniformities in the flow per unit cavity width exiting the inner slot due to pressure variations in the inner cavity. However, significant flow occurs in the cross section of the outer cavity (Fig. 1.2) between the exit of the inner slot and entrance to the outer slot, such that the primary flow of the outer cavity is no longer oriented widthwise along the cavity axis but predominantly along the length of the die. It is important to consider the optimum use of the outer cavity cross sectional area as the influence of streamlining, wall shear stress, and residence time distribution of fluid within the outer cavity are crucial considerations of coating die design.

Vortex formation and fluid stagnation in the cross section of the outer cavity not only diminish the ability of the cavity to dampen nonuniformities in the flow per unit cavity width exiting the inner slot, but also result in gelation, due to a cross linking agent or flocculated rheology, as well as the sedimentation of pigments in certain applications. Near the exit of the inner slot and entrance of the outer slot, the formation of vortices reduces the effective cross sectional area available in the outer cavity for the widthwise redistribution of flow along the cavity axis. Outer cavity geometries which demonstrate an ineffective use

of available cross sectional area commonly exhibit an increase in fluid residence time, often raising the maintenance costs associated with the removal of settling and reactive materials. Therefore, typical outer cavity design utilizes a streamlined shape such that the expansion and contraction angles of the geometry may be determined to minimize or eliminate these undesirable effects for a range of fluids and flow conditions.

Three dimensional numerical simulation in the current literature (Chapter 2) has been a valuable tool for the prediction of vortex formation in the cross flow of the outer cavity regions of a dual cavity coating die. Flow patterns of fluids obeying a power law dependence of viscosity on shear rate within semicircular and tear drop outer cavity cross sections were computed by the finite element method to reveal the formation of vortices with increased fluid inertia (Lee and Liu, 1989). The effects of cavity shape, particularly the expansion and contraction angles, as well as the rheological properties of polymeric fluids on vortex formation in the outer cavity of a dual cavity coating die have also been examined by Lee et al. (1990).

In addition to the streamline considerations of vortex formation and recirculation, the magnitude of the cavity wall shear stress is a further concern which must be considered in the design of the outer cavity cross sectional shape. The stiffening of generalized Newtonian fluids with a power law dependence of viscosity on shear rate occurs as a result of insufficient shear stresses along the lower boundaries of the outer cavity cross section and a consequential increase in fluid viscosity. For flow conditions of moderate Reynolds number, regions of stagnation appear at the cavity walls where the velocity gradients which determine the magnitude of the local shear rate diminish with the expansion of the outer cavity cross sectional area. A reduction in the height of the cross section (Fig. 3.1) perpendicular to the direction of flow is required to maintain sufficient shear stresses at the lower boundaries of the cavity wall and prevent the stagnation and stiffening of shear thinning fluids.

The current literature (Chapter 2) has only focused on the design of the outer cavity cross sectional shape with respect to streamline considerations, and thus an extension of this research is made to incorporate the concern of cavity wall shear stress in a two dimensional investigation of the design of the outer cavity cross section. This is accomplished in the proposed outer cavity design through a truncation of the streamlined thirty-sixty degree expansion and contraction angle triangular outer cavity cross section, producing a flattened boundary of the lower geometry (Fig. 3.1) parallel to the direction of the primary flow. In this way, the proposed optimum outer cavity design maintains sufficient shear stresses along the lower boundaries of the geometry to prevent the stiffening of shear thinning fluids, while utilizing the streamlined shape of the triangular outer cavity cross section to reduce vortex formation and recirculation.

It is important to note that the reduction of cross sectional area associated with the proposed outer cavity design, which is necessary to maintain sufficient wall shear stresses at the lower boundary of the geometry, results in an increase of the resistance to flow along the width of the cavity. Consequently, the ability of the outer cavity to dampen nonuniformities in the flow per unit cavity width exiting the inner slot, due to pressure variations in the inner cavity, is diminished. The requirement for sufficient shear stresses to prevent fluid stagnation in the cross section of the outer cavity negatively affects the widthwise redistribution of flow along the outer cavity, and thus the relative increase in cavity wall shear stress is examined in its interaction with the damping ability of the proposed outer cavity design.

The impact of geometrical adjustments in the proposed outer cavity design must be established to consider the optimum use of the outer cavity cross sectional area through the influence of streamlining, wall shear stress, and residence time distribution of fluid within the outer cavity. In the solution of the outer cavity approximate model (Chapter 4), a method for obtaining the widthwise distribution of the flow per unit cavity width exiting the outer slot of a dual cavity coating die has been demonstrated. The outer cavity damping dimensionless group, which arises in the solution of the outer cavity approximate model, allows for the direct comparison of the relative effect of the reduced cross sectional area in the proposed outer cavity design on the widthwise redistribution of flow through the outer cavity shape factor.

To determine a reasonable outer cavity design for a suitable range of flow conditions and fluid rheologies, a characteristic flat bottom length in the outer cavity is defined as the ratio of the length of the outer cavity flat bottom to the length of the outer cavity (Fig. 3.1), which relatively measures the reduction of cross sectional area for the proposed outer cavity design. Three specific flat bottomed triangular outer cavity cross sections, which include 0.316, 0.416, and 0.516 ratios of the characteristic flat bottom length, are considered in the proposed outer cavity design. In this way, the relative influence of the reduction of area in the proposed outer cavity design on the cavity wall shear stress, as well as the ability of the cavity to dampen nonuniformities in the flow per unit cavity width exiting the inner slot, are effectively investigated through the solution of the outer cavity approximate model (Chapter 4).

A method for obtaining the outer cavity shape factor (Chapter 5) utilizing commercially available software has been established to correlate the perturbed equations (Eqs. 5.1.1a to 5.1.1e) of the outer cavity approximate model with those implemented within ANSYS Fluent. The numerical procedure for the computation of the outer cavity shape factor as well as the solution of the outer cavity approximate model (Chapter 4) have been generalized in a form which is valid for the design of more complex geometries of any arbitrary, yet widthwise

constant, cross sectional shape. Therefore, identical considerations in mesh generation as well as the specification of material properties, boundary conditions, and solver models for the traditional outer cavity designs outlined previously are utilized in the computation of the outer cavity shape factor for the proposed optimum outer cavity design.

Model Specific Simulation Parameters	
θ	30.0
ϕ	60.0
H_{is}	0.048
H_{oc}	0.344
H_{os}	0.048
L_{is}	0.096
L_{fb}	0.316
L_{os}	0.480
M_c	0.0010

Table 7.1: Simulation Parameters Specific to the Triangular 30.0-60.0 Flat Bottom 0.316 Cross Section in the Computation of the Outer Cavity Shape Factor

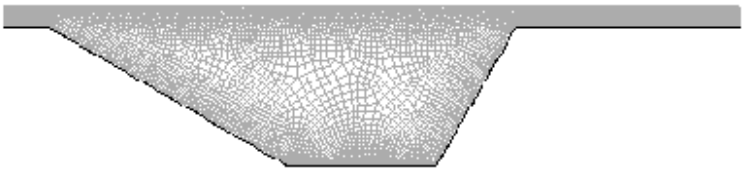

Figure 7.1: Triangular 30.0-60.0 Flat Bottom 0.316 Final Mesh

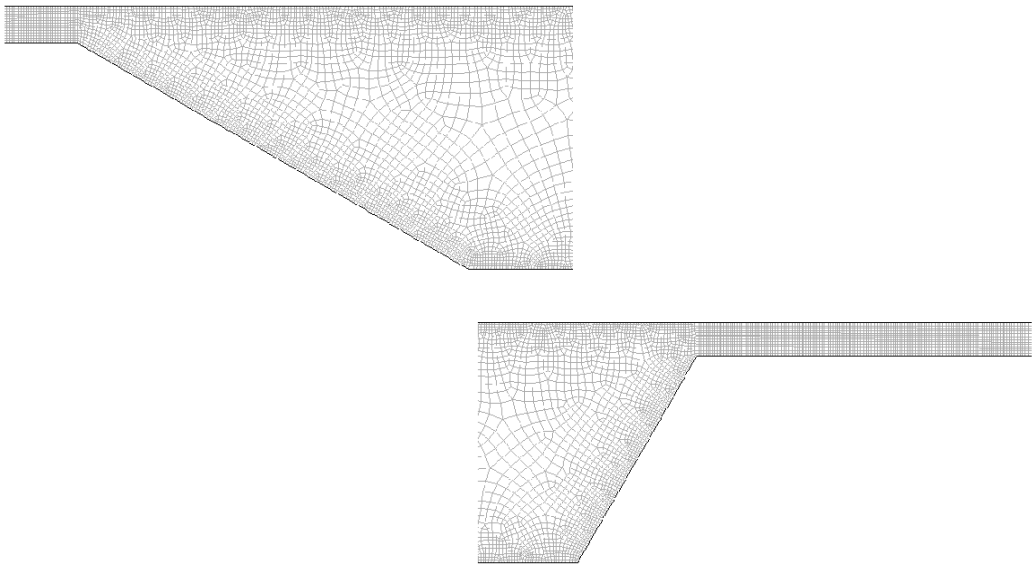

Figure 7.2: Triangular 30.0-60.0 Flat Bottom 0.316 Final Mesh Magnified

Model Specific Simulation Parameters	
θ	30.0
ϕ	60.0
H_{is}	0.048
H_{oc}	0.300
H_{os}	0.048
L_{is}	0.096
L_{fb}	0.416
L_{os}	0.480
M_c	0.0010

Table 7.2: Simulation Parameters Specific to the Triangular 30.0-60.0 Flat Bottom 0.416 Cross Section in the Computation of the Outer Cavity Shape Factor

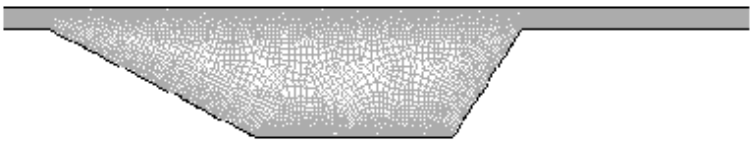

Figure 7.3: Triangular 30.0-60.0 Flat Bottom 0.416 Final Mesh

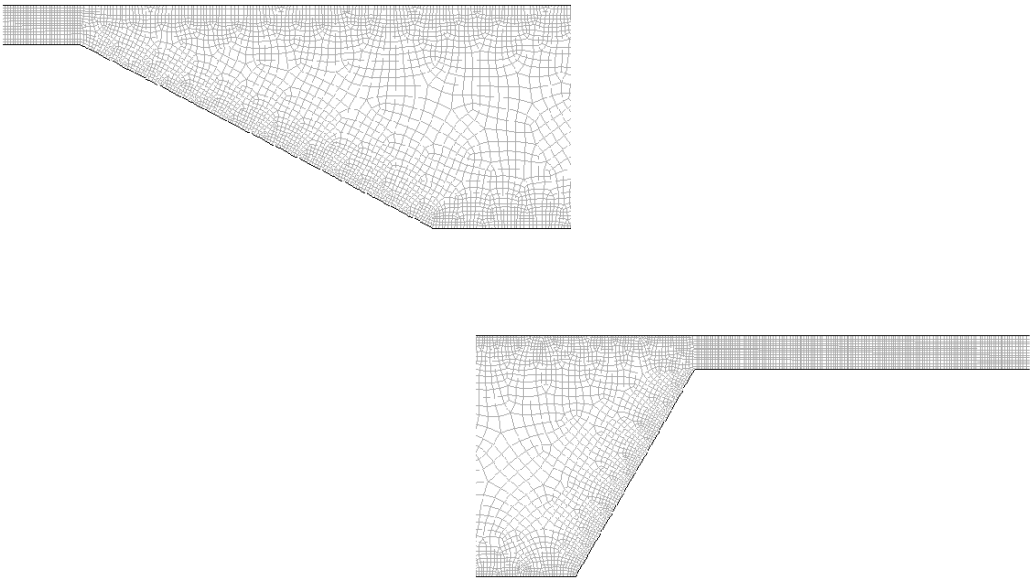

Figure 7.4: Triangular 30.0-60.0 Flat Bottom 0.416 Final Mesh Magnified

Model Specific Simulation Parameters	
θ	30.0
ϕ	60.0
H_{is}	0.048
H_{oc}	0.258
H_{os}	0.048
L_{is}	0.096
L_{fb}	0.516
L_{os}	0.480
M_c	0.0010

Table 7.3: Simulation Parameters Specific to the Triangular 30.0-60.0 Flat Bottom 0.516 Cross Section in the Computation of the Outer Cavity Shape Factor

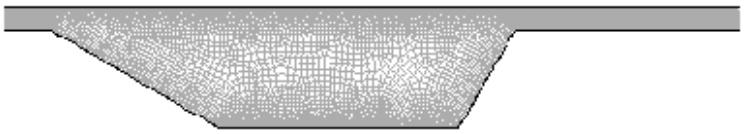

Figure 7.5: Triangular 30.0-60.0 Flat Bottom 0.516 Final Mesh

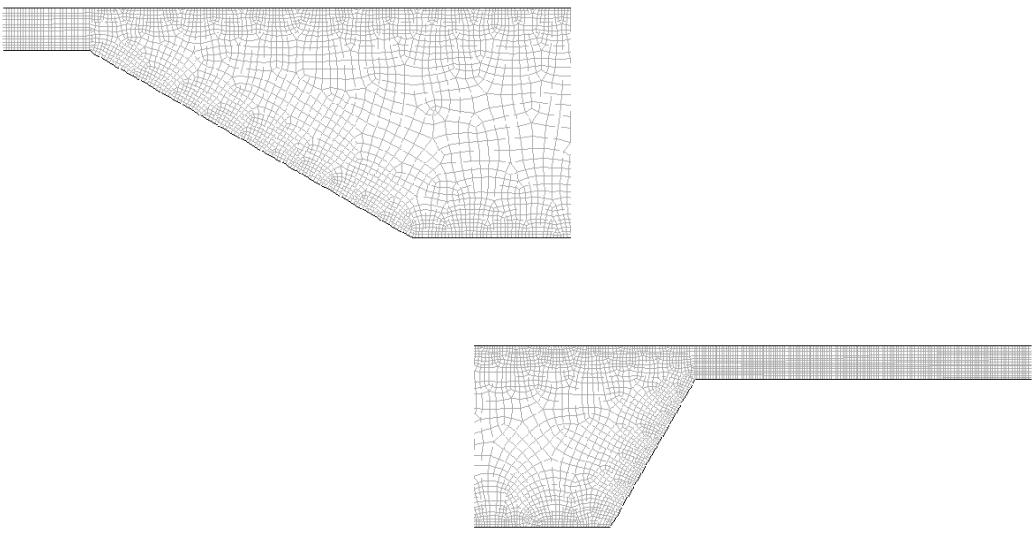

Figure 7.6: Triangular 30.0-60.0 Flat Bottom 0.516 Final Mesh Magnified

Once the solution for the perturbed set of three dimensional equations (Eqs. 5.1.1a to 5.1.1e) governing flow in the outer cavity is converged and the outer cavity shape factor has been determined, no additional post processing is required to determine the effect of the reduction of cross sectional area on cavity wall shear stress in the proposed outer cavity design. From the correlation of the analogous ANSYS Fluent momentum and energy equations (Chapter 5), the spatial coordinates and velocity components in the two dimensional cross section of the outer cavity scale such that the dimensional forms of the ANSYS Fluent model are numerically equivalent to the dimensionless forms of the derivation of the outer cavity approximate model. Therefore, the shear stress at the lower boundary of the outer cavity cross section is extracted directly from the ANSYS Fluent post processor, from which the statistical mean is determined and examined as a relative increase from the traditional, untruncated outer cavity design.

Outer Cavity Wall Shear Stress

	$L_{fb} = 0.000$	$L_{fb} = 0.316$		$L_{fb} = 0.416$		$L_{fb} = 0.516$	
n	Statistical Mean	Statistical Mean	Percent Increase	Statistical Mean	Percent Increase	Statistical Mean	Percent Increase
1.0	217.486162	235.691073	8.4	273.116900	25.6	256.962147	18.2
0.9	114.344902	124.379282	8.8	143.710293	25.7	137.191485	20.0
0.8	63.630019	69.467127	9.2	80.684994	26.8	77.063181	21.1
0.7	34.221742	37.530409	9.7	43.326842	26.6	42.060036	22.9
0.6	18.634134	20.565604	10.4	23.145207	24.2	23.411191	25.6
0.5	10.380006	11.527053	11.1	13.123125	26.4	13.115697	26.4
0.4	5.843242	6.546465	12.0	7.330639	25.5	7.546567	29.2
	$L_{fb} = 0.000$	$L_{fb} = 0.316$		$L_{fb} = 0.416$		$L_{fb} = 0.516$	
n	Standard Deviation	Standard Deviation	Percent Difference	Standard Deviation	Percent Difference	Standard Deviation	Percent Difference
1.0	542.820642	567.847005	4.6	580.157785	6.9	566.640441	4.4
0.9	272.073306	284.457753	4.6	290.577163	6.8	282.495761	3.8
0.8	122.830116	127.022579	3.4	129.619785	5.5	125.811433	2.4
0.7	62.436793	64.425614	3.2	65.590028	5.1	63.426304	1.6
0.6	32.159012	33.147694	3.1	33.670063	4.7	32.307647	0.5
0.5	15.075828	15.272919	1.3	15.368395	1.9	14.811220	1.8
0.4	7.391838	7.369088	0.3	7.358811	0.4	7.068275	4.4

Table 7.4: Proposed Outer Cavity Design Wall Shear Stress Statistical Data Summary

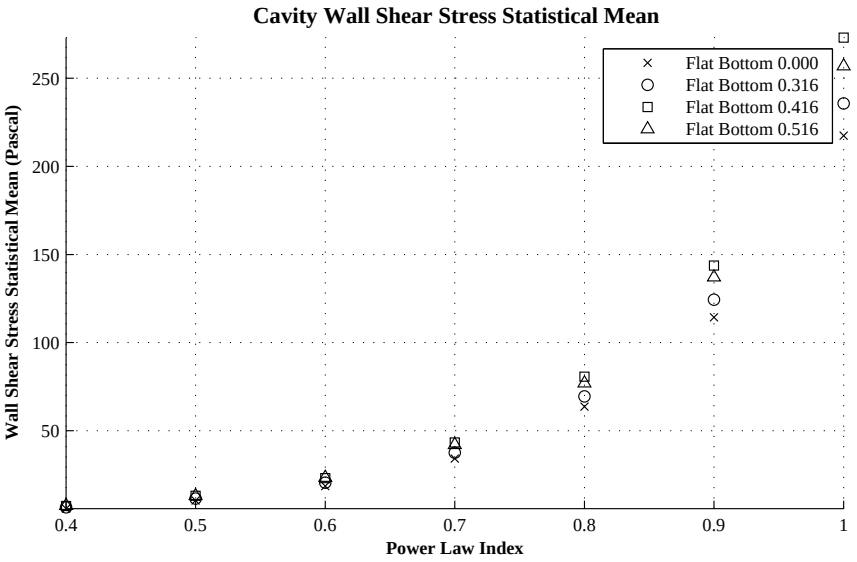

Figure 7.7: Proposed Outer Cavity Design Cavity Wall Shear Stress Statistical Mean Plotted Results

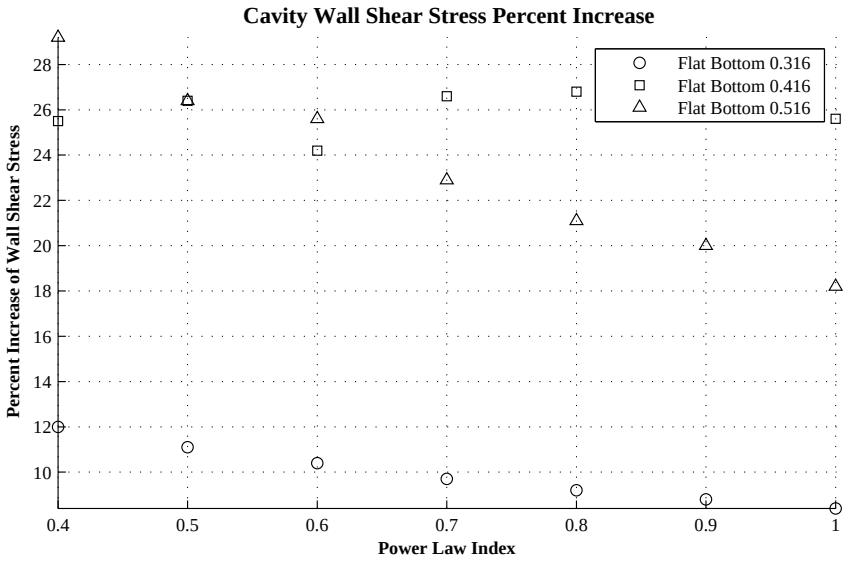

Figure 7.8: Proposed Outer Cavity Design Cavity Wall Shear Stress Percent Increase Plotted Results

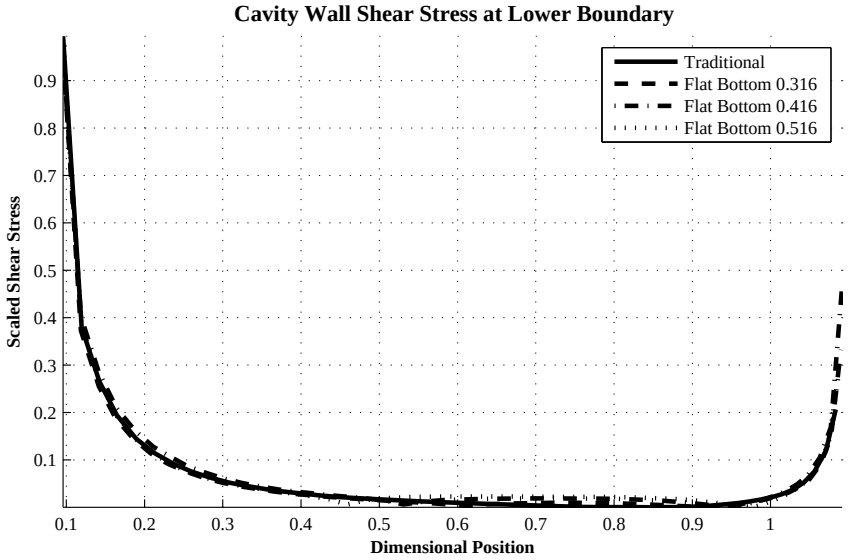

Figure 7.9: Proposed Outer Cavity Design Newtonian Cavity Wall Shear Stress Profile $n = 1.0$ and $Re = 0.1$

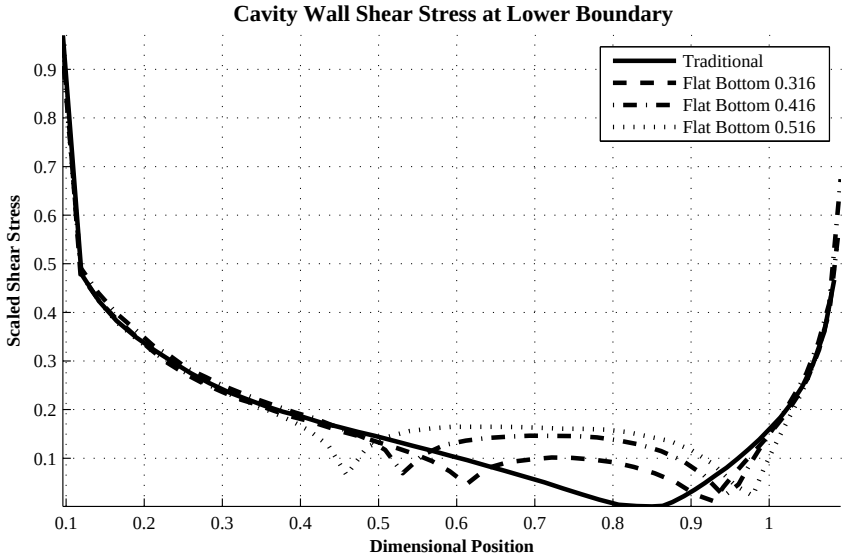

Figure 7.10: Proposed Outer Cavity Design Non-Newtonian Cavity Wall Shear Stress Profile $n = 0.4$ and $Re = 0.1$

For each of the cases considered in the proposed outer cavity design, the thirty-sixty degree expansion and contraction angle triangular cross sections with 0.316, 0.416, and 0.516 ratios of the characteristic flat bottom length, cognitive results for the statistical mean of outer cavity wall shear stress were obtained for shear thinning fluids, ranging in power law index as low as $n = 0.4$ to the Newtonian case of $n = 1.0$, of generalized Newtonian rheology. The numerically obtained data in the tabulated results (Table 7.4) as well as the presentation of the plotted curves (Figs. 7.7 to 7.10) illustrate two important effects of the reduction in the height of the cross section (Fig. 3.1) perpendicular to the direction of flow on cavity wall shear stress and fluid stagnation. First, a relative increase in the outer cavity wall shear stress statistical mean of 9.9, 25.8, and 23.3 percent for the respective thirty-sixty degree expansion and contraction angle triangular cross sections with 0.316, 0.416, and 0.516 ratios of the characteristic flat bottom length from the traditional, untruncated outer cavity design is demonstrated with a corresponding reduction in the height of the cross section perpendicular to the direction of flow. As expected, the stiffening of generalized Newtonian fluids with a power law dependence of viscosity on shear rate occurs as a result of insufficient shear stresses along the lower boundaries of the outer cavity cross section where the velocity gradients which determine the magnitude of the local shear rate diminish with the expansion of the outer cavity cross sectional area. Second, a reduction in the height of the cross section perpendicular to the direction of flow demonstrates a diminishing return in the relative increase of the outer cavity wall shear stress statistical mean, evident with the continued reduction from the 0.416 to 0.516 ratios of the characteristic flat bottom length respectively. This observed phenomena cannot be explained with the available data numerically obtained in the design of the outer cavity cross section, nor through an assessment of the fundamental physics associated with the design of dual cavity coating dies; therefore, a further investigation is required beyond the scope of the current research. These observations of the numerically obtained outer cavity wall shear stress in the proposed outer cavity design offer valuable information for the investigation into the the optimum design of the outer cavity cross section beyond the traditional concerns of streamlining.

The reduction of cross sectional area associated with the proposed outer cavity design, which is necessary to maintain sufficient wall shear stresses at the lower boundary of the geometry, results in an increase of the resistance to flow along the width of the cavity. To achieve a redistribution of fluid along the widthwise direction of the coating die, the resistance to flow in the outer cavity is made low by choosing a relatively large cross sectional area, while the slot geometry is designed such that the resistance to flow is high, accomplished by choosing a relatively small slot height and long slot length (Fig. 3.1). Therefore, the requirement for sufficient shear stresses to prevent fluid stagnation in the cross section

of the outer cavity negatively affects the widthwise redistribution of flow along the outer cavity, and thus the relative increase in cavity wall shear stress is examined in its interaction with the damping ability of the proposed outer cavity design.

The relative influence of the reduction of area in the proposed outer cavity design on the ability of the cavity to dampen nonuniformities in the flow per unit cavity width exiting the inner slot is effectively investigated through the solution of the outer cavity approximate model (Chapter 4). In the ANSYS Fluent post processor, the volume integral of the perturbed axial component of velocity in the outer cavity provides the required data for the computation of the outer cavity viscous shape factor. The outer cavity damping dimensionless group (Eq. 4.0.10b), which arises in the solution of the outer cavity approximate model (Chapter 4), allows for the direct comparison of the relative effect of the reduced cross sectional area in the proposed outer cavity design on the widthwise redistribution of flow, and is examined as a relative decrease from the traditional, untruncated outer cavity design.

Outer Cavity Shape Factor

$n = 1.0$		$n = 0.9$		$n = 0.8$		$n = 0.7$	
Re	Fluent λ_{oc}	Re	Fluent λ_{oc}	Re	Fluent λ_{oc}	Re	Fluent λ_{oc}
0.10	0.023578	0.10	0.035120	0.10	0.052474	0.10	0.078655
1.00	0.023324	1.00	0.034417	1.00	0.050495	1.00	0.073117
5.00	0.020089	5.00	0.026933	2.00	0.046434	2.00	0.063533
10.0	0.015970	10.0	0.019800	3.00	0.042051	3.00	0.054834
15.0	0.013112	15.0	0.015573	4.00	0.038052	4.00	0.047800
20.0	0.011122	20.0	0.012848	5.00	0.034590	5.00	0.042182
25.0	0.009674	25.0	0.010927	10.0	0.023414	7.50	0.032241
30.0	0.008575	30.0	0.009459	15.0	0.017490	10.0	0.025497
40.0	0.007024						
50.0	0.005982						

$n = 0.6$		$n = 0.5$		$n = 0.4$	
Re	Fluent λ_{oc}	Re	Fluent λ_{oc}	Re	Fluent λ_{oc}
0.10	0.118095	0.10	0.177882	0.10	0.268136
1.00	0.103313	0.50	0.164389	0.50	0.230420
2.00	0.082954	1.00	0.140177	1.00	0.178324
3.00	0.067551	1.50	0.118672	1.50	0.138973
4.00	0.056233	2.00	0.101324	2.00	0.109976
5.00	0.047526	2.50	0.087290	2.50	0.088638
6.00	0.040591	3.00	0.075734		
7.00	0.036087	4.00	0.057995		

Table 7.5: Triangular 30.0-60.0 Flat Bottom 0.316 ANSYS Fluent Outer Cavity Shape Factor Data Summary

Fitting Constants

Rheological and Model Specific		Model Specific	
n	c_1		
1.0	0.024145	c_2	0.023826
0.9	0.035000	c_3	3.945039
0.8	0.051797	c_4	1.751500
0.7	0.076784	c_5	0.000000
0.6	0.114533	c_6	2.944230
0.5	0.170916	c_7	0.513065
0.4	0.257564	c_8	1.336871

Table 7.6: Triangular 30.0-60.0 Flat Bottom 0.316 Curve Fitting Constants Summary

Outer Cavity Shape Factor

$n = 1.0$				$n = 0.9$			
Re	Fitted λ_{oc}	Percent Error λ_{oc}	Percent Error ε	Re	Fitted λ_{oc}	Percent Error λ_{oc}	Percent Error ε
0.10	0.023807	1.0	1.0	0.10	0.035305	0.5	0.5
1.00	0.023411	0.4	0.4	1.00	0.034406	0.0	0.0
5.00	0.020557	2.3	1.6	5.00	0.028255	4.9	4.7
10.0	0.016688	4.5	4.3	10.0	0.020925	5.7	5.4
15.0	0.013401	2.2	2.2	15.0	0.015733	1.0	1.0
20.0	0.010907	1.9	2.0	20.0	0.012540	2.4	2.5
25.0	0.009142	5.5	5.8	25.0	0.010748	1.6	1.7
30.0	0.007956	7.2	7.8	30.0	0.009812	3.7	3.6
40.0	0.006714	4.4	4.6				
50.0	0.006257	4.6	4.4				
$n = 0.8$				$n = 0.7$			
Re	Fitted λ_{oc}	Percent Error λ_{oc}	Percent Error ε	Re	Fitted λ_{oc}	Percent Error λ_{oc}	Percent Error ε
0.10	0.052342	0.3	0.3	0.10	0.077557	1.4	1.4
1.00	0.050246	0.5	0.5	1.00	0.072527	0.8	0.8
2.00	0.047124	1.5	1.5	2.00	0.065375	2.9	2.8
3.00	0.043749	4.0	3.9	3.00	0.058109	6.0	5.6
4.00	0.040364	6.1	5.7	4.00	0.051330	7.4	6.8
5.00	0.037105	7.3	6.8	5.00	0.045304	7.4	6.9
10.0	0.024442	4.4	4.2	7.50	0.033903	5.2	4.9
15.0	0.017810	1.8	1.8	10.0	0.027044	6.1	5.7
$n = 0.6$				$n = 0.5$			
Re	Fitted λ_{oc}	Percent Error λ_{oc}	Percent Error ε	Re	Fitted λ_{oc}	Percent Error λ_{oc}	Percent Error ε
0.10	0.114791	2.8	2.9	0.10	0.169488	4.7	4.9
1.00	0.102316	1.0	1.0	0.50	0.156669	4.7	4.9
2.00	0.086031	3.7	3.6	1.00	0.137525	1.9	1.9
3.00	0.071302	5.6	5.2	1.50	0.118900	0.2	0.2
4.00	0.059285	5.4	5.1	2.00	0.102369	1.0	1.0
5.00	0.050073	5.4	5.0	2.50	0.088460	1.3	1.3
6.00	0.043322	6.7	6.2	3.00	0.077191	1.9	1.9
7.00	0.038549	6.8	6.3	4.00	0.061508	6.1	5.6

$n = 0.4$			
Re	Fitted λ_{oc}	Percent Error λ_{oc}	Percent Error ε
0.10	0.248716	7.2	7.7
0.50	0.212392	7.8	8.3
1.00	0.165706	7.1	7.4
1.50	0.128908	7.2	7.6
2.00	0.103299	6.1	6.3
2.50	0.086833	2.0	2.0

Table 7.7: Triangular 30.0-60.0 Flat Bottom 0.316 Fitted Curve Outer Cavity Shape Factor Data Summary

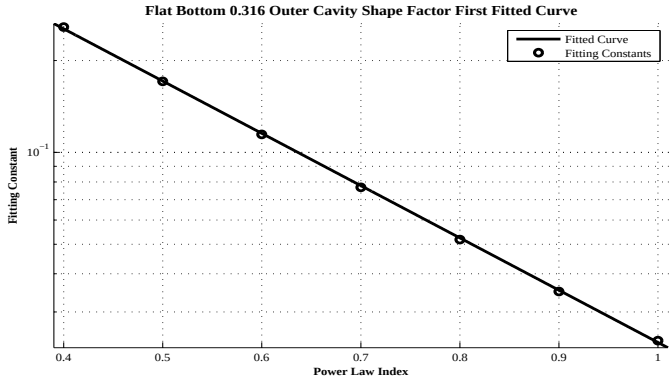

Figure 7.11: Triangular 30.0-60.0 Flat Bottom 0.316 Outer Cavity Shape Factor First Fitted Curve Plotted Results

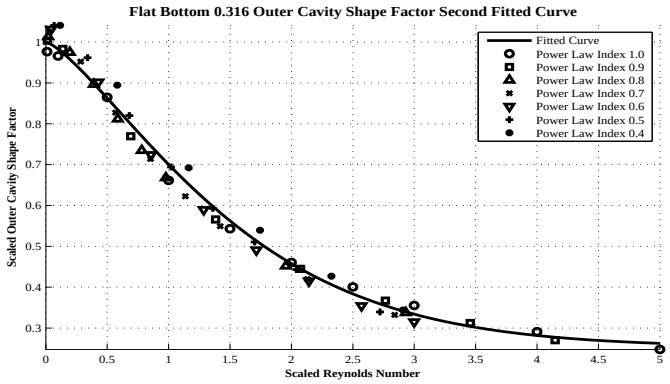

Figure 7.12: Triangular 30.0-60.0 Flat Bottom 0.316 Outer Cavity Shape Factor Second Fitted Curve Plotted Results

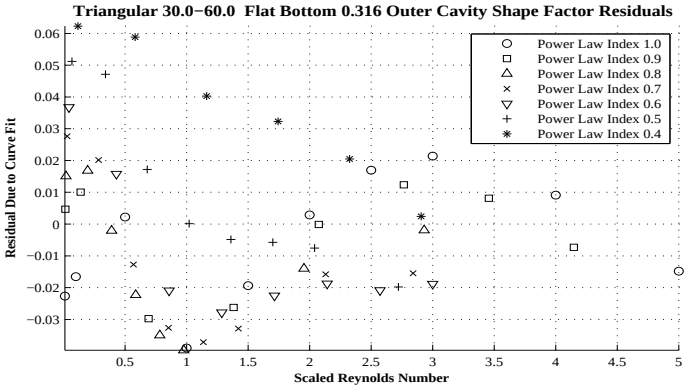

Figure 7.13: Triangular 30.0-60.0 Flat Bottom 0.316 Outer Cavity Shape Factor Second Fitted Curve Plotted Residuals

Outer Cavity Shape Factor

$n = 1.0$		$n = 0.9$		$n = 0.8$		$n = 0.7$	
Re	Fluent λ_{oc}	Re	Fluent λ_{oc}	Re	Fluent λ_{oc}	Re	Fluent λ_{oc}
0.10	0.020443	0.10	0.031465	0.10	0.048571	0.10	0.075221
1.00	0.020270	1.00	0.030946	1.00	0.046983	1.00	0.070380
5.00	0.017983	5.00	0.025087	2.00	0.043658	2.00	0.061820
10.0	0.014735	10.0	0.018904	3.00	0.039947	3.00	0.053823
15.0	0.012299	15.0	0.015029	4.00	0.036455	4.00	0.047208
20.0	0.010529	20.0	0.012466	5.00	0.033356	5.00	0.041849
25.0	0.009207	25.0	0.010651	10.0	0.022967	7.50	0.032282
30.0	0.008188	30.0	0.009283	15.0	0.017352	10.0	0.025894
40.0	0.006722						
50.0	0.005719						

$n = 0.6$		$n = 0.5$		$n = 0.4$	
Re	Fluent λ_{oc}	Re	Fluent λ_{oc}	Re	Fluent λ_{oc}
0.10	0.116912	0.10	0.182308	0.10	0.283997
1.00	0.102719	0.50	0.167909	0.50	0.242296
2.00	0.083181	1.00	0.143503	1.00	0.187425
3.00	0.068142	1.50	0.121834	1.50	0.146283
4.00	0.057049	2.00	0.104299	2.00	0.116333
5.00	0.048540	2.50	0.090201	2.50	0.095205
6.00	0.041792	3.00	0.079109		
7.00	0.036493	4.00	0.061309		

Table 7.8: Triangular 30.0-60.0 Flat Bottom 0.416 ANSYS Fluent Outer Cavity Shape Factor Data Summary

Fitting Constants

Rheological and Model Specific		Model Specific	
n	c_1		
1.0	0.021671	c_2	0.020796
0.9	0.031749	c_3	4.477007
0.8	0.049374	c_4	2.104691
0.7	0.077163	c_5	0.478820
0.6	0.119799	c_6	0.210303
0.5	0.195965	c_7	0.000000
0.4	0.318093	c_8	0.672537

Table 7.9: Triangular 30.0-60.0 Flat Bottom 0.416 Curve Fitting Constants Summary

Outer Cavity Shape Factor

$n = 1.0$				$n = 0.9$			
Re	Fitted λ_{oc}	Percent Error λ_{oc}	Percent Error ε	Re	Fitted λ_{oc}	Percent Error λ_{oc}	Percent Error ε
0.10	0.020714	1.3	1.3	0.10	0.032355	2.8	2.7
1.00	0.019992	1.4	1.4	1.00	0.030754	0.6	0.6
5.00	0.017138	4.7	4.9	5.00	0.024723	1.5	1.5
10.0	0.014258	3.2	3.3	10.0	0.019179	1.5	1.4
15.0	0.011992	2.5	2.6	15.0	0.015247	1.5	1.4
20.0	0.010208	3.0	3.1	20.0	0.012458	0.1	0.1
25.0	0.008804	4.4	4.6	25.0	0.010480	1.6	1.6
30.0	0.007699	6.0	6.3	30.0	0.009077	2.2	2.3
40.0	0.006144	8.6	9.4				
50.0	0.005181	9.4	10.3				

$n = 0.8$				$n = 0.7$			
Re	Fitted λ_{oc}	Percent Error λ_{oc}	Percent Error ε	Re	Fitted λ_{oc}	Percent Error λ_{oc}	Percent Error ε
0.10	0.050491	4.0	3.8	0.10	0.078659	4.6	4.4
1.00	0.046865	0.3	0.3	1.00	0.070256	0.2	0.2
2.00	0.043204	1.0	1.0	2.00	0.062191	0.6	0.6
3.00	0.039896	0.1	0.1	3.00	0.055278	2.7	2.6
4.00	0.036907	1.2	1.2	4.00	0.049354	4.5	4.3
5.00	0.034205	2.5	2.5	5.00	0.044277	5.8	5.4
10.0	0.024133	5.1	4.8	7.50	0.034537	7.0	6.5
15.0	0.018061	4.1	3.9	10.0	0.027914	7.8	7.2

$n = 0.6$				$n = 0.5$			
Re	Fitted λ_{oc}	Percent Error λ_{oc}	Percent Error ε	Re	Fitted λ_{oc}	Percent Error λ_{oc}	Percent Error ε
0.10	0.122155	4.5	4.3	0.10	0.188482	3.4	3.2
1.00	0.102212	0.5	0.5	0.50	0.164781	1.9	1.9
2.00	0.084659	1.8	1.7	1.00	0.140198	2.3	2.3
3.00	0.070931	4.1	3.9	1.50	0.120231	1.3	1.3
4.00	0.060195	5.5	5.2	2.00	0.104015	0.3	0.3
5.00	0.051798	6.7	6.2	2.50	0.090844	0.7	0.7
6.00	0.045230	8.2	7.5	3.00	0.080148	1.3	1.3
7.00	0.040094	9.9	8.8	4.00	0.064404	5.0	4.7

$n = 0.4$			
Re	Fitted λ_{oc}	Percent Error λ_{oc}	Percent Error ε
0.10	0.286523	0.9	0.9
0.50	0.224671	7.3	7.7
1.00	0.169860	9.4	10.0
1.50	0.132552	9.4	10.0
2.00	0.107158	7.9	11.8
2.50	0.089874	5.6	5.6

Table 7.10: Triangular 30.0-60.0 Flat Bottom 0.416 Fitted Curve Outer Cavity Shape Factor Data Summary

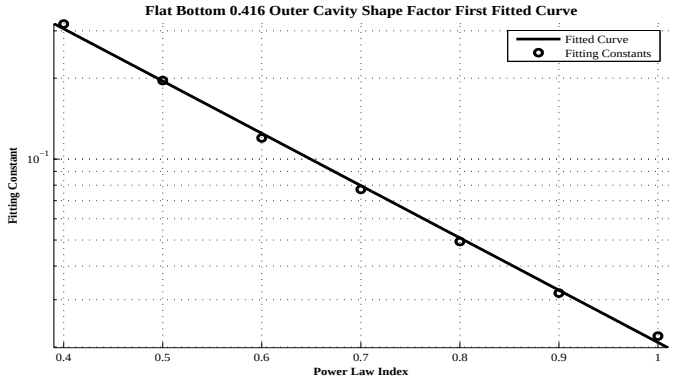

Figure 7.14: Triangular 30.0-60.0 Flat Bottom 0.416 Outer Cavity Shape Factor First Fitted Curve Plotted Results

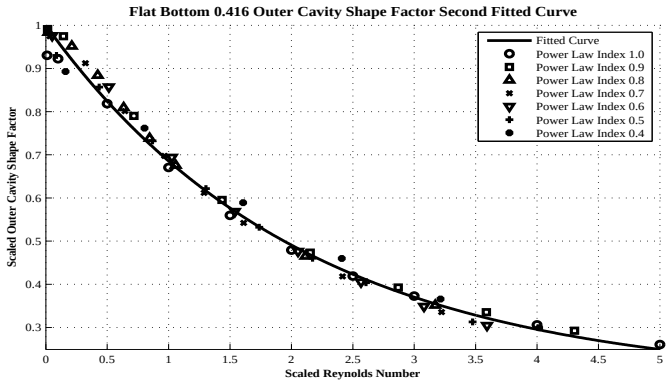

Figure 7.15: Triangular 30.0-60.0 Flat Bottom 0.416 Outer Cavity Shape Factor Second Fitted Curve Plotted Results

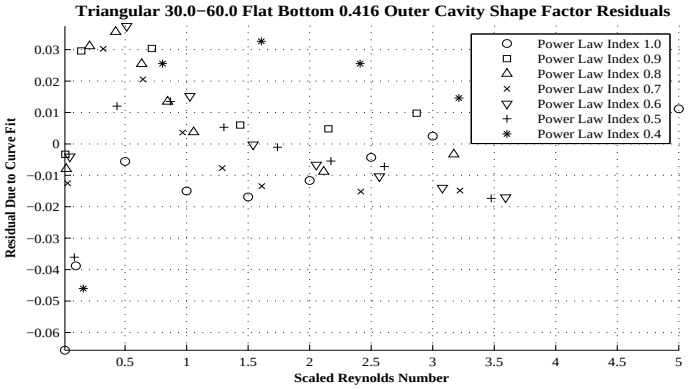

Figure 7.16: Triangular 30.0-60.0 Flat Bottom 0.416 Outer Cavity Shape Factor Second Fitted Curve Plotted Residuals

Outer Cavity Shape Factor

$n = 1.0$		$n = 0.9$		$n = 0.8$		$n = 0.7$	
Re	Fluent λ_{oc}	Re	Fluent λ_{oc}	Re	Fluent λ_{oc}	Re	Fluent λ_{oc}
0.10	0.019495	0.10	0.030237	0.10	0.047023	0.10	0.073351
1.00	0.019349	1.00	0.029783	1.00	0.045582	1.00	0.068819
5.00	0.017362	5.00	0.024480	2.00	0.042540	2.00	0.060749
10.0	0.014386	10.0	0.018614	3.00	0.039089	3.00	0.053088
15.0	0.012077	15.0	0.014850	4.00	0.035792	4.00	0.046673
20.0	0.010371	20.0	0.012331	5.00	0.032832	5.00	0.041432
25.0	0.009084	25.0	0.010523	10.0	0.022733	7.50	0.031921
30.0	0.008085	30.0	0.009147	15.0	0.017116	10.0	0.025474
40.0	0.006640						
50.0	0.005642						

$n = 0.6$		$n = 0.5$		$n = 0.4$	
Re	Fluent λ_{oc}	Re	Fluent λ_{oc}	Re	Fluent λ_{oc}
0.10	0.114754	0.10	0.179764	0.10	0.282815
1.00	0.101159	0.50	0.165982	0.50	0.240004
2.00	0.082281	1.00	0.142141	1.00	0.186206
3.00	0.067543	1.50	0.120840	1.50	0.144259
4.00	0.056450	2.00	0.103414	2.00	0.114915
5.00	0.047799	2.50	0.089127	2.50	0.098190
6.00	0.041289	3.00	0.077406		
7.00	0.037918	4.00	0.062827		

Table 7.11: Triangular 30.0-60.0 Flat Bottom 0.516 ANSYS Fluent Outer Cavity Shape Factor Data Summary

Fitting Constants

Rheological and Model Specific		Model Specific	
n	c_1		
1.0	0.020474	c_2	0.019812
0.9	0.031749	c_3	4.457637
0.8	0.048327	c_4	2.010408
0.7	0.073404	c_5	0.478762
0.6	0.114131	c_6	0.224531
0.5	0.187674	c_7	0.000000
0.4	0.297042	c_8	0.651407

Table 7.12: Triangular 30.0-60.0 Flat Bottom 0.516 Curve Fitting Constants Summary

Outer Cavity Shape Factor

$n = 1.0$				$n = 0.9$			
Re	Fitted λ_{oc}	Percent Error λ_{oc}	Percent Error ε	Re	Fitted λ_{oc}	Percent Error λ_{oc}	Percent Error ε
0.10	0.019734	1.2	1.2	0.10	0.030768	1.8	1.7
1.00	0.019055	1.5	1.5	1.00	0.029278	1.7	1.7
5.00	0.016367	5.7	6.1	5.00	0.023655	3.4	3.5
10.0	0.013656	5.1	5.3	10.0	0.018471	0.8	0.8
15.0	0.011522	4.6	4.8	15.0	0.014782	0.5	0.5
20.0	0.009843	5.1	5.4	20.0	0.012156	1.4	1.4
25.0	0.008521	6.2	6.6	25.0	0.010287	2.2	2.3
30.0	0.007480	7.5	8.1	30.0	0.008957	2.1	2.1
40.0	0.006016	9.4	10.3				
50.0	0.005109	9.4	10.4				
$n = 0.8$				$n = 0.7$			
Re	Fitted λ_{oc}	Percent Error λ_{oc}	Percent Error ε	Re	Fitted λ_{oc}	Percent Error λ_{oc}	Percent Error ε
0.10	0.047928	1.9	1.9	0.10	0.074544	1.6	1.6
1.00	0.044594	2.2	2.2	1.00	0.066917	2.8	2.8
2.00	0.041222	3.1	3.2	2.00	0.059562	2.0	2.0
3.00	0.038168	2.4	2.4	3.00	0.053225	0.3	0.3
4.00	0.035403	1.1	1.1	4.00	0.047767	2.3	2.3
5.00	0.032898	0.2	0.2	5.00	0.043065	3.9	3.8
10.0	0.023504	3.4	3.3	7.50	0.033967	6.4	6.0
15.0	0.017781	3.9	3.7	10.0	0.027701	8.7	8.0
$n = 0.6$				$n = 0.5$			
Re	Fitted λ_{oc}	Percent Error λ_{oc}	Percent Error ε	Re	Fitted λ_{oc}	Percent Error λ_{oc}	Percent Error ε
0.10	0.115611	0.7	0.7	0.10	0.178283	0.8	0.8
1.00	0.097746	3.4	3.5	0.50	0.157420	5.2	5.4
2.00	0.081849	0.5	0.5	1.00	0.135524	4.7	4.8
3.00	0.069270	2.6	2.5	1.50	0.117505	2.8	2.8
4.00	0.059319	5.1	4.8	2.00	0.102676	0.7	0.7
5.00	0.051445	7.6	7.0	2.50	0.090472	1.5	1.5
6.00	0.045215	9.5	8.5	3.00	0.080428	3.9	3.7
7.00	0.040285	6.2	5.8	4.00	0.065361	4.0	3.8

$n = 0.4$			
Re	Fitted λ_{oc}	Percent Error λ_{oc}	Percent Error ε
0.10	0.271402	4.0	2.1
0.50	0.217620	9.3	6.0
1.00	0.168590	9.5	8.0
1.50	0.134136	7.0	9.4
2.00	0.109925	4.3	7.7
2.50	0.092912	5.4	0.3

Table 7.13: Triangular 30.0-60.0 Flat Bottom 0.516 Fitted Curve Outer Cavity Shape Factor Data Summary

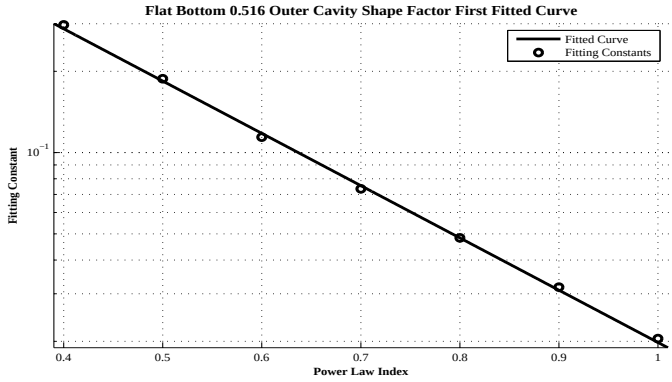

Figure 7.17: Flat Bottom 0.516 Outer Cavity Shape Factor First Fitted Curve Plotted Results

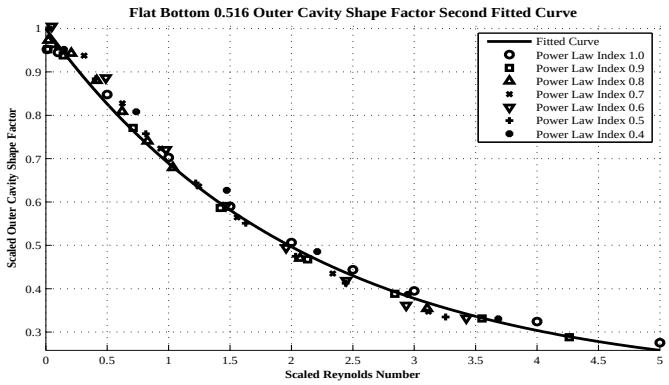

Figure 7.18: Flat Bottom 0.516 Outer Cavity Shape Factor Second Fitted Curve Plotted Results

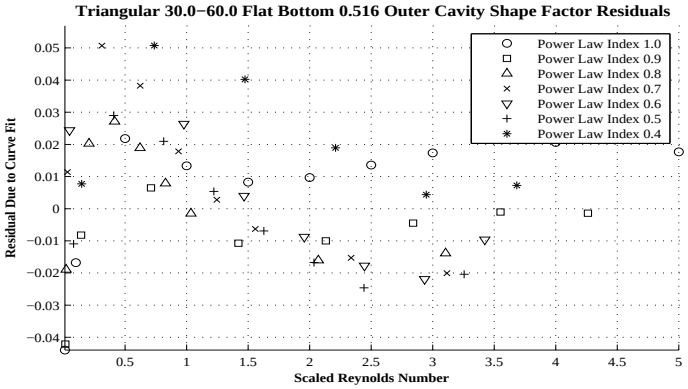

Figure 7.19: Triangular 30.0-60.0 Flat Bottom 0.516 Outer Cavity Shape Factor Second Fitted Curve Plotted Residuals

	Outer Cavity Damping Dimensionless Group		
n	ς Percent Increase		
	$L_{fb} = 0.316$	$L_{fb} = 0.416$	$L_{fb} = 0.516$
1.0	20.9	75.7	83.9
0.9	18.1	67.9	75.3
0.8	15.4	62.4	69.5
0.7	12.9	54.3	60.3
0.6	10.8	47.6	51.8
0.5	8.6	41.4	45.6
0.4	7.0	35.9	39.3

Table 7.14: Proposed Outer Cavity Design Outer Cavity Damping Dimensionless Group Data Summary

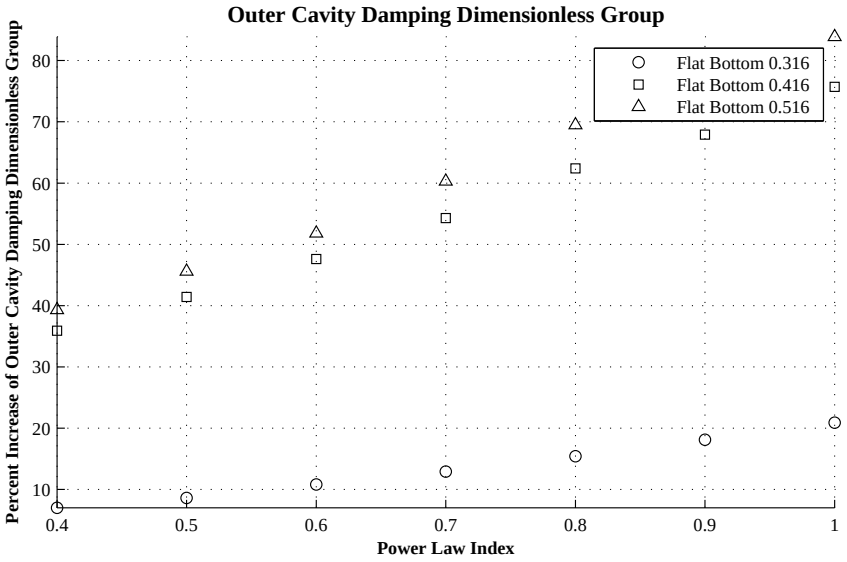

Figure 7.20: Proposed Outer Cavity Design Outer Cavity Damping Dimensionless Group Percent Increase Plotted Results

For each of the cases considered in the proposed outer cavity design, the thirty-sixty degree expansion and contraction angle triangular cross sections with 0.316, 0.416, and 0.516 ratios of the characteristic flat bottom length, cognitive results for the outer cavity shape factor and corresponding outer cavity damping dimensionless group (Eq. 4.0.10b) were obtained for shear thinning fluids, ranging in power law index as low as $n = 0.4$ to the Newtonian case of $n = 1.0$, of generalized Newtonian rheology. The theoretically obtained data in the tabulated results (Table 7.14) of the outer cavity damping dimensionless

group as well as the presentation of the plotted curve (Fig. 7.20) illustrate three important observations associated with the reduction in the height of the cross section (Fig. 3.1) perpendicular to the direction of flow on the relative ability of the proposed outer cavity design to dampen nonuniformities in the flow per unit cavity width exiting the inner slot. First, a relative increase in the outer cavity damping dimensionless group is demonstrated with the continued successive reduction in the height of the cross section perpendicular to the direction of flow. Here, the truncation of the outer cavity cross sectional area results in an maximum percent increase in the outer cavity damping dimensionless group of 20.9, 75.7, and 83.9, with a minimum of 7.0, 35.9, and 39.3, for the respective thirty-sixty degree expansion and contraction angle triangular cross sections with 0.316, 0.416, and 0.516 ratios of the characteristic flat bottom length. Similar to the function of the inner cavity, the presence of disparate resistances to flow in the outer cavity geometry, such that the resistance to flow along the width of the cavity is made low by choosing a relatively large cross sectional area, can effectively reduce nonuniformities in the flow per unit cavity width exiting the inner slot due to pressure variations in the inner cavity. Second, the resulting increase in the outer cavity damping dimensionless group becomes less severe with a corresponding decrease of the power law index for a given flow condition. It is important to note that although shear thinning behavior promotes the widthwise redistribution of flow along the width of a dual cavity coating die by reducing the resistance to flow along the outer cavity, this effect is amplified in the cross section of the outer slot, thus hindering the overall performance of the outer cavity. Third, the resulting increase in the outer cavity damping dimensionless group also becomes less severe with the successive continued reduction in the height of the cross section perpendicular to the direction of flow. As expected, the negative impact on the ability of the outer cavity to improve flow uniformity due to the continued reduction of the outer cavity cross sectional area is recoverable through the outer cavity shape factor, as the shear thinning behavior of generalized Newtonian rheological models reduces the resistance to flow along the width of the outer cavity. These observations of the numerically obtained outer cavity damping dimensionless group in the proposed design of the outer cavity shape are consistent with the fundamental physics observed in the outer cavity of a dual cavity coating die, providing valuable information for the investigation into the the optimum design of the outer cavity cross section.

Investigation of the outer cavity damping dimensionless group (Eq. 4.0.10b) provides meaningful insight into the relative impact of the ability of the outer cavity to improve flow uniformity, however the primary interest of coating die design is the peak to peak variation in the widthwise flow distribution exiting the outer slot. Through the solution of the outer cavity approximate model (Chapter 4), a method for obtaining the desired expression for

the widthwise uniformity of the final coating film has been demonstrated, which allows many flow conditions and geometric parameters to be tested efficiently and effectively. In a practical demonstration of the solution of the outer cavity approximate model, identical considerations in the geometrical parameters of the computational domain employed in the three dimensional validation of the theoretical approximate modeling approach (Chapter 6), with the exception of those associated with the specific cross sectional shape, are utilized to examine the proposed outer cavity design. Here, the solution of the outer cavity approximate model illustrates the relative performance of the proposed outer cavity designs through the peak to peak variation in the widthwise flow distribution exiting the outer slot as well as the outer cavity damping factor (Eq. 4.0.14).

Outer Cavity Damping Factor			
n	ε Percent Increase		
	$L_{fb} = 0.316$	$L_{fb} = 0.416$	$L_{fb} = 0.516$
1.0	16.7	76.2	86.8
0.9	15.9	67.1	76.6
0.8	14.6	62.9	73.2
0.7	13.2	54.5	63.2
0.6	11.6	46.4	52.9
0.5	10.0	41.6	47.5
0.4	7.8	36.3	39.8

Table 7.15: Proposed Outer Cavity Design Outer Cavity Damping Factor Data Summary

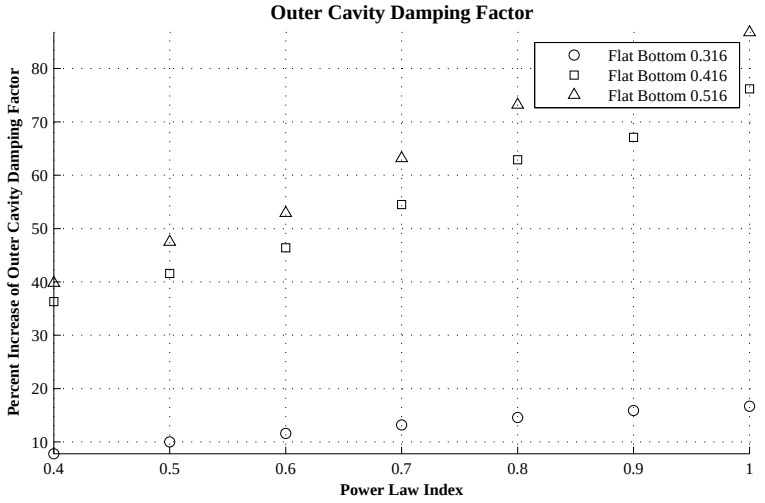

Figure 7.21: Proposed Outer Cavity Design Outer Cavity Damping Factor Percent Increase Plotted Results

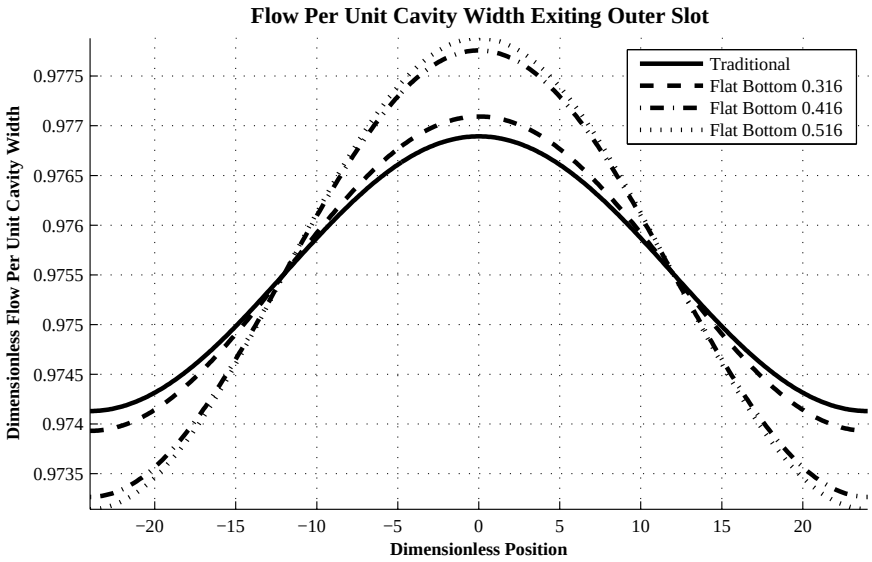

Figure 7.22: Proposed Outer Cavity Design Newtonian Flow Per Unit Cavity Width Profile $n = 1.0$ and $Re = 0.1$

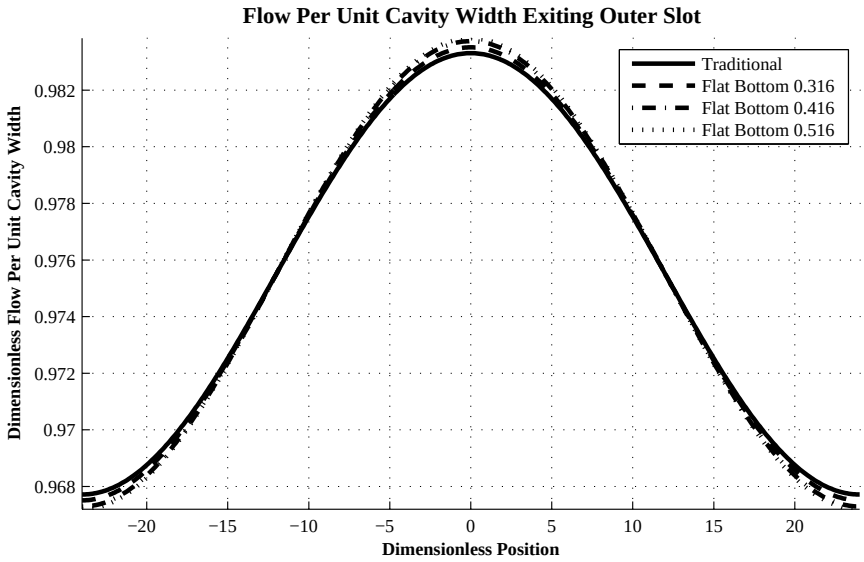

Figure 7.23: Proposed Outer Cavity Design Non-Newtonian Flow Per Unit Cavity Width Profile $n = 0.4$ and $Re = 0.1$

For each of the cases considered in the proposed outer cavity design, results for the peak to peak variation in the widthwise flow distribution exiting the outer cavity as well as the outer cavity damping factor (Eq. 4.0.14) were obtained for shear thinning fluids of generalized Newtonian rheology with a power law index of $n = 1.0$ and $n = 0.4$ at negligible Reynolds number. The general observations of the theoretically obtained data in the tabulated results (Table 7.15) of the outer cavity damping factor as well as the presentation of the plotted curves (Figs. 7.21 to 7.23) of the peak to peak variation in the predicted flow per unit cavity width entering the outer slot are consistent with those examined in the outer cavity dimensionless group (Eq. 4.0.10b). Here, a relative increase in the outer cavity damping factor, and thus amplified peak to peak variation in the flow per unit cavity width exiting the outer slot, is demonstrated with the continued successive reduction in the height of the cross section (Fig. 3.1) perpendicular to the direction of flow. In the proposed outer cavity design, the truncation of the outer cavity cross sectional area results in a maximum percent increase in the outer cavity damping factor of 16.7, 76.2, and 86.8, with a minimum of 7.8, 36.3, and 39.8, for the respective thirty-sixty degree expansion and contraction angle triangular cross sections with 0.316, 0.416, and 0.516 ratios of the characteristic flat bottom length. As expected, the continued reduction of the outer cavity cross sectional area consequently homogenizes the resistances to flow demonstrated in the outer cavity geometry, whereas the presence of disparate resistances to flow is required for the widthwise redistribution of the flow per unit cavity width. Shear thinning rheology, however, counteracts this increase in resistance to flow along the axis of the outer cavity, and thus the diminishing ability of the outer cavity to improve flow uniformity is less sensitive for fluids of generalized Newtonian rheology with a power law dependence of viscosity on shear rate. It is important to note that the resulting relative increase in the outer cavity damping factor, and thus amplified peak to peak variation in the flow per unit cavity width exiting the outer slot, demonstrates good agreement with the observed relative percent increase of the outer cavity damping dimensionless group. Therefore, an investigation of the outer cavity damping dimensionless group offers meaningful insight into the relative impact of the proposed design on the ability of the outer cavity to improve flow uniformity and the desired peak to peak variation of the flow per unit cavity width exiting the outer slot. These observations of the theoretically obtained data are consistent with the fundamental physics expected in the outer cavity of a dual cavity coating die and demonstrate the utility of the approximate die design modeling approach through a quantitative examination of the outer cavity damping factor as well as the visual representation of the flow distribution profile.

It has been demonstrated that the reduction in the height of the cross section (Fig. 3.1) perpendicular to the direction of primary flow in the outer cavity, which is necessary to

maintain sufficient shear stress along the lower boundary of the streamlined triangular outer cavity cross section, results in a diminished ability of the outer cavity to improve flow uniformity. This negative impact on the damping ability of the outer cavity is associated with the corresponding loss in cross sectional area, which results in an increased resistance to flow along the width of the outer cavity and subsequent decrease in the gross partitioning of flow resistances which drive the axial flow responsible for damping nonuniformities in the flow per unit cavity width. A possible counter balance to restore the original damping ability of the untruncated triangular outer cavity cross sectional design to the proposed flat bottom outer cavity design is to increase length of the outer cavity, the flow path length, and consequently increase the outer cavity cross sectional area.

Outer Cavity Flow Path Length			
n	L_{oc} Percent Increase		
	$L_{fb} = 0.316$	$L_{fb} = 0.416$	$L_{fb} = 0.516$
1.0	7.0	22.7	28.6
0.9	6.6	22.5	28.7
0.8	6.1	22.9	29.8
0.7	5.7	22.3	29.6
0.6	5.2	22.0	29.4
0.5	4.7	21.8	30.3
0.4	4.3	21.8	31.3

Table 7.16: Proposed Outer Cavity Design Required Flow Path Length Data Summary

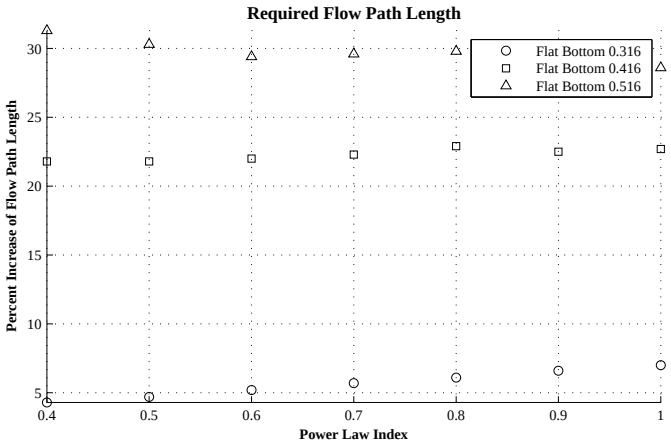

Figure 7.24: Proposed Outer Cavity Design Required Flow Path Length Plotted Results

As evident from the theoretically obtained data in the tabulated results (Table 7.16) as well as the presentation of the plotted curve (Fig. 7.24), a successive increase in the additional

flow path length (Fig. 3.1) required is demonstrated with the corresponding reduction in the height of the cross section perpendicular to the direction of flow. To achieve a widthwise redistribution of fluid in the proposed flat bottom outer cavity design which is equivalent to the untruncated triangular outer cavity design, a corresponding 5.7, 22.3, and 29.7 average percent increase of the original flow path length is required for the respective triangular outer cavity cross sections of 0.316, 0.416, and 0.516 ratios of the characteristic flat bottom length. In this way, the reduced height of the outer cavity cross section perpendicular to the direction of the primary flow maintains sufficient shear stress along the lower boundary, while the streamlined shape of the triangular cross section is preserved to prevent vortex formation and the cross sectional area is now suitable to promote the disparate resistance to flow necessary for adequate damping.

Although the expansion of the outer cavity cross sectional area through an increase in the flow path length (Fig. 3.1) fundamentally improves the ability of the outer cavity to dampen flow nonuniformities, mechanical constraints are another important consideration in the optimum outer cavity design. In practical applications, a dual cavity coating die design may be required to fit within an existing process, restricting the allowable size of the design, while an extension of the cantilevered outer slot can result in mechanical deflections which distort the intended geometry of the cross sectional design, thus altering the flow uniformity or inducing additional mechanical stress. Therefore, an extension of the flow path length in the proposed outer cavity design, intending to expand the cross sectional area of the outer cavity and improve flow uniformity, requires further consideration and investigation of the associated mechanical constraints.

The goal of dual cavity coating die design is to deliver a uniform liquid film for a wide range of fluid rheologies and flow conditions within specified uniformity limits, where the design of the optimum outer cavity cross sectional shape must consider the effects of streamlining and recirculation as well as fluid stagnation and cavity wall shear stress. A viable method for maintaining sufficient shear stress along the lower boundary of the outer cavity cross section while preserving the traditional streamlined shape necessary to eliminate vortex formation and recirculation has been investigated in the proposed outer cavity design. It is important to note that the reduction in the height of the cross section associated with the proposed outer cavity design, required to prevent the stagnation of shear thinning fluids, results in an increase in the resistance to flow along the width of the outer cavity and corresponding diminished ability of the outer cavity to dampen nonuniformities in the flow per unit cavity width exiting the inner slot. The ultimate design of the optimum outer cavity cross sectional shape, given a range of fluid rheologies and flow conditions, must often result from a compromise of the effects due to vortex formation and recirculation, fluid stagnation,

and mechanical deflections and stresses.

Chapter 8

Final Conclusions

The focus of this research was to utilize Computational Fluid Dynamics as idealized experimental data, which was to be used for the improvement and verification of the theoretical outer cavity approximate die design model, as well as the provision of the first numerical computations of the generalized outer cavity shape factor. Here, a two dimensional validation of the fundamental assumptions utilized in the derivation of the outer cavity approximate model was performed, while an attempted three dimensional validation of the predicted flow per unit cavity width exiting the outer slot provided confidence in the validity of the approximate modeling approach. A final, practical demonstration of the solution of the outer cavity approximate model provided valuable information for the investigation into the the optimum design of the outer cavity cross section.

Beginning with the derivation of the outer cavity approximate model, a method for obtaining the flow equations of the outer cavity of a dual cavity coating die has been demonstrated, which accounted for the three dimensional nature of the equations of motion and coupled the flow through nonlinearities in the governing equations occurring due to inertia or non-Newtonian rheologies. An expression for the desired relationship between the axial pressure gradient and volumetric flow along the outer cavity axis has been provided, which was a valuable tool for the determination of the desired peak to peak variation in widthwise flow uniformity exiting the outer slot of a dual cavity coating die. The system of equations that governed the combined inner slot and outer cavity flows has been solved through a Fourier analysis, such that any desired form of the flow per unit cavity width exiting the inner slot could be represented in the outer cavity approximate model, which provided the desired expression for the widthwise uniformity of the final coating film.

The outer cavity shape factor was a necessary input to the approximate die design models which incorporated the specific cross sectional shape of the cavity domain into the pressure drop flow relationship, and the determination of the outer cavity shape factor required the

solution to the perturbed set of three dimensional equations that governed fluid flow in the outer cavity domain. A method for obtaining the outer cavity shape factor, which utilized commercially available software, has been established to correlate the perturbed equations of the outer cavity approximate model with those implemented within the ANSYS Fluent package. The design of the outer cavity required a more complex shape than that of the inner cavity, which prevented regions of stagnation and recirculation, thus three specific triangular outer cavity designs were considered in the computation of the outer cavity shape factor. For each of the cases considered in the computation of the outer cavity shape factor, the triangular fifteen-fifteen, thirty-thirty, and thirty-sixty degree expansion and contraction angles respectively, cognitive results for the outer cavity shape factor were obtained for shear thinning fluids of generalized Newtonian rheology, which ranged in power law index as low as $n = 0.4$ to the Newtonian case of $n = 1.0$, with numerous flow conditions. A particularly convenient representation of the outer cavity shape factor for a given cross sectional design characterized the numerically determined data over the entire range of fluid rheologies and flow conditions considered through a bipartite series of fitted curves. In this way, the outer cavity shape factor for a given cross sectional design could be extracted for any given fluid rheology and flow condition, within the limits of the plotted data, as input to the outer cavity approximate die design model.

In the derivation of the outer cavity approximate model, it was anticipated that the back pressure of the outer slot greatly exceeded pressure variations in the outer cavity cross section, due to the typical aspect ratios demonstrated in the geometry of dual cavity coating die design as the ratio of the length of the outer slot to the height of the outer slot greatly exceeded the ratio of the length of the outer cavity to the height of the outer cavity. Validation of the anticipated dominant back pressure of the outer slot directly corresponded to the simulation of the two dimensional base flow in the computation of the outer cavity shape factor, and thus could be investigated in the two dimensional cross section of the outer cavity. Observations of the numerically obtained pressure variations in the cross section of the outer cavity provided validation of the anticipated dominant back pressure of the outer slot assumed in the derivation of the outer cavity approximate model.

The flow in dual cavity coating die designs was three dimensional in nature, and thus the most accurate approach to the analysis of widthwise flow uniformity and ultimate geometrical designs was to solve the complete set of three dimensional equations governing flow, without simplifications, through numerical computation. These simulations were numerically intensive, and required over three hundred hours of continuous run time to accurately simulate a single die flow condition with no guarantee a solution would even converge. Observations of the numerically obtained flow per unit cavity width exiting the outer cavity

provided good agreement and confidence in the validity of the theoretical approximate modeling approach. In the three dimensional validation of the outer cavity approximate model, the realistic aspect ratios demonstrated in dual cavity coating die designs utilized in typical industrial applications, specifically the coating width and slot height, could not be obtained with the available resources of the Rochester Institute of Technologys Research Computing Large Memory Computer. Therefore, the limitations of the validity of the outer cavity approximate model could not be identified, however, the attempts of the complete three dimensional numerical simulation of the outer cavity further demonstrated the utility and importance of theoretical approximate die design models.

A viable method for maintaining sufficient shear stress along the lower boundary of the outer cavity cross section, which preserved the traditional streamlined shape necessary to eliminate vortex formation and recirculation, has been investigated in the proposed outer cavity design. It is important to note that the reduction in the height of the cross section associated with the proposed outer cavity design, required to prevent the stagnation of shear thinning fluids, resulted in an increase in the resistance to flow along the width of the outer cavity and corresponding diminished ability of the outer cavity to dampen nonuniformities in the flow per unit cavity width exiting the inner slot.

Ultimately, this research provided a firmer foundation for the design of the outer cavity in a dual cavity coating die, and further demonstrated the utility and importance of the theoretical approximate die design modeling approach; however, there are several opportunities present for future research of the analysis and design of dual cavity coating dies. In the derivation of the outer cavity approximate model, the complete set of three dimensional governing momentum equations were applied for generalized Newtonian fluids with a power law dependence of viscosity on shear rate, which is also common of the previously cited analyses in the current literature (Ruschak and Weinstein, 1997a). However, typical rheological curves of polymers may approach a constant Newtonian viscosity at low and high rates of strain, making the power law model inadequate for fluids that may be classified as moderately shear thinning. Future research of the outer cavity approximate die deign model could incorporate more complex, yet general, rheological models to more accurately represent the fluid rheology of polymers in the outer cavity of a dual cavity coating die design. The outer cavity shape factor has also been determined through an approximate method, as reported by Weinstein (2010), utilizing an assumed velocity distribution in the two dimensional cross section of the outer cavity. Velocity profiles extracted from the numerical solution of the base flow computation could provide suggestion for a more appropriate form of the assumed velocity distribution and improvement to this efficient estimation of the outer cavity shape factor. The realistic aspect ratios demonstrated in the dual cavity

coating die designs utilized in typical industrial applications could not be obtained in the three dimensional validation of the outer cavity approximate model with the available computational resources. An important step in the future work of dual cavity coating die design would establish an explicit identification of the limitations and applicability of the theoretical outer cavity approximate model and the corresponding pressure drop flow relationship provided. Furthermore, an investigation of mechanical constraints, specifically the sensitivity of mechanical deflections and surface roughness effects on film thickness uniformity, could be incorporated in future examination of the optimum outer cavity cross sectional design.

An advantageous aspect of dual cavity coating die design is the ability of the outer cavity to dampen nonuniformities in the flow per unit cavity width exiting the inner slot due to pressure variations in the inner cavity. This feature improves the versatility of coating die design while reducing the negative effects of uncertainties associated with vortex formation in the inlet region, stagnation or stiffening of shear thinning fluids, and fabrication tolerances. The outer cavity approximate die design model is an essential tool for the design of dual cavity coating dies, as full numerical computation of the complete set of three dimensional equations governing fluid flow is numerically intensive, often requiring long computational times to accurately simulate a single die flow condition with no guarantee a solution will converge, and a meaningful experimental verification of lateral flow uniformity requires expensive hardware, while there are too many geometric and flow parameters for a purely experimental approach to be efficient .

References

Atkinson B., Brocklebank M.P., Card C.C.H., and Smith J.M., *Low Reynolds Number Developing Flows*, American Institute of Chemical Engineers, **15**, 1969

Carly J.F., *Flow of Melts in Crosshead Slit Dies; Criteria for Die Design*, Journal of Applied Physics, **25**, 1954

Durst F., Lange U., and Raszillier H., *Optimization of Distribution Chambers of Coating Facilities*, Chemical Engineering Science, **49**, 1994

Durst F., Ray S., Ünsal B., and Bayoumi O.A., *The Development Lengths of Laminar Pipe and Channel Flows*, American Society of Mechanical Engineers, **127**, 2005

Hanks R.W., *On the Prediction of Non-Newtonian Flow Behavior in Ducts of Noncircular Cross Section*, Industrial and Engineering Chemistry Fundamentals, **13**, 1974

Huang J.C.P and Yu H.S., *Pressure Distribution in Porous Ducts of Arbitrary Cross Section*, Journal of Fluids Engineering, **95**, 1973

Kozicki W., Chou C.H., and Tiu C., *Non-Newtonian Flow in Ducts of Arbitrary Cross Sectional Shape*, Chemical Engineering Science, **21**, 1966

Lee K.Y. and Liu T.J., *Design and Analysis of a Dual Cavity Coat Hanger Die*, Polymer Engineering and Science, **29**, 1989

Lee K.Y., Wen S.H., and Liu T.J., *Vortex Formation in a Dual Cavity Coat Hanger Die*, Polymer Engineering and Science, **30**, 1990

Leonard W.K., *Effects of Secondary Cavities, Inertia, and Gravity on Extrusion Dies*, SPE ANTEC Technical Papers, **31**, 1985

Leonard W.K., *Inertia and Gravitational Effects in Extrusion Dies for Non-Newtonian Fluids*, Polymer Engineering and Science, **25**, 1985

Liu L.D., Wen S.H., and Liu T.J., *Extrusion Die Design for Viscoplastic Fluids*, Advances in Polymer Technology, **13**, 1994

Liu T.J., *Fully Developed Flow of Power Law Fluids in Ducts*, American Chemical Society, **22**, 1983

Liu T.J. and Hong C.N., *The Pressure Drop Flow Rate Equation for Non-Newtonian Flow in Channels of Irregular Cross Section*, Polymer Engineering and Science, **28**, 1988

Miller C., *Predicting Non-Newtonian Flow Behavior in Ducts of Unusual Cross Section*, Industrial and Engineering Chemistry Fundamentals, **11**, 1972

Ruschak K.J., Personal communication, 2010

Ruschak K.J. and Weinstein S.J., *Modeling the Secondary Cavity of Two Cavity Dies*, Polymer Engineering and Science, **37**, 1997

Ruschak K.J. and Weinstein S.J., *Perturbation Solution for Flow in Two Cavity Dies*, Journal of Fluids Engineering, **119**, 1997

Schechter R.S., *On the Steady Flow of a Non-Newtonian Fluid in Cylinder Ducts*, American Institute of Chemical Engineers, **7**, 1961

Schlichting H., **Boundary Layer Theory**, 7th ed. New York, NY: McGraw Hill, 1979

Various, **Fluent 6.3 User's Guide**, Lebanon, NH: Fluent Inc., 2006

Vrahopoulou E.P., *A Model for Fluid Flow in Dies*, Chemical Engineering Science, **46**, 1991

Wang Y., *The Flow Distribution of Molten Polymers in Slit Dies and Coat Hanger Dies Through Three Dimensional Finite Element Analysis*, Polymer Engineering and Science, **31**, 1991

Weinstein S.J., Personal communication, 2010

Weinstein S.J. and Ruschak K.J., *Asymptotic Analysis of Die Flow fir Shear Thinning Fluids*, American Institute of Chemical Engineers, **42**, 1996

Weinstein S.J. and Ruschak K.J., *One Dimensional Equations Governing Single Cavity Die Design*, American Institute of Chemical Engineers, **42**, 1996

Wen S.H. and Liu T.J., *Three Dimensional Finite Element Analysis of Polymeric Fluid Flow in an Extrusion Die part I: Entrance Effect*, Polymer Engineering and Science, **34**, 1994

Wheeler J.A. and Wissler E.H., *The Fristion Factor Reynolds Number Relation for the Steady Flow of Pseudoplastic Fluids Through Rectangular Ducts Part I: Theory*, American Institute of Chemical Engineers, **11**, 1965

References

Yu Y.W., Wu P.Y., and Liu T.J., *Validity of One Dimensional Equation Governing Extrusion Die Flow*, American Institute of Chemical Engineers, **43**, 1997

Yuan S.L., *A Flow Model for Non-Newtonian Liquids Inside a Slot Die*, Polymer Engineering and Science, **35**, 1995

Appendix A

User Defined Functions

A.1 Two Dimensional Velocity Inlet Profile

```
/***** Fluent Directories *****/
#include "udf.h"
/***** Parameter Constants *****/
#define Hos xx.xxx
#define Loc xx.xxx
#define n x.x
#define m x.x
/***** Define Velocity Profile *****/
DEFINE_PROFILE(velocity_profile,thread,position)
{
  real x[ND_ND];
  real y;
  real q;
  face_t f;
  begin_f_loop(f,thread);
    {
      F_CENTROID(x,f,thread);
      y = fabs(x[1]);
      q = (pow((m*(pow((Los),(2.0*(1.0-n))))),(1.0/(2.0-n))));
      F_PROFILE(f,thread,position) = ((2.0+(1.0/n))/(1.0+(1.0/n))) \
        *(q/Hos) \
        *(1.0-pow((y/(Hos/2.0)),(1.0+(1.0/n))));
    }
  end_f_loop(f,thread)
}
```

A.2 Three Dimensional Velocity Inlet Profile

```
/***** Fluent Directories *****/
#include "udf.h"
/***** Parameter Constants *****/
#define Hos xx.xxx
#define Loc xx.xxx
#define Woc xx.xxx
#define n x.x
#define m x.x
#define amplitude x.xx
#define pi 3.141593
/***** Define Velocity Profile *****/
DEFINE_PROFILE(velocity_profile,thread,position)
{
  real x[ND_ND];
  real y;
  real z;
  real q;
  face_t f;
  begin_f_loop(f,thread);
    {
      F_CENTROID(x,f,thread);
      y = fabs(x[1]);
      z = x[2];
      q = (amplitude)*cos((z/Woc)*pi) \
        +(pow((m*(pow((Los),(2.0*(1.0-n))))),(1.0/(2.0-n))));
      F_PROFILE(f,thread,position) = ((2.0+(1.0/n))/(1.0+(1.0/n))) \
        *(q/Hos) \
        *(1.0-pow((y/(Hos/2.0)),(1.0+(1.0/n))));
    }
  end_f_loop(f,thread)
}
```

A.3 Thermal Conductivity by Viscosity Duplication

```
/***** Fluent Directories *****/
#include "udf.h"
/***** Define Thermal Conductivity *****/
DEFINE_PROPERTY(thermal_conductivity,cell,thread)
{
  real k;
  real eta = C_MU_L(cell,thread);
  k = eta;
  return k;
}
```

A.4 Density by Reynolds Number Duplication

```
/***** Fluent Directories *****/
#include "udf.h"
/***** Parameter Constants *****/
#define Re xx.xx
/***** Define Thermal Conductivity *****/
DEFINE_PROPERTY(density,cell,thread)
{
  real rho;
  rho = Re;
  return rho;
}
```

Appendix B

Gambit Journal

```
/ Journal File for Gambit 2.3.16
/ Three Dimensional Validation
/
/ Define Geometry Property Parameters
/
$Theta=xx.x
$Phi=xx.x
$foo8os=x.xxx
$Woc=xxx*$foo8os
$foo8oc=xxx*$foo8os
$Loc=xx.xx*$foo8os
$Lis=xx.xx$foo8os
/
/ Define Mesh Property Parameters
/
$Mesh = x.xxxx
$Ratio = x.xx
/
/ Preliminary Calculations
/
$foo6oo1=0.5*$foo8os
$foo6oo2=-$foo6oo1
$foo6oo3=-($foo8oc-(0.5*$foo8os))
$foo6oo4=$Lis+($foo8oc-$foo8os)/TAN($Theta)
$foo6oo5=$foo6oo4+($foo8oc-$foo8os)/TAN($Phi)
$foo6=$foo6oo5+$Los
/
$foo7=$foo8os/$Mesh
```

```
$foo8=$foo7*$Ratio
/
/ Define Vertices
/
vertex create coordinates 0    $foo6oo2 0
vertex create coordinates $Lis $foo6oo2 0
vertex create coordinates $foo6oo4   $foo6oo3 0
vertex create coordinates $foo6oo5   $foo6oo2 0
vertex create coordinates $foo6   $foo6oo2 0
vertex create coordinates $foo6   $foo6oo1 0
vertex create coordinates $foo6oo5   $foo6oo1 0
vertex create coordinates $Lis $foo6oo1 0
vertex create coordinates 0    $foo6oo1 0
/
vertex create coordinates 0    $foo6oo2 $Woc
vertex create coordinates $Lis $foo6oo2 $Woc
vertex create coordinates $foo6oo4   $foo6oo3 $Woc
vertex create coordinates $foo6oo5   $foo6oo2 $Woc
vertex create coordinates $foo6   $foo6oo2 $Woc
vertex create coordinates $foo6   $foo6oo1 $Woc
vertex create coordinates $foo6oo5   $foo6oo1 $Woc
vertex create coordinates $Lis $foo6oo1 $Woc
vertex create coordinates 0    $foo6oo1 $Woc
/
/ Define Edges
/
edge create straight "vertex.1" "vertex.2"
edge create straight "vertex.2" "vertex.3"
edge create straight "vertex.3" "vertex.4"
edge create straight "vertex.4" "vertex.5"
edge create straight "vertex.5" "vertex.6"
edge create straight "vertex.6" "vertex.7"
edge create straight "vertex.7" "vertex.8"
edge create straight "vertex.8" "vertex.9"
edge create straight "vertex.9" "vertex.1"
edge create straight "vertex.8" "vertex.2"
edge create straight "vertex.7" "vertex.4"
/
edge create straight "vertex.10" "vertex.11"
```

```
edge create straight "vertex.11" "vertex.12"
edge create straight "vertex.12" "vertex.13"
edge create straight "vertex.13" "vertex.14"
edge create straight "vertex.14" "vertex.15"
edge create straight "vertex.15" "vertex.16"
edge create straight "vertex.16" "vertex.17"
edge create straight "vertex.17" "vertex.18"
edge create straight "vertex.18" "vertex.10"
edge create straight "vertex.17" "vertex.11"
edge create straight "vertex.16" "vertex.13"
/
edge create straight "vertex.9" "vertex.18"
edge create straight "vertex.1" "vertex.10"
edge create straight "vertex.8" "vertex.17"
edge create straight "vertex.2" "vertex.11"
edge create straight "vertex.3" "vertex.12"
edge create straight "vertex.7" "vertex.16"
edge create straight "vertex.4" "vertex.13"
edge create straight "vertex.6" "vertex.15"
edge create straight "vertex.5" "vertex.14"
/
/ Define Faces
/
face create wireframe "edge.9" "edge.23" "edge.20" \
  "edge.24" real
face create wireframe "edge.1" "edge.24" "edge.12" \
  "edge.26" real
face create wireframe "edge.10" "edge.25" "edge.21" \
  "edge.26" real
face create wireframe "edge.8" "edge.23" "edge.19" \
  "edge.25" real
face create wireframe "edge.19" "edge.20" "edge.12" \
  "edge.21" real
face create wireframe "edge.8" "edge.9" "edge.1" \
  "edge.10" real
/
face create wireframe "edge.2" "edge.26" "edge.13" \
  "edge.27" real
face create wireframe "edge.3" "edge.27" "edge.14" \
```

```
  "edge.29" real
face create wireframe "edge.11" "edge.28" "edge.22" \
  "edge.29" real
face create wireframe "edge.7" "edge.25" "edge.18" \
  "edge.28" real
face create wireframe "edge.18" "edge.21" "edge.13" \
  "edge.14" "edge.22" real
face create wireframe "edge.7" "edge.10" "edge.2" \
  "edge.3" "edge.11" real
/
face create wireframe "edge.4" "edge.29" "edge.15" \
  "edge.31" real
face create wireframe "edge.5" "edge.30" "edge.16" \
  "edge.31" real
face create wireframe "edge.6" "edge.28" "edge.17" \
  "edge.30" real
face create wireframe "edge.17" "edge.22" "edge.15" \
  "edge.16" real
face create wireframe "edge.6" "edge.11" "edge.4" \
  "edge.5" real
/
/ Define Volumes
/
volume create stitch "face.1" "face.2" "face.3" "face.4" \
  "face.5" "face.6" real
volume create stitch "face.3" "face.7" "face.8" "face.9" \
  "face.10" "face.11" "face.12" real
volume create stitch "face.9" "face.13" "face.14" "face.15" \
  "face.16" "face.17" real
/
/ Define Continuim Type
/
physics create "Inner_Slot" ctype "FLUID" volume "volume.1"
physics create "Outer_Cavity" ctype "FLUID" volume "volume.2"
physics create "Outer_Slot" ctype "FLUID" volume "volume.3"
/
/ Define Boundary Conditions
/
physics create "Inlet" btype "VELOCITY_INLET" face "face.1"
```

```
physics create "Outlet" btype "PRESSURE_OUTLET" face "face.14"
/
physics create "Slip_Center_Inner" btype "WALL" face "face.6"
physics create "Slip_Center_Cavity" btype "WALL" face "face.12"
physics create "Slip_Center_Outer" btype "WALL" face "face.17"
/
physics create "Slip_End_Inner" btype "WALL" face "face.5"
physics create "Slip_End_Cavity" btype "WALL" face "face.11"
physics create "Slip_End_Outer" btype "WALL" face "face.16"
/
physics create "Top_Inner" btype "WALL" face "face.4"
physics create "Top_Cavity" btype "WALL" face "face.10"
physics create "Top_Outer" btype "WALL" face "face.15"
/
physics create "Bottom_Inner" btype "WALL" face "face.2"
physics create "Bottom_Cavity1" btype "WALL" face "face.7"
physics create "Bottom_Cavity2" btype "WALL" face "face.8"
physics create "Bottom_Outer" btype "WALL" face "face.13"
/
/ Mesh Inner Slot
/
face mesh "face.5" map size $foo7
face mesh "face.6" map size $foo7
volume mesh "volume.1" cooper source "face.5" "face.6" \
  size $foo8
/
/ Mesh Outer Slot
/
edge mesh "edge.22" successive ratio1 1 size $foo7
sfunction create sourceedges "edge.22" startsize $foo7 \
  growthrate 1.01 sizelimit 10 attachfaces "face.16" fixed
sfunction bgrid attachfaces "face.16"
face mesh "face.16" map size $foo7
sfunction delete "sfunc.1"
edge mesh "edge.11" successive ratio1 1 size $foo7
sfunction create sourceedges "edge.11" startsize $foo7 \
  growthrate 1.01 sizelimit 10 attachfaces "face.17" fixed
sfunction bgrid attachfaces "face.17"
face mesh "face.17" map size $foo7
```

```
volume mesh "volume.3" cooper source "face.16" "face.17" \
  size $foo8
/
/ Mesh Outer Cavity
/
sfunction delete "sfunc.1"
sfunction create sourceedges "edge.21" "edge.13" "edge.14" \
  "edge.22" "edge.18" startsize $foo7 growthrate 1.1 \
  sizelimit 10 attachfaces "face.11" fixed
sfunction bgrid attachfaces "face.11"
face mesh "face.11" pave size $foo7
volume mesh "volume.2" cooper size $foo8
/
/ Export Mesh
/
export fluent5 "Three_Dimensional_Validation.msh"
```

Appendix C

Matlab Functions

C.1 OuterCavityApproximation.m

```
function [qis,qos,qis_bar,qos_bar,z,z_bar] = ...
  OuterCavityApproximation(m,n,Hos,Los,Woc,Loc,A,theta,...
  phi,Re,profile,varargin)
%
% Revision 1.0
% Mark Andrew Livelli
% Rochester Institute of Technology
% April 11, 2010
%
%%%%%%%%%%%%%%%%%%
% Matlab Formatting
%%%%%%%%%%%%%%%%%%

% Create Symbolic Integration Variable
syms xi

% Create Symbolic Fourier Mode Number
syms iota

%%%%%%%%%%%%%%%%%%%%%%%%%%%%%%%%
% Define Fluid Property Parameters
%%%%%%%%%%%%%%%%%%%%%%%%%%%%%%%%

% Define Fluid Consistency
m;
```

```
% Define Power Law Index
n;

%%%%%%%%%%%%%%%%%%%%%%%%%%%%%%%%%%%%
% Define Geometry Property Parameters
%%%%%%%%%%%%%%%%%%%%%%%%%%%%%%%%%%%%

% Define Outer Slot Height
Hos;

% Outer Slot Length
Los;

% Define Outer Cavity Width
Woc;

% Define Outer Cavity Length
Loc;

% Define Outer Cavity Cross Sectional Area
A;

% Define Outer Cavity Entrance Angle
theta;

% Define Outer Cavity Exit Angle
phi;

%%%%%%%%%%%%%%%%%%%%%%%%
% Define Flow Conditions
%%%%%%%%%%%%%%%%%%%%%%%%

% Define Reynolds Number
Re;

% Define Inlet Flow Profile Representation
profile;
```

```
%%%%%%%%%%%%%%%%%%%%%%%%%%%%%%%%%%%%
% Define Variable Argument Parameters
%%%%%%%%%%%%%%%%%%%%%%%%%%%%%%%%%%%%

% Define Outer Cavity Flat Bottom
if nargin >= 12
  Lfb = varargin{1};
else
  Lfb = 0.0;
end

% Define Discretization Points
if nargin >= 13
  points = varargin{2};
else
  points = 500.0;
end

% Define Fourier Modes
if nargin >= 14;
  modes = varargin{3};
else
  modes = 1.0;
end

%%%%%%%%%%%%%%%%%%%%%%%%%%
% Preallocate Memory Storage
%%%%%%%%%%%%%%%%%%%%%%%%%%

% Preallocate Dimensional Coordinates
z = zeros(points,1);

% Preallocate Dimensionless Coordinates
z_bar = zeros(points,1);

% Preallocate Fourier Coefficients
alpha = zeros(1,1);
beta = zeros(modes,1);
gamma = zeros(modes,1);
```

```
% Preallocate Condensed Fourier Coefficients
Alpha = zeros(modes,1);
Beta = zeros(modes,1);

% Preallocate Differential Equation Coefficients
kappa = zeros(modes,1);

% Preallocate Dimensional Solution Results
qis = zeros(points,1);
qos = zeros(points,1);

% Preallocate Dimensionless Solution Results
qis_bar = zeros(points,1);
qos_bar = zeros(points,1);

%%%%%%%%%%%%%%%%%%%%%%%%%
% Preliminary Calculations
%%%%%%%%%%%%%%%%%%%%%%%%%

% Outer Cavity Shape Factor
lambda = OuterCavityShapeFactor(n,theta,phi,Re,Lfb);

% Outer Cavity Damping Dimensionless Group
varsigma = (((Hos/Loc)^(2.0*(n+1.0)))...
           *(Loc^3.0)...
           *(Woc^2.0))...
           /...
           ((2.0^(n+1.0))...
           *((2.0+(1.0/n))^n)...
           *Los...
           *n...
           *lambda...
           *(A^2.0));

% Dimensional Coordinates
for i = 1:points
  z(i,1) = ((Woc*((2.0*i)...
           -(points+1.0)))...
```

```
          /...
          (points-1.0));
end

% Dimensionless Coordinates
for i = 1:points
  z_bar(i,1) = (((2.0*i)...
               -(points+1.0))...
               /...
               (points-1.0));
end

% Dimensional Flow Profile Representation
symqis = sym(strrep(profile,'z','xi'));

% Average Slot Flow Rate Per Unit Cavity Width
qa = (1.0...
     /...
     (2.0*Woc))...
     *subs(int(symqis,xi,-Woc,Woc));

% Dimensionless Flow Profile Representation
symqis_bar = sym((strrep(profile,'z',['(xi*' num2str(Woc) ')'])))/qa;

%%%%%%%%%%%%%%%%%%%%%%
% Fourier Decomposition
%%%%%%%%%%%%%%%%%%%%%%

% Determine Fourier Coefficients
alpha = subs((1.0/2.0)*int(symqis_bar,xi,-1.0,1.0));
for i = 1:modes
  beta(i,1) = int(subs(symqis_bar*cos(iota*pi*xi),{iota},i),xi,-1.0,1.0);
  gamma(i,1) = int(subs(symqis_bar*sin(iota*pi*xi),{iota},i),xi,-1.0,1.0);
end

% Determine Condensed Fourier Coefficients
for i = 1:modes
  if beta(i,1) < 0 || gamma(i,1) < 0
    Alpha(i,1) = (-1.0)...
```

```
                *sqrt(((beta(i,1))^2.0)...
                +((gamma(i,1))^2.0));
  else
    Alpha(i,1) = (1.0)...
                *sqrt(((beta(i,1))^2.0)...
                +((gamma(i,1))^2.0));
  end
  if gamma(i,1) == 0
    Beta(i,1) = 0;
  else
    Beta(i,1) = atan(beta(i,1)/gamma(i,1))...
                -(pi/2.0);
  end
end

%%%%%%%%%%%%%%%%%%%%%%%%%%%%%%
% Differential Equation Solution
%%%%%%%%%%%%%%%%%%%%%%%%%%%%%%

% Particular Solution Coefficients
for i = 1:modes
  kappa(i,1) = (Alpha(i,1)*i*pi))...
               /...
               ((i*pi)^2.0)...
               +varsigma);
end

%%%%%%%%%%%%%%%%%%%%%%%%%%%%
% Outer Cavity Appromximation
%%%%%%%%%%%%%%%%%%%%%%%%%%%%

% Inlet Flow Profile
for i = 1:points
  qis(i,1) = subs(symqis,z(i,1));
  qis_bar(i,1) = subs(symsqis_bar,z_bar(i,1));
end

% Outlet Flow Profile
for i = 0:modes
```

```
  for j = 1:points
    if i == 0
      qos_bar(j,1) = alpha;
    else
      qos_bar(j,1) = qos_bar(j,1)...
                     +((Alpha(i,1)-(kappa(i,1)*i*pi))...
                     *cos((i*pi*z_bar(j,1))+Beta(i,1)))...
                     -(((sqrt(varsigma)*kappa(i,1)*((-1.0)^(i+1.0))...
                     *sin(Beta(i,1)))...
                     /...
                     cosh(sqrt(varsigma))))...
                     *sinh(sqrt(varsigma)*z_bar(j,1)));
    end
  end
end
qos = qos_bar*qa;

%%%%%%%%%%%%%
% Plot Results
%%%%%%%%%%%%%

% Open Figure
fig1 = 'Outer Cavity Dimensional Flow Profile Damping Representation';
plotfig1 = figure('name',fig1);

% Plot Data
plot(...
    z,qis,'k-.',...
    z,qos,'r-.',...
    'LineWidth',2);

% Format Plot
legend('Inlet Flow Profile','Outlet Flow Profile');
title('Dimensional Flow Profile Damping');
xlabel('Dimensional Position');
ylabel('Dimensional Flow Per Unit Cavity Width');
grid on

% Open Figure
```

```
fig2 = 'Outer Cavity Dimensionless Flow Profile Damping Representation';
plotfig2 = figure('name',fig2);

% Plot Data
plot(...
    z_bar,qis_bar,'k-.',...
    z_bar,qos_bar,'r-.',...
    'LineWidth',2);

% Format Plot
legend('Inlet Flow Profile','Outlet Flow Profile');
title('Dimensionless Flow Profile Damping');
xlabel('Dimensionless Position');
ylabel('Dimensionless Flow Per Unit Cavity Width');
grid on

% Standardize Plot
StandardizePlot(plotfig1);
StandardizePlot(plotfig2);
```

C.2 OuterCavityShapeFactor.m

```
function [lambda] = OuterCavityShapeFactor(...
  n,theta,phi,Re,varargin);
%
% Revision 1.0
% Mark Andrew Livelli
% Rochester Institute of Technology
% April 11, 2010
%
%%%%%%%%%%%%%%%%%%%%%%%%%%%%%%%%
% Define Fluid Property Parameters
%%%%%%%%%%%%%%%%%%%%%%%%%%%%%%%%

% Define Power Law Index
n;

%%%%%%%%%%%%%%%%%%%%%%%%%%%%%%%%%%%%
% Define Geometry Property Parameters
%%%%%%%%%%%%%%%%%%%%%%%%%%%%%%%%%%%%

% Define Outer Cavity Entrance Angle
theta;

% Define Outer Cavity Exit Angle
phi;

%%%%%%%%%%%%%%%%%%%%%%%%
% Define Flow Conditions
%%%%%%%%%%%%%%%%%%%%%%%%

% Define Reynolds Number
Re;

%%%%%%%%%%%%%%%%%%%%%%%%%%%%%%%%%%%%
% Define Variable Argument Parameters
%%%%%%%%%%%%%%%%%%%%%%%%%%%%%%%%%%%%

% Define Outer Cavity Flat Bottom
if nargin >= 5
```

```
  Lfb = varargin{1};
else
  Lfb = 0.0;
end

%%%%%%%%%%%%%%%%%%%%%%%%%%
% Preallocate Memory Storage
%%%%%%%%%%%%%%%%%%%%%%%%%%

% Preallocate Fitting Constants
c = zeros(8,1);

%%%%%%%%%%%%%%%%%%%%%%%%%%
% Determine Fitting Constants
%%%%%%%%%%%%%%%%%%%%%%%%%%

% Test Angle Match
GeometryTest(theta,phi,Lfb);

% Match Fittinc Constants
switch theta
  case 15
    switch phi
      case 15
        switch Lfb
          case 0.000
            c(2,1) = 0.0107040440;
            c(3,1) = 5.9320346674;
            c(4,1) = 2.9193211662;
            c(5,1) = 0.0160728211;
            c(6,1) = 2.9065624487;
            c(7,1) = 0.2265322358;
            c(8,1) = 1.2357169021;
        end
    end
  case 30
    switch phi
      case 30
        switch Lfb
```

```
        case 0.000
          c(2,1) = 0.0182850064;
          c(3,1) = 4.7402136792;
          c(4,1) = 2.2465417632;
          c(5,1) = 0.0000000000;
          c(6,1) = 2.9204875968;
          c(7,1) = 0.4398851296;
          c(8,1) = 1.2541337095;
      end
    case 60
      switch Lfb
        case 0.000
          c(2,1) = 0.0236279773;
          c(3,1) = 3.9179661904;
          c(4,1) = 1.8901885291;
          c(5,1) = 0.0015942915;
          c(6,1) = 3.1199949179;
          c(7,1) = 0.5252376827;
          c(8,1) = 1.2464161356;
        case 0.316
          c(2,1) = 0.0238259449;
          c(3,1) = 3.9450394744;
          c(4,1) = 1.7515002864;
          c(5,1) = 0.0000000000;
          c(6,1) = 2.9442298150;
          c(7,1) = 0.5130645275;
          c(8,1) = 1.3368708468;
        case 0.416
          c(2,1) = 0.0207958295;
          c(3,1) = 4.4770066593;
          c(4,1) = 2.1046905138;
          c(5,1) = 0.4788195378;
          c(6,1) = 0.2103027900;
          c(7,1) = 0.0000000000;
          c(8,1) = 0.6725366389;
        case 0.516
          c(2,1) = 0.0198115099;
          c(3,1) = 4.4576372653;
          c(4,1) = 2.0104080098;
```

```
            c(5,1) = 0.4787621007;
            c(6,1) = 0.2245314076;
            c(7,1) = 0.0000000000;
            c(8,1) = 0.6514074575;
        end
    end
end

%%%%%%%%%%%%%%%%%%%%%%%%%%
% Shape Factor Approximation
%%%%%%%%%%%%%%%%%%%%%%%%%%

% Approxiamted Zero Reynolds Number Shape Factor
c(1,1) = c(2,1)...
             *exp(c(3,1)*(1.0-n));

% Scaled Reynolds Number
Re_bar = (1.0...
         /...
         (n^c(4,1)))...
         *(((2.0+(1.0/n))^(1.0-n))...
         /...
         ((3.0+(2.0/n))...
         *(2.0^n)))...
         *Re;

% Approximated Shape Factor
lambda = c(1,1)...
         *(((exp(-c(5,1)*Rebar))...
         +(c(6,1)...
         *exp(-c(7,1)*(Rebar^c(8,1)))))...
         /...
         (1+c(6,1)));
```

C.3 GeometryTest.m

```
function GeometryTest(theta,phi,varargin)
%
% Triangular 15.0-15.0
%   Flat Bottom Length 0.000
% Triangular 30.0-30.0
%   Flat Bottom Length 0.000
% Triangular 30.0-60.0
%   Flat Bottom Length 0.000
%   Flat Bottom Length 0.316
%   Flat Bottom Length 0.416
%   Flat Bottom Length 0.516
%
% Revision 1.0
% Mark Andrew Livelli
% Rochester Institute of Technology
% April 11, 2010
%
%%%%%%%%%%%%%%%%%%%%%%%%%%%%%%%%%%%
% Define Geometry Property Parameters
%%%%%%%%%%%%%%%%%%%%%%%%%%%%%%%%%%%

% Define Outer Cavity Entrance Angle
theta;

% Define Outer Cavity Exit Angle
phi;

%%%%%%%%%%%%%%%%%%%%%%%%%%%%%%%%%%%
% Define Variable Argument Parameters
%%%%%%%%%%%%%%%%%%%%%%%%%%%%%%%%%%%

% Define Outer Cavity Flat Bottom
if nargin >= 3
  Lfb = varargin{1};
else
  Lfb = 0.0;
end
```

```
%%%%%%%%%%%%%%%%%%%%%%%%
% Test Available Matches
%%%%%%%%%%%%%%%%%%%%%%%%

% Initialize Test
test = 0;

% Test Geometrical Parameters
if theta == 15
  if phi == 15
    if Lfb == 0.000
      test = 1;
    end
  end
elseif theta == 30
  if phi == 30
    if Lfb == 0.000
      test = 1;
    end
  elseif phi == 60
    if Lfb == 0.000 | 0.316 | 0.416 | 0.516
      test = 1;
    end
  end
end

if test == 0
  message = ['Data for this geometry is not available. '...
             'You have specified the following parameters: \n\n'...
             'Entrance Angle ==> %4.3f \n'...
             'Exit Angle ==> %4.3f \n'...
             'Flat Bottom Length ==> %4.3f \n\n'...
             'Please check the help section of this function '...
             'by typing "help GeometryTest" '...
             'for a list of currently available '...
             'outer cavity shape factor data'];
  error('ErrorTests:convertTest',...
        message,...
        theta,...
```

```
        phi,...
        Lfb);
end
```

C.4 StandardizePlot.m

```
function StandardizePlot(fignum,varargin)
%
% Revision 1.0
% Coded: Rebecca Jaiven
% Assisted: Bill Seely
% General Electric
% August 29, 2008
%
% Revision 2.0
% Mark Andrew Livelli
% Rochester Institute of Technology
% April 11, 2010
%
%%%%%%%%%%%%%%%%%%%%%%%%%
% Define Figure Parameters
%%%%%%%%%%%%%%%%%%%%%%%%%

% Define Figure Number
fignum;

%%%%%%%%%%%%%%%%%%%%%%%%%%%%%%%%%%%
% Define Variable Argument Parameters
%%%%%%%%%%%%%%%%%%%%%%%%%%%%%%%%%%%

% Define Window Scale
if nargin >= 2
  wscale = varargin{1};
else
  wscale = 0.35;
end

% Define Graph Size
if nargin >= 3
  gscale = varargin{2};
else
gscale = 0.75;
end
```

```
% Define Title Font Size
if nargin >= 4
  tsize = varargin{3};
else
  tsize = 10;
end

% Define Label Font Size
if nargin >= 5
  lsize = varargin{4};
else
  lsize = 8;
end

% Define Font Type
if nargin >= 6
  font = varargin{5};
else
  font = 'Times New Roman';
end

% Define Background Color
if nargin >= 7
  bcolor = varargin{6};
else
  bcolor = [1 1 1];
end

% Define Generic Font Size
if nargin >= 8
  fsize = varargin{7};
else
  fsize = 8;
end

%%%%%%%%%%%%%%%%%%%%%%%
% Extract Figure Handles
%%%%%%%%%%%%%%%%%%%%%%%
```

```
% Extract Figure Handle
hfigure = figure(fignum);

% Extract Axis Handle
haxis = get(fignum,'Children');

% Include Figure Interior
set(hfigure,'ActivePositionProperty','OuterPosition');

% Remove Legend Handle
if strcmpi(get(haxis(1),'Tag'),'legend') == 1
  hax = haxis(2:end);
  ltag = 1;
else
  hax = haxis;
  ltag = 0;
end

%%%%%%%%%%%%%%%%%%%
% Adjust Figure Size
%%%%%%%%%%%%%%%%%%%

% Define Figure Units
set(0,'units',pixels');

% Determine Screen Size
screen = get(0,'Screensize');

% Adjust Figure Size
width = wscale*screen(3);
height = wscale*screen(4);
size = [screen(3)/2-width/2 screen(4)/2-height/2 width height];

% Format Figure Size
set(hfigure,'position',size,'paperpositionmode','auto');

%%%%%%%%%%%%%%%%%%%%%%%%%%%%%%%
% Format General Figure Properties
%%%%%%%%%%%%%%%%%%%%%%%%%%%%%%%
```

```
for i = 1:length(hax)

  % Format Font Type
  set(hax(i),'fontname',font);

  % Remove Boxed Border
  set(hax(i),'box','off');

  % Normalize Unit Values
  set(hax(i),'units','normalized');

  % Format Graph Size
  pos = get(hax(i),'position');
  set(hax(i),'position',[pos(1) pos(2) pos(3) gscale]);

end

% Format Background Color
set(hfigure,'Color',bcolor);

% Format Grid
grid(hax(length(hax)),'on');

%%%%%%%%%%%%%%%%%%%%%%
% Format Axis Properties
%%%%%%%%%%%%%%%%%%%%%%

for j = 1:length(hax)

  % Format Tick Font Size
  set(hax(j),'fontsize',fsize);

  % Format Axis Range
  axis(hax(j),'tight');

  % Format Y-Axis
  ylabel(hax(j),get(get(hax(j),'ylabel'),'string'),...
    'fontsize',lsize,...
```

```
    'fontweight','b',...
    'fontname',font);

  % Format X-Axis
  xlabel(hax(j),get(get(hax(j),'xlabel'),'string'),...
    'fontsize',lsize,...
    'fontweight','b',...
    'fontname',font);

  % Format Title
  title(hax(j),get(get(hax(j),'title'),'string'),...
    'fontsize',lsize,...
    'fontweight','b',...
    'fontname',font);

end

%%%%%%%%%%%%%%%%%%%%%%%%
% Format Legend Properties
%%%%%%%%%%%%%%%%%%%%%%%%

if ltag == 1
  if length(haxis) == 3

  % Normalize Unit Values
  set(haxis(1),'units','normalized');

  % Format Font Type
  set(haxis(1),'fontname',font);

  % Format Font Size
  set(haxis(1),'fontsize',fsize);

  end
end
```

C.5 ThreeDimensionalValidation.m

```
%%%%%%%%%%%%%%%%%%%%%%%%%%%%%%%%
% Define Fluid Property Parameters
%%%%%%%%%%%%%%%%%%%%%%%%%%%%%%%%

% Define Fluid Consistency
m = x.x;

% Define Power Law Index
n = x.x;

%%%%%%%%%%%%%%%%%%%%%%%%%%%%%%%%%%%%
% Define Geometry Property Parameters
%%%%%%%%%%%%%%%%%%%%%%%%%%%%%%%%%%%%

% Define Outer Slot Height
Hos = xx.xxx;

% Outer Slot Length
Los = xx.xxx;

% Define Outer Cavity Width
Woc = xx.xxx;

% Define Outer Cavity Length
Loc = xx.xxx;

% Define Outer Cavity Cross Sectional Area
A = xx.xxxxx;

% Define Outer Cavity Entrance Angle
theta = xx.xx;

% Define Outer Cavity Exit Angle
phi = xx.xx;

%%%%%%%%%%%%%%%%%%%%%%%
% Define Flow Conditions
%%%%%%%%%%%%%%%%%%%%%%%
```

```
% Define Reynolds Number
Re = xx.x;

% Define Inlet Flow Profile Representation
profile = 'x.xx*cos((z/xx.xxx)*pi)+x.xxxx;

%%%%%%%%%%%%%%%%%%%%%%%%
% Define Fluent Data Files
%%%%%%%%%%%%%%%%%%%%%%%%

% Define Inlet Data
inlet = 'xxxxxxxxxxxx.csv';

% Define Outlet Data
outlet = 'xxxxxxxxxxx.csv';

%%%%%%%%%%%%%%%%%%%%%%
% Fluent Inlet Solution
%%%%%%%%%%%%%%%%%%%%%%

% Load Data
Fluent(inlet);
Inlet = [ycoordinate round(zcoordinate*10000)/10000 xvelocity];

% Sort Data
SortInlet = sortrows(Inlet,[2.1]);

% Determine Flow Per Unit Cavity Width
[zinlet,qinlet] = FlowPerUnitCavityWidth(...
  SortInlet(:,1),...
  SortInlet(:,2),...
  SortInlet(:,3));

%%%%%%%%%%%%%%%%%%%%%%%
% Fluent Outlet Solution
%%%%%%%%%%%%%%%%%%%%%%%

% Load Data
```

```
Fluent(outlet);
Outlet = [ycoordinate round(zcoordinate*10000)/10000 xvelocity];

% Sort Data
SortOutlet = sortrows(Outlet,[2.1]);

% Determine Flow Per Unit Cavity Width
[zoutlet,qoutlet] = FlowPerUnitCavityWidth(...
  SortOutlet(:,1),...
  SortOutlet(:,2),...
  SortOutlet(:,3));

%%%%%%%%%%%%%%%%%%%%%%%%%%%%%%%%%%%%%%%%
% Outer Cavity Approximate Model Solution
%%%%%%%%%%%%%%%%%%%%%%%%%%%%%%%%%%%%%%%%

% Approximate Model Solution
[qis,qos,qis_bar,qos_bar,z,z_bar] = ...
  OuterCavityApproximation(m,n,Hos,Los,Woc,Loc,A,theta,...
  phi,Re,profile);

% Close Figures
close all

%%%%%%%%%%%%
% Plot Results
%%%%%%%%%%%%

% Open Figure
fig1 = 'Dimensional Flow Per Unit Cavity Width Entering Outer Cavity';
plotfig1 = figure('name',fig1);

% Plot Data
plot(...
  z,qis,'k-',...
  zinlet(1:round(length(zinlet)/50):end),...
  qinlet(1:round(length(qinlet)/50):end),...
  'ko',...
  -zinlet(1:round(length(zinlet)/50):end),...
```

```
  qinlet(1:round(length(qinlet)/50):end),...
  'ko',...
  'LineWidth',2,...
  'MarkerSize',1.5);

% Format Plot
legend('Approximate Model','Fluent');
title('Dimensional Flow Per Unit Cavity Width Entering Outer Cavity');
xlabel('Dimensional Position')
ylabel('Dimensional Flow Per Unit Cavity Width');

% Open Figure
fig2 = 'Dimensional Flow Per Unit Cavity Width Exiting Outer Cavity';
plotfig2 = figure('name',fig2);

% Plot Data
plot(...
  z,qos,'k-',...
  zoutlet(1:round(length(zoutlet)/50):end),...
  qoutlet(1:round(length(qoutlet)/50):end),...
  'ko',...
  -zoutlet(1:round(length(zoutlet)/50):end),...
  qoutlet(1:round(length(qoutlet)/50):end),...
  'ko',...
  'LineWidth',2,...
  'MarkerSize',1.5);

% Format Plot
legend('Approximate Model','Fluent');
title('Dimensional Flow Per Unit Cavity Width Exiting Outer Cavity');
xlabel('Dimensional Position')
ylabel('Dimensional Flow Per Unit Cavity Width');

% Standardize Plot
Standardize(plotfig1);
Standardize(plotfig2);
```

C.6 Fluent.m

```
function Fluent(openfile)
%
% Revision 1.0
% Mark Andrew Livelli
% Rochester Institute of Technology
% April 11, 2010
%
%%%%%%%%%%%%%%%%%%%%%%%%
% Define File Parameters
%%%%%%%%%%%%%%%%%%%%%%%%

% Define Data File
openfile;

%%%%%%%%%%%%%%%%%%%%%%%%
% Preliminary Preparations
%%%%%%%%%%%%%%%%%%%%%%%%

% Define File Delimiter
delim = ',';

% Preallocate Format Placeholder
dataformat = [];

% Load File
fid = fopen(openfile,'r');
if fid == -1
  error('File Not Found')
end

%%%%%%%%%%%%%%%%%%%%%%
% Prepare Data Formats
%%%%%%%%%%%%%%%%%%%%%%

% Read File Header
headerstring = fgetl(fid);

% Parse File Header
```

```
headercell = textscan(headerstring,'%s','delimiter',delim);
headercell = headercell{1};

% Parse Data
data = textscan(fid,'%s',length(headerstring),'delimiter,delim);
data = data{1};

% Construct Column Formats
for i = 1:length(data)

  % If Number
  if ~isnan(str2double(data{i}))
    columnformat = '%f ';

  % If String
  else
    columnformat = '%s ';

  % Store Format
  end
  dataformat = [dataformat columnformat];
end

% Return To File Start
frewind(fid);

%%%%%%%%%%%%%%%%%%%
% Create Data Fields
%%%%%%%%%%%%%%%%%%%

% Read File Data With Column Formats
data = textscan(fid,dataformat,'delimiter',delim,'headerlines',1);

% Close File
fclose(fid);

%%%%%%%%%%%%
% Assign Data
%%%%%%%%%%%%
```

```
% Assign Data To Corresponding Variable
for i = 1:length(headercell)

  % Retrieve Variable Name
  variable = headercell{i};

  % Ensure Acceptable Format
  variable = strrep(variable,'-','');
  variable = lower(genvarname(variable));

  % Replace Improperly Formatted
  headercell{i} = variable;

  % Assign Data
  assignin('base',variable,data{i});
  eval([variable '=data{i}' ';']);
end
```

C.7 FlowPerUnitCavityWidth.m

```
function [z,q] = FlowPerUnitCavityWidth(ycoordinate,zcoordinate,xvelocity)
%
% Revision 1.0
% Mark Andrew Livelli
% Rochester Institute of Technology
% April 11, 2010
%
%%%%%%%%%%%%%%%%%%%%%
% Define Fluent Inputs
%%%%%%%%%%%%%%%%%%%%%

% Define Y Coordinate
ycoordinate;

% Define Z Coordinate
zcoordinate;

% Define Velocity Component
xvelocity;

%%%%%%%%%%%%%%%%%%%%%%%%
% Preliminary Preparations
%%%%%%%%%%%%%%%%%%%%%%%%

% Define Test Parameters
Test = 0;
Count = 0;
Old = 0;
New = 0;

% Determine Characteristic Mesh Size
while Test ~= 1
  Count = Count+1;
  New = zcoordinate(Count);
  if Count > 1
    if New ~= Old
      Test = 1;
      Nodes = Count-1;
```

```
    end
  end
Old = New;
end

%%%%%%%%%%%%%%%%%%%%%%%%%%%%%%%%%%%%
% Integrate Flow Per Unit Cavity Width
%%%%%%%%%%%%%%%%%%%%%%%%%%%%%%%%%%%%

% Define Integration Parameters
% Count = 0;

% Extract Nodes Across Height
for i = 1:Nodes:(length(xvelocity)-Nodes)
  Height = ycoordinate(i:(i+(Nodes-1)));
  Width = zcoordinate(i:(i+(Nodes-1)));
  Velocity = xvelocity(i:(i+(Nodes-1)));

  % Check For Fluent Output Error
  if sum(Width-ones(length(Width,1)*Width(1)) == 0

    % Integrate Across Height
    Count = Count+1;
    z(Count) = zcoordinate(i);
    q(Count) = trapz(Height,Velocity);
  end
end
```